Optimization and Control in Deep Hyperthermia

Clinical implementation of hyperthermia treatment planning in cervical cancer treatment to obtain higher treatment quality

R.A.M. Canters

Colofon

The investigations presented in this thesis was performed within the framework of the Erasmus MC Postgraduate School Molecular Medicine, at the Department of radiation Oncology, Erasmus MC – Daniel den Hoed Cancer Center, Rotterdam, the Netherlands.

Molecular Medicine
Postgraduate School

The research was financially supported by the Dutch Cancer Society (KWF kankerbestrijding). Printing of this thesis was kindly supported by Dr. Sennewald Medizintechnik and the Dutch Cancer Society.

DUTCH CANCER SOCIETY

DR. SENNEWALD
medizintechnik gmbh

Optimization and control in deep hyperthermia
R.A.M. Canters
PhD thesis Erasmus University Rotterdam
ISBN 978-90-8891-607-1

Printed by: Proefschriftmaken.nl || Uitgeverij BOXPress

Optimization and Control in Deep Hyperthermia

Optimalisatie en beheersing van diepe hyperthermie behandelingen

Proefschrift

ter verkrijging van de graad van doctor aan de
Erasmus Universiteit Rotterdam
op gezag van de rector magnificus
Prof.dr. H.G. Schmidt

en volgens besluit van het College voor Promoties.

De openbare verdediging zal plaatsvinden op
woensdag 22 mei 2013 om 11:30 uur

Door

Richard Adrianus Maria Canters

geboren te Venlo

Promotiecommissie

Promotor:	Prof.dr.ing. G.C. van Rhoon
Overige leden:	Prof.dr.ir. N. de Jong
	Dr. L. Incrocci
	Prof.dr. C.L. Creutzberg
Copromotor:	Dr. J. van der Zee

Ad maiorem Dei gloriam

Contents

1 Introduction

This chapter is based on:
Canters RAM, Paulides MM, Van der Zee J, Van Rhoon GC. Implementation of treatment planning in the routine clinical procedure of regional hyperthermia treatment of cervical cancer, an overview and the Rotterdam experience, Int J Hyperthermia 2012, 28(6):570-581

1.1 Introduction

Today, in a growing number of hospitals worldwide, hyperthermia is added to radiotherapy and/or chemotherapy in the treatment of cancer. After the publication of Robinson et al [1] in the 1970's showing that hyperthermia had a selective cytotoxic effect on hypoxic cells at low pH, research for the use of hyperthermia for the treatment of cancer increased considerably [1-2]. From that time until now, a series of phase III trials demonstrated the clinical effect of hyperthermia [3-25]. Additionally, several studies indicate that the clinical efficacy of a hyperthermia treatment is correlated to the applied thermal dose, i.e. the summation of the temperature-time profile that is achieved in the tumor volume over the treatment time [26-33]. A review by Wust et al. shows the background of these developments in hyperthermia treatment [34], while a review of Van der Zee et al. focuses on cervical cancer [35]. When hyperthermia is applied in the combined treatment of cervical cancer, heat is usually delivered by using electromagnetic (EM) energy in the radiofrequency range. To control the shape of the heating pattern and to adapt this pattern to the target volume, phased array applicators were developed. Multipath phenomena due to the dielectric contrast of different tissues make the energy distributions during treatment with phased-array applicators difficult to predict intuitively and these energy distributions differ greatly from the distribution in simple homogenous phantoms. Although clinical results using this intuitive approach showed a clear benefit of hyperthermia, further improvement requires a more advanced prediction and control of the energy distribution. Since the 1980's computer power was greatly enhanced and reached a sufficient level to initiate interest in the development of hyperthermia treatment planning (HTP) codes aiming at the prediction and optimization of the EM energy distribution in the patient [36]. First, these treatment planning codes were mainly used for research purposes, but with growing computer power, calculation times are reduced and accuracy was improved to allow full 3D representation of the patient. Nowadays, treatment planning enables the calculation of EM-fields, online optimization, and adjustment of power and phase settings of the hyperthermia treatment in a few minutes.

1.2 Treatment planning techniques

1.2.1 Treatment planning workflow

Before a hyperthermia treatment can start, the following workflow needs to be followed when including HTP:

Patient imaging. As a basis for the patient-specific simulation model, a computerized tomography (CT) or magnetic resonance imaging (MRI) scan is necessary. The highest accuracy is obtained when during this scan the patient is in an identical position as during the hyperthermia treatment.

Segmentation. The patient anatomy has to be segmented into various tissues, according to relevant differences in dielectric and thermal properties.

Model generation. From the segmented slices, a 3D patient model can be generated, that needs to be placed inside a validated applicator model, containing the detailed antenna structures, that reflects the clinically used applicator.

EM and thermal calculations. After the model generation, EM and thermal calculations are carried out using numerical methods.

Optimization. After calculation, the SAR or thermal distribution needs to be optimized to obtain the initial settings of phase and amplitudes for each antenna as used at the start of the hyperthermia treatment.

Translation to the clinic; from monitor to reality. Maximum exploitation of the improved treatment quality from optimized settings requires matching the setup in the clinic to the setup that was used during simulations. Hence, the patient and the applicator need to be positioned as accurately as possible compared to the simulation, to reduce deviations between planned and real application. Furthermore, the amplitude and phase of the signals emitted by the antennas need to be controlled accurately.

HTP assisted treatment can start after all these steps have been taken. In the next chapters, some of the steps are further explained.

1.2.2 Numerical simulation techniques

Since the 1980's, many studies have been performed to asses the influence of various parameters, and to develop applicators. The developments in hyperthermia treatment planning in the decades up to 2000 are extensively discussed in Lagendijk et al [36].

Two main numerical methods are predominantly used: the integral finite element method (FEM) [37] or finite difference time domain (FDTD) method using the Yee cell structure [38]. While the FE method can model complex geometries easily and is able to handle higher order approximations, it becomes memory consuming with large domains

and contains no time dependent information. The FDTD method on the other hand contains time information and needs less memory when dealing with large problem, but is less suitable for modeling complex structures due to the rectangular voxels. Sreenivasa et al [39] compared both methods and found that SAR predictions were approximately equal. Two main steps can be recognized in treatment planning: calculation of RF-power deposition and temperature distribution. In the power deposition calculations, the Maxwell equations are solved and a distribution of specific absorption rates (SAR) [W/kg] is obtained. For the thermal calculations, two approaches are usually taken: the Pennes bioheat equation (PBHE) [40] or the discrete vasculature (DIVA) model [41-44]. The PBHE, which is essentially the energy equation with an extra term added for blood perfusion, estimates the extraction of heat by the blood flow with a heat sink term, i.e. a perfusion of tissues with a blood flow of constant temperature. To also add vessel information to the energy equation, a discrete vasculature (DIVA) model was developed at the University of Utrecht that takes into account thermal equilibrium lengths of the vascular network [41-44]. The disadvantage of this approach is that it requires very precise 3D imaging of the vessel structure which is presently still a too much time consuming procedure. Alternatively, one could limit the HTP to SAR modeling only and use SAR based parameters that correlate with temperature, as was shown by the Rotterdam group to be a valid alternative [45]. Nevertheless, with the increasing potential in computing power and MR angiography, the ultimate objective remains to perform discrete vasculature HTP modeling, as this is expected to be the most reliable predictor of the temperature distribution.

Currently, a range of software packages is available for electromagnetic and thermal modeling. Most of these software packages are not custom-written for use in a hyperthermia environment and require a substantial effort to create applicator models and optimization routines. One package, Sigma Hyperplan (Dr. Sennewald Medizintechnik GmbH), was developed especially for hyperthermia purposes and is also aimed for clinical use [46]. In the Hyperthermia groups of Rotterdam, Berlin, Munich and elsewhere, Sigma Hyperplan is regularly used for treatment planning of loco-regional deep heating with the BSD2000 Sigma 60 or Sigma Eye applicator. Full clinical use in terms of HTP guided steering however, still requires adaptation of the software [47]. These adaptations are illustrated in chapter 8. Besides Sigma Hyperplan, in Rotterdam and in other institutes also the Semcad-X package is used (SPEAG, i.e. Schmid & Partner Engineering AG), that also contains several hyperthermia specific routines. Despite the fact that clinical application of this package is more labor intensive, it has the advantage of custom

antenna design and can be used to generate information for the design and development of new applicators.

1.2.3 Patient modeling

For the result of HTP calculations, the incorporated dielectric and thermal parameters are of great importance. Naturally, these parameters need to be chosen such, that they resemble the actual patient as closely as possible. The main sources for dielectric parameters (i.e. permittivity and effective conductivity) are the studies of Gabriel et al [48-50]. From these studies, a parametric model is derived for each tissue that is dependent on frequency. For easiness of use and for a more uniform use of these parameters they are available at a number of websites, e.g. [51]. For thermal parameters (i.e. blood perfusion, thermal conductivity, heat capacity, density, and metabolic heat generation), there are two main databases available, that summarize the known literature: the IT'IS database [51], and the McIntosh database [52]. In Rotterdam, both these databases are used as the basis for model generation.
When using these database values, one has to realize that the presented values are averages over various studies and measurements, and that uncertainties exist in each of the dielectric and thermal parameters. Additionally, often animal tissue was used in determining the parameters. From the Gabriel measurements, we derived an uncertainty in permittivity of 15% (standard deviation) and 25% for effective conductivity [49]. From the IT'IS database, uncertainties were derived of 30% for perfusion, 8% for thermal conductivity and 13% for heat capacity [51]. Note that for perfusion, both databases contain only data for tissue in resting condition. Several studies have shown that perfusion is an important parameter in tumor heating [53-56]. Perfusion levels change considerably under thermal stress [53, 57-59]. The influence of uncertainties in perfusion and dielectric constants was partly assessed by De Greef et al [60-61], who showed that realistic uncertainties in perfusion lead to sub-optimal temperatures in the tumor of around 0.5^{o}C. A further analysis indicated that there might be a positive correlation between the number of antennas in an applicator and the level of uncertainty [61]. To complete the analysis of uncertainties with a statistically relevant number nof patients, more research is needed, e.g. a full Monte Carlo analysis. Once these consequences are clear, actions can be taken to reduce them, or modeling can be adapted to take uncertainties into account in treatment planning for individual patients.

1.2.4 Applicator modeling

With the rise of the use of treatment planning, it became clear that accurate antenna modeling is highly important. When there is an impedance mismatch between antenna and coax cable, this will result in unpredictable behavior of the electromagnetic fields in the applicator, i.e. unknown phase shifts and amplitude changes of the fields of each antenna [62-63]. Further, cross coupling and reflection between antennas plays are role in the EM-field sitribution. Several approaches were taken to reduce the effect of mismatch. Increased control of the electromagnetic fields was proposed , first by Wust et al by measuring the electromagnetic field in the applicator [64-65], second by an MR supported feedback loop to correct for mismatch [66-73]. Further, with help of numerical simulations, several groups have developed new multi-ring applicators with good matching characteristics [74-76]. Reduction of the uncertainty arising from the mismatch from antennas is mandatory in the clinical application of hyperthermia.

1.2.5 Optimization and goal functions

Along with the calculation of SAR and temperature in patient models, optimization of the SAR and/or temperature distributions is an important issue. With the increasing numbers of antennas, and thus degrees of freedom, intuitive determination of the treatment settings is no longer an option, i.e. impossible.
In optimization algorithms, two main strategies exist: local and global. Commonly local strategies use the gradient of an optimization landscape e.g. the line search method. This means that this strategy can get to a minimum accurately, but has a high probability to get stuck in local minima. Global optimization (e.g. particle swarm / genetic algorithms) strategies generally make us of random methods to come to an optimum and are useful to approach global optima [77]. However, the precision with which the optimum is determined is low. In Rotterdam we use both methods sequentially: first the global optimum is estimated by a particle swarm method, and then the optimum is approached by a line search method.
Extensive research has been conducted to find SAR indicators, which could also be used in optimization [78-96] (also summarized in chapter 2). From the latter study, the indicator correlating best with the calculated median tumor temperature (predicted using PBHE) was the hotspot tumor quotient (HTQ). HTQ is the quotient of the hotspot SAR (average SAR in x^{th} volume percentile) and the average tumor SAR (see chapter 2.).
For temperature optimization, two main types of goal functions are found: maximization of tumor temperature [60-61, 97-98], or a combination of maximizing tumor temperature

and minimizing hotspots in healthy tissues [39, 81, 99-102]. The latter has the advantage of unconstrained goal function, which is less likely to be stuck in local minima.

1.2.6 Validation

An essential step in the clinical introduction of treatment planning in hyperthermia is model validation. Validation consists of three steps: first the mathematical calculation model has to be validated, which is usually done by the manufacturer against algebraic solutions. Second, the applicator models have to be validated in a controlled setup, i.e. measurements in a homogeneous or heterogeneous phantom must be compared against model results. The validation of the applicator model in a controlled setup was done in various studies and showed good resemblance between model predictions and measurements [76, 103-107]. Third, clinical validation of HTPhas to take place, i.e. does the application of HTP lead to the expected temperatures in the tumor in practice. MRI thermometry appears exceptionally useful for validation of treatment planning models. Clinical validation was done by Sreenivasa et al, who found a good agreement between clinically measured temperatures and model predictions [39]. Some years ago, a study was started in Rotterdam to assess the effect on tumor temperature of using 3D EM models to find optimal treatment settings. In a randomized setup, intuition based TCP steering (see chapter 3) was compared to HTP guided steering for 36 patients in the Sigma 60 applicator. The result of this study showed that HTP guided steering performed equal to TCP steering in terms of temperatures representative for the tumor temperature, and that HTP guided steering is feasible in the clinic [39, 108].

1.2.7 Translation from model to clinic

The transfer of hyperthermia treatment planning based predictions to the clinic consists mainly of the reduction of differences between the set-up of the model used in the calculations and the patient set-up during the actual treatment situation. Besides the uncertainties arising from selected tissue parameters and actual patient properties, there are several important factors that determine a successful transition from monitor to clinic: a treatment representative CT/MRI scan of the patient as basis for the models (preferably in the same position as during treatment), accurate segmentation of these images into different tissues, and reproduction of the patient position in the clinic. After all preparations have been performed in good order and accuracy, the treatment can start. There are several options to apply treatment planning in the clinic: the classical target center point (TCP) steering [47, 74], pre-treatment planning [100], complaint

adaptive steering [47], and MR image guided hyperthermia [68-71, 109]. In the next sections, an overview is given of segmentation, positioning, and the different treatment strategies. In chapter 8, the treatment workflow is explained using the Rotterdam experience as an example.

Tissue segmentation

Between the different tissues in the pelvic region, considerable differences in dielectric and thermal constants exist. If imaging is done using a CT, three major types of tissue can be segmented automatically, using the difference in Hounsfield units: bone, muscle-like (muscle + organs) and fat. Discrimination between muscle and organs is not possible from the CT-scan, while the quite substantial differences in perfusion would require, at least in our opinion, additional segmentation to separately segment muscle and the various organs. Since manual organ segmentation still requires an unacceptable amount of time, the possibility for atlas based segmentation is currently investigated. It is important to notice that similar techniques are already in use in radiation therapy segmentation [110-111].

Patient and tumor positioning

Several studies have been published that show the importance of accurate patient, and thus tumor positioning, i.e. to obtain an accurate match between model and patient [97, 112-113]. These studies show that position deviations of more than 1cm should be avoided. To obtain position accuracies of this kind without image guidance from an MR system in the treatment room, it is necessary to apply precise systems of positioning. Two types of positioning can be distinguished: patient positioning on the treatment table/hammock, and applicator positioning with respect to the patient. Currently, markers on the patient, line lasers, ultrasound probes, and simple rulers are used. The main problem with most of the applied methods is that measurement becomes hard once the water bolus of the applicator is filled. For accurate routine clinical application of HTP, it is necessary to use the more precise means of positioning, i.e. laser or ultrasound. The use of rulers tend to result in deviations of >1 cm. If an MR is available however, precise positioning in the order of a few mm can be achieved by overlaying of the model and the MR-image, although at the edges of the MRI image this becomes less accurate. Additionally to patient positioning, several studies have also investigated the influence of tumor position inside the patient on the heating quality [80, 82]. Generally, higher frequencies lead to better tumor heating, since the focus becomes smaller. However, for tumors positioned centrally in the body, the studies report that the gain is less, probably

because of the smaller penetration depth at higher frequencies or the low number of antennas.

Table 1.1: Summary of the main factors involved in the outcome of treatment planning

Factor	Explanation
Patient imaging (CT or MR)	Patient position and posture during imaging should be identical to that during treatment.
Tissue segmentation	CT and / or MRI resolution are sufficient for accurate patient geometry reconstruction. In manual segmentation, interobserver differences play a role, while in autosegmentation the accuracy of the method is important.
Model generation	The generation of a 3D model from the segmentation causes potential changes in geometry due to discretization (voxels or thetrahedra)
Dielectric and thermal parameters	Dielectric and thermal parameters from literature [49, 51-52] have considerable uncertainties (5 to 30%)
Applicator model	Accurate implementation of the antennas is required for correct prediction of EM-fields, hence validation of the applicator model is needed. Correction for antenna mismatch is possible via a feedback loop with the power system.
Optimization	The optimization algorithm must be able to find a global optimum, or at least a value close to this optimum
Transfer into clinic : positioning	Clinical reproduction of patient positioning and posture in the model must be within 1 cm.
Transfer into clinic : amplitude and phase	Amplitude and phase of the signals emitted by the antennas should be identical to the requested values.

1.2.8 Overview of uncertainties in clinical application of HTP

In the previous sections, various factors involved in successful translation from HTP to the clinic were mentioned. In table 1.1, the various factors affecting the clinical outcome, i.e. tumor temperature, are summarized.

1.3 Steering strategies

There are several approaches to apply treatment planning in the clinic. These approaches are explained in the next sections.

TCP steering

This is the oldest procedure for SAR steering and is based on TCP (target center point) steering of the focus of the EM (electromagnetic) field. The procedure is based on a simple analytical model in which the treatment settings are calculated on basis of the path length from the antennas to the focal point, under the assumption that the patient is a uniform homogeneous cylinder. Besides this rather crude approximation of the patient, there is no unequivocal reaction to a patient complaint. Quality assurance guidelines only state that the energy in the complaint region needs to be reduced [114]. In many hyperthermia centers, TCP steering is used as the standard method to calculate the phase settings of the antennas.

Pre treatment planning

Especially in applicators with multiple antennas, placed in a single or more rings, and thus large numbers of degrees of freedom, a significant effect of optimization is expected [80]. Many institutes that use HTP and optimization routines to calculate optimal treatment settings use HTP to calculate starting phase and amplitude settings for a treatment, as we observed. Again, there is no unequivocal reaction to a patient complaint. Although this is a relatively simple method, it disregards the fact that treatment limiting hotspots could occur at locations that were not predicted, due to the previously mentioned uncertainties. In this case, only power reduction can be applied.

HTP guided steering

Because of the disadvantages mentioned in the last section, in Rotterdam an alternate method of using HTP in the clinic is adopted: complaint adaptive steering [47]. The treatment is monitored by using a pre-calculated EM distribution and feed the EM-model

with the actual measured phase and amplitude settings applied to the applicator such that the displayed SAR distribution reflects the real situation present at the patient. This option makes online treatment optimization a realistic feature. In addition, the response of the operator to a patient complaint of discomfort can be made uniform and is automatically recorded. As already pointed out in a previous study [47], re-optimizations are performed in case of discomfort by adding constraint factors for the region with the complaint. Of course, the intention of re-optimization is to retain or increase tumor heating. Here again, the model predictions can be used to quantify and evaluate the effectiveness of the optimization procedure. To reduce uncertainties due to mismatch of antennas, RF sensors are under development to measure the E-field distribution in the water bolus. The measured signals function as input to calculate antenna offset correction values [64, 115]. This might provide a method to reduce uncertainties without the need for acquiring an MR scanner to assess the shifts between predicted and measured 3D-temperature distributions.

HTP in combination with non-invasive thermometry

Using non-invasive MR thermometry (NIT) in hyperthermia, 3D temperature maps became available during hyperthermia treatment. This created the possibility for treatment optimization with help of actually measured temperature data. The HT-groups of Munich, Berlin and Durham belonged to the first to apply HTP in combination with temperature measurements in a feedback loop in order to optimize the temperature distribution [68-71, 109]. This is a promising new development that uses the benefits of both 3D temperature information and optimization capabilities of the numerical models. Uncertainties that normally affect HTP can be corrected for by the instantly measured 3D-temperature data. A disadvantage however, is the reactive nature of NIT: the current temperature is available, but in order to know how to reach the desired temperature distribution, treatment planning is an absolute requirement.

1.4 Outline of this thesis

In this thesis, the path towards controlled and optimized hyperthermia treatments by applying hyperthermia treatment planning is discussed. The main items that are investigated are optimization of power deposition patterns in the patient, uncertainties and their influence on heating quality, and application of hyperthermia treatment planning in a clinical setting to achieve controlled and optimal heating of the patient.

In chapter 1, an introduction and overview is given over the field of hyperthermia, and more specifically, hyperthermia treatment planning and clinical steering strategies.
The first main item, optimization is assessed in chapters 2 and 3. In chapter 2, a literature survey on optimization goal functions is presented, along with an analysis of the effectiveness of each of these functions. In chapter 3, a newly developed complaint adaptive optimizations strategy, designed for clinical use is evaluated and tested in an experimental setup.
The second main item, uncertainties, is assessed in chapters 4 and 5. In chapter 4, the influence of positioning accuracy on treatment outcome is assessed, while chapter 5 addresses the possibilities of increasing the number of degrees of freedom by introducing the Sigma Eye, taking into account uncertainties in dielectric and thermal parameters.
The third main item, application of hyperthermia treatment planning in a clinical setting, is addressed in chapters 6, 7, and 8. Chapter 6 shows the results of the first clinical application of HTP guided steering: a “cross-over” clinical trial assessing the effect of using HTP optimized settings during treatment. Chapter 7 evaluates the treatments where HTP was used on the predicted hotspot locations. Chapter 8 illustrates the current clinical implementation of HTP in Rotterdam that results from this research.
Finally, in chapter 9, the relevance of the results of this research is discussed.

2 A literature survey on indicators for characterization and optimization of SAR distributions in deep hyperthermia, a plea for standardization

This chapter was published as:

Canters RAM, Wust P, Bakker JF, Van Rhoon GC. A literature survey on indicators for characterization and optimization of SAR distributions in deep hyperthermia, a plea for standardization. Int J Hyperthermia 2009, 25(7): 593-608.

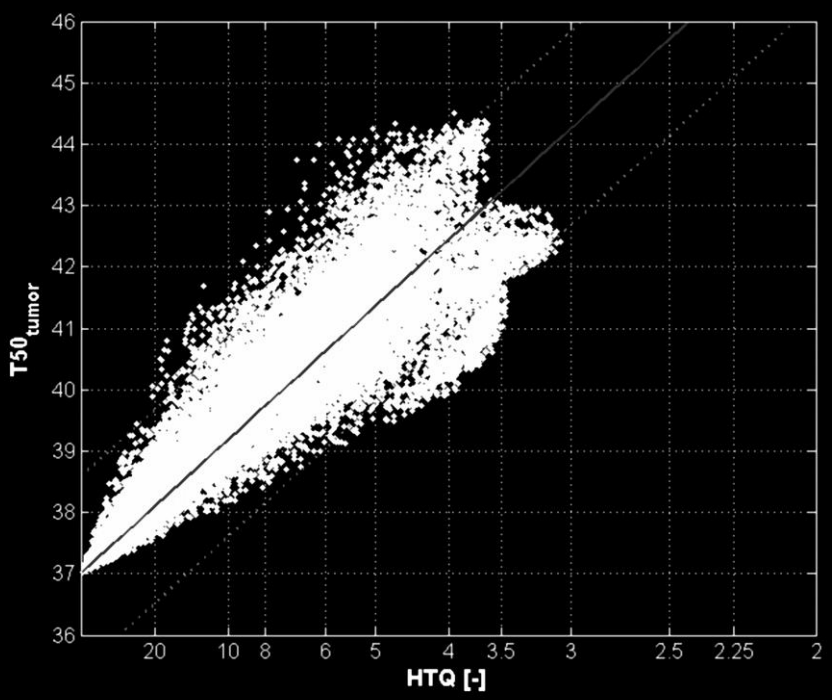

Abstract

Purpose: To evaluate the predictive value of SAR-indicators by assessing the correlation of a SAR-indicator with the corresponding predicted temperature. Ultimately, this should lead to a number of verified SAR-indicators for characterization and optimization of a predicted SAR distribution.
Methods: A literature survey is followed by an evaluation of the SAR-indicators on their functionality, using a set of heuristic classification criteria. To obtain an objective assessment of the predictive value for SAR-characterization, all SAR-indicators are evaluated by correlating the value of the SAR-indicator to the predicted target temperature when heated with the BSD2000 Sigma 60 applicator. Two methods were followed. First, the specificity of the SAR-indicator to target temperature was assessed for each of the 36 patient specific models, using 30 randomly chosen phase and amplitude settings. Secondly, each SAR-indicator was used as a goal function to assess its suitability for optimization purposes.
Results: Only a selected number of SAR-indicators correlate well with tumor/target-temperature. Hence, for target-related properties, an adequate set of SAR-indicators is found in the literature. For hotspots, modifications are desirable. For optimization purposes, improved objective functions have been defined.
Conclusions: From the correlation of the SAR-indicators with tumor temperature, a preferred set of SAR-indicators is derived:
For target heating, *'average SAR(-ratio)', 'Hotspot-target SAR-ratio'* , and *'homogeneity coefficient'* provide suitable objective criteria, while for hotspot reduction, '*Hotspot-target SAR-ratio'* is considered the most useful indicators.
For optimization procedures, '*Hotspot-target SAR-ratio*' is currently the most suitable objective function.

Nomenclature

Symbol	Unit	Description
SAR_{tot}	[W/kg]	Volume averaged SAR in the total patient volume (the part of the patient inside the applicator)
SAR_{targ}	[W/kg]	Volume averaged SAR in the target volume
SAR_{max}	[W/kg]	Maximum SAR in the total patient volume
$SAR_{targ\ max}$	[W/kg]	Maximum SAR inside the target volume
$SAR_{complaint\ region}$	[W/kg]	Volume averaged SAR in a complaint region
$SAR5_{tot}$	[W/kg]	SAR exceeded in 5% of the total patient volume
$SAR5_{targ}$	[W/kg]	SAR exceeded in 5% of the target volume
$SAR5_{region}$	[W/kg]	SAR exceeded in 5% of a region volume
$25\%SAR_{max}$	[W/kg]	25% of the maximum SAR
$25\%SAR_{max}\ coverage$	[-]	Ratio of the target enclosed by $25\%SAR_{max}$ isosurface
P_{tot}	[W]	Deposited power in the total patient volume
$P_{t\,\mathrm{arg}}$	[W]	Deposited power in the target volume
$\vec{x}$	[m]	A location inside the patient
w_b	[ml/kg/min]	Blood perfusion
V_{tot}	[m^3]	Total volume
V_{targ}	[m^3]	Target volume
$V1$	[m^3]	Volume where SAR>SAR1, i.e. the percent of the patient

		volume with the highest power absorption.
$V_{x\%SARmax}$	[m^3]	Volume enclosed by $x\%SAR_{max}$
$V_{x\%SAR\ targ\ \ max}$	[m^3]	Volume enclosed by $x\%SAR_{targ\_max}$
$T50_{targ}$	[^oC]	Temperature exceeded in 50% of the target volume
$T50_{\ targ\ max\ tolerance}$	[^oC]	Temperature exceeded in 50% of the target volume, at maximum patient tolerance

2.1 Introduction

Within the hyperthermia community, general consensus exists that quality of the hyperthermia treatment is a key factor for treatment outcome. In various clinical trials, a correlation between treatment outcome and various retrospectively assessed thermal dose parameters has been demonstrated [26-33]. The derivation of a prescriptive quality parameter, preferably prognostic for treatment outcome, would have a great potential in further positioning hyperthermia as a practical and widespread adjunct to radiotherapy and chemotherapy [116].
A major limitation for further enhancement of hyperthermia treatment quality is the difficulty to define the most relevant dose parameter [117-119], to adequately monitor temperature distribution [120], or to reliably predict the temperature- (blood flow changes with temperature and over time) or SAR (specific absorption rate)-distribution [36], and thus it is still not feasible to prescribe a dose to a target volume. Important preconditions for solutions to overcome these limitations are that they must be economically as well as clinically acceptable [121].
To improve hyperthermia treatment quality, research is currently focusing on two approaches:
Improvement of temperature monitoring during treatment by introducing non-invasive thermometry by magnetic resonance imaging (MRI) [70, 122]. However, it should be noted that this innovative approach improves monitoring and control, but provides no a-priori information on treatment quality.
Optimization of the temperature- or SAR-distribution by hyperthermia treatment planning (HTP). In strong contrast to the first research approach, a major benefit of HTP is that it offers a tool to a-priori assess the temperature- or SAR-distribution and to apply optimization methods prior to the actual treatment [47, 123-124].
As the potential of electromagnetic models has increased dramatically over recent years, the presently available HTP systems provide excellent opportunities to perform optimization of the 3D SAR- and, to a lesser extent, temperature distributions before and during treatment, i.e. prescribe the amplitude and phase settings for optimal hyperthermia quality [47, 124].

Already, a few groups have demonstrated the great potential of 3D electromagnetic models to establish new quality assurance and control guidelines for superficial hyperthermia [125-131]. De Bruijne et al. [132] has demonstrated the new prospects that

extensive electromagnetic modeling offers to elegantly characterize the performance of the Lucite Cone applicator or superficial applicators in general. More recently, our group exploited electromagnetic modeling as the foundation for the development of a complex phased array applicator for hyperthermia treatment of head and neck tumors [47, 75, 80, 124, 133-135].

Besides the initial use of HTP in characterization of SAR-distributions for applicator development and quality assurance studies, HTP is used more and more to guide optimization of the hyperthermia treatment quality prior to or during treatment. In various publications, the Rotterdam and Berlin hyperthermia groups [100, 131-132] reported increased tumor temperatures following adaptation of the applicator settings or even by selecting a different applicator following extensive HTP to improve electromagnetic energy deposition in the tumor. The work of Paulides et al. [75, 133] showed that if the applicator is also designed with electromagnetic modeling, excellent agreement exists between predicted and measured SAR distribution in phantoms. De Bruijne et al.[107] report a relative dose difference of 2% and a distance to agreement of 2 mm between predicted and measured data. The latter demonstrates that, under laboratory conditions, the accuracy of electromagnetic modeling in hyperthermia is comparable to the accuracy in radiotherapy treatment planning.

Various modeling packages are in use for hyperthermia, such as Sigma Hyperplan (finite element method or finite difference time domain) [39, 100], the Utrecht- [124, 136] and SEMCAD-X HTP model (both finite difference time domain) [107, 137], as well as Comsol (finite element method), and CST (finite element method). Despite the fact that these electromagnetic models are using different mathematical concepts to describe the interaction between the electromagnetic field and tissue, all of them have been proved to be valid when compared against analytical solutions for specific configurations. At present, the reliability of an electromagnetic model is mostly governed by the precision of the antenna implementation in the electromagnetic model. In the Hyperthermia groups of Rotterdam, Berlin, Munich and several others, Sigma Hyperplan is regularly used for treatment planning of loco-regional deep heating with the BSD2000 Sigma 60 or Sigma Eye applicator.

In order to exploit HTP to improve the quality of deep hyperthermia, it is mandatory that a comprehensive set of indicators is available to characterize and optimize the SAR distribution and to assess hyperthermia treatment quality. For both SAR-characterization and SAR-optimization, it is necessary to define objective criteria. Preferably consensus exists on a set of quality indicators in order to enable quantitative comparison of different treatments, i.e. in the same patient with a single system, as well as in different patients,

and even more importantly, with regard to treatments by different institutes and different treatment systems. Clearly, for optimization so-called objective functions for the selected SAR-indicator are required, allowing it to be maximized or minimized using solver algorithms.
The objective of this study is to create a verified set of indicators for characterization and optimization of predicted SAR distributions. Hereto, the predictive value of SAR-indicators is specified by assessing the correlation of a SAR-indicator with the corresponding predicted temperature.

2.2 Methods

2.2.1 General outline of the study

The general outline of the study is the following: First, in the methods section, the literature search, the set of heuristics for quality indicators, and the setup for the calculations for an objective evaluation through a correlation between temperature and SAR-indicators are presented. In the results section, the outcome of the literature search is presented and evaluated according to the previously defined heuristic criteria. On basis of this evaluation, modifications of existing indicators or new indicators are proposed. The last part of the results section deals with objectively assessing the correlations between temperature models and the different indicators as well as the optimization outcomes for the different indicators in order to evaluate their practical value, both in characterization and in optimization. After the discussion, this leads to the proposal of a preferred set of indicators that can be used in analysis or optimization of SAR distributions. The outline is schematically depicted in figure 2.1.

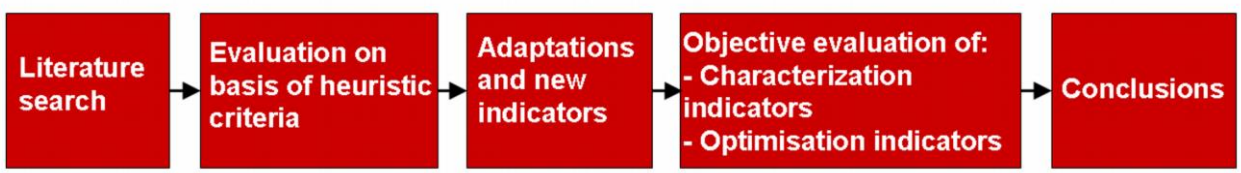

Figure 2.1: Outline of the study

2.2.2 Literature search

A literature search in PubMed is performed to make a survey of various quality indicators used for SAR-characterization and -optimization. Typical keywords used in this search

were ‘treatment planning’, ‘SAR optimization’, ‘SAR dosimetry’, ‘SAR analysis’ and ‘SAR treatment planning’ in combination with ‘Hyperthermia’. Subsequently, these quality indicators are evaluated on their usefulness for quality assurance and optimization. A subjective evaluation is performed, using a set of heuristics considering various aspects of characterization- and optimization modeling. These criteria are defined in section 2.2.3.

2.2.3 Criteria for subjective evaluation of SAR quality indicators

The quality of a hyperthermia treatment strongly depends on the balance between SAR in the target volume and SAR peaks outside this target volume, i.e. hotspots. Therefore, the SAR in target and hotspots are considered as most important for the analysis of SAR distributions. The SAR in the target is an indicator that needs to be maximized to elevate temperatures in the tumor. Hotspots, on the other hand, limit the applied power if they cause patient discomfort, further referred to as patient complaints, and thus must be minimized. Indicators providing information about the SAR in target and/or hotspots must be evaluated in terms of their ability to differentiate between poor and good treatment plans. Furthermore, the scale on which an indicator is defined is considered important, e.g. does the indicator contain absolute values, or is it defined relative to a certain average or maximum value?
For quality indicators in characterization of SAR distributions, it is very important to have a comparative value. Intra- and inter-patient comparison should be possible with a quality indicator. Additionally, a comparison of clinical results as obtained by different treatment systems or institutes should be possible.
Over the years, many different quality indicators have been introduced. We may question whether many of these indicators are needed. However, for selection of the most appropriate indicator, an evaluation of the various quality indicators on their ability to characterize SAR distributions or to optimize a SAR distribution is required. For such an evaluation, a set of subjective and objective criteria are required. The definitions of the set of heuristics as used in the subjective evaluation are formulated below and provide a boolean (yes or no) as answer. The objective criteria are explained in section 2.2.4.

Characterization of SAR distributions, SAR_{max} independency
A general criterion for quality indicators is SAR_{max} independency. In SAR distributions, either modeled or measured, the outliers tend to be more sensitive to the setup of the model or measurement than the average. Clearly, comparison of measured data (mostly with a course data sampling) with predicted data (fine data sampling) will also improve

when normalization on SAR_{max} is replaced by for instance on $SAR_{average}$. It is our experience that SAR_{max} is potentially easily disrupted by details of the model. Tissue segmentation inaccuracies and inaccuracies in conformality of the tetrahedral grid can easily lead to local peaks in SAR that do not correspond with the actual situation. SAR_{max} is potentially far easier affected by these inaccuracies than the volume averaged SAR. Additionally, tetrahedron - or voxel size will influence the SAR_{max} value. In finite element method, but also in finite difference time domain models with dynamic voxel sizes, the element size often differs considerably over the patient anatomy, generally being particularly small at tissue interfaces with strong curvatures. If tetrahedra or voxels are large, maxima in SAR will be averaged over the element volume and thus will be smoothed. Average SAR however, is less sensitive for changes in value of SAR_{max}, either in finite element method or finite difference time domain. Although the effect of size could be counteracted with a finer grid, SAR_{max} will remain more sensitive to segmentation errors than average SAR.

Characterization of SAR distributions, target or region related criteria

With respect to the target region, a first sub-criterion is quantification of deposited SAR in the target (and/or other regions) in absolute values, i.e. W/kg. Deposited SAR has a direct relationship to the quality of heating.

A second sub-criterion is the quantification of the deposited SAR in the target (and/or other regions) relative to the whole body average SAR, i.e. selectivity of tumor heating.

A third sub-criterion is the analysis of the homogeneity of the target. Temperature homogeneity would be the first goal. However, this requires detailed knowledge of perfusion in the target. To be able to distinguish inhomogeneities in perfusion on a sub-target scale, it would be necessary to incorporate accurate perfusion data, a large vessel model and the dynamic behavior of the perfusion. Acquiring these data is still very hard and their practical implementation has been limited so far to small volumes such as used in interstitial HT [138]. At present, we consider aiming for SAR-homogeneity as the best alternative for homogeneity of heating. Moreover, at the frequency we used (i.e. 77MHz), it is impossible to focus heating on a sub-target size, e.g. cm^3, scale. As a consequence, we anticipate that the SAR distribution in the target area will finally determine the quality of the treatment. With current available electromagnetic phased array systems, we may at best aim for low heterogeneity of the SAR distribution in the target volume.

Indicators obeying the three sub-criteria mentioned above are always comparable between heat sessions, patients, institutes, systems and studies, assuming that the efficiency of the system is known.

Characterization of SAR distributions, *hotspot related criteria*
Quality indicators should provide information about the absolute SAR level in hotspots, as well as relative to the target. Indicators obeying these criteria are comparable between heat sessions, patients, institutes, systems and studies.
Optimization-criteria for SAR objective functions
For goal functions in optimization, there are two important criteria. Maximization of SAR in the target area is the most important objective. However, hotspots typically limit the SAR level in the target and therefore the goal function should additionally restrict hotspot SAR.

2.2.4 Objective evaluation of quality indicators for characterization of SAR distribution through model calculations for 36 patients

All subjective criteria mentioned in the previous paragraph lead to a set of indicators that theoretically allow SAR characterization and optimization. In case one of the aspects is covered insufficiently, new or modified indicators need to be proposed.
To assess the predictive value of the quality indicators, the SAR and temperature part of the Sigma Hyperplan model is used, to investigate the correlation of T50 with the associated quality indicator. A high correlation between T50 and a quality indicator means that the specific quality indicator has a high predictive value for the target temperature, i.e. a high value of this indicator will lead to a high temperature. Preferably, a quality indicator should provide patient specific information, and should also enable comparison between different patients, treatments, institutes and treatment settings. The SAR part of Sigma Hyperplan is based on the finite element method calculation of Maxwell's equations, the temperature part is based on the Pennes bio-heat equation [40]. Using Sigma Hyperplan with a model of the BSD2000 Sigma 60, we calculated electromagnetic and temperature distributions for 36 patients, with 30 different amplitude and phases settings each, to verify the functionality of the proposed indicators [39, 100]. These 30 different settings are chosen randomly (amplitude = random (0.5, 1), phase = random (-180, 180)), but are the same for all 36 patients. To asses the functionality of each quality indicator for optimization, each indicator is used as a goal function for a patient specific SAR-optimization. The same 36 patient models as mentioned in the previous paragraph have been used for individual optimization and the results are reported as the average for 36 patients. The resulting temperature model

outcomes provide information about the suitability of each indicator as a goal function. The characteristics of the used 36 patient models are summarized in table 2.1.

Table 2.1 : Characteristics of the 36 patient models that were used to verify the found indicators. Averages and standard deviations are given.

	average	SD
# tetrahedra	248011	49747
Patient volume inside applicator [cm3]	31715	7820
Tumor volume [cm^3]	129	98
Fat [%]	47	13
Muscle [%]	32	7
Bone [%]	7	2

2.2.5 Equipment

All calculation models are representative for a regular treatment of cervical cancer in the BSD2000 Sigma 60 [139-140]. This applicator has a diameter of 60 cm and a length of 50 cm. Furthermore, it consists of a ring of 8 dipole antennas that are coupled in 4 channels of two antennas each, which is schematically depicted in figure 2.2.

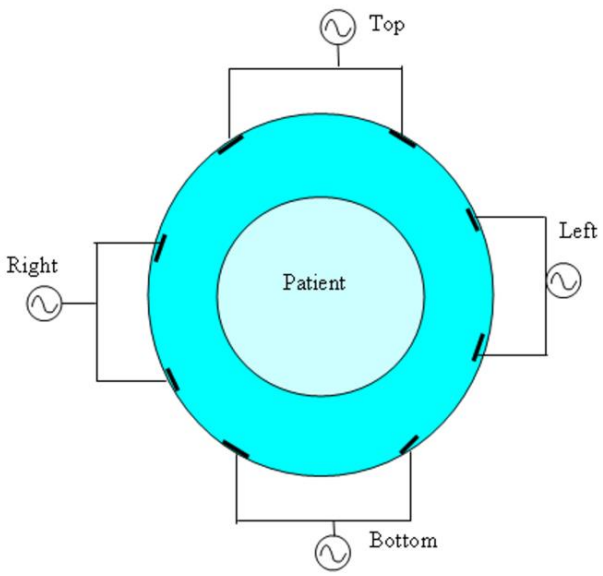

Figure 2.2: Axial view from the caudal direction of the Sigma 60 applicator, with the four channels, each connected to two antennas

E-fields are calculated for a frequency of 77 MHz, which is the standard treatment frequency for deep hyperthermia treatment in Rotterdam [4]. For all models, the E-field for all antennas is calculated at an applicator input power of 400 W. Calculations take approximately 1.5 hours on a 2.8GHz Pentium 4 PC. Tissues are defined in the model on basis of a CT-scan, made with the patient in a hyperthermia hammock, i.e. equivalent to the position during hyperthermia treatment. Dielectric properties of these tissues are defined in table 2.2 [49]. All tissues defined in table 2.2 are actually used in the segmentation of the patient model.

Table 2.2: Tissues, defined in the patient model and their electromagnetic and thermal properties at 77 MHz, 37°C and under thermal stress [39, 49, 113]

Tissue	Relative permittivity	Effective electric conductivity [S/m]	Blood perfusion (ml/kg/min)	Mass density (kg/m^3)	Heat capacity ($J\ kg^{-1}\ K^{-1}$)	Thermal conductivity ($W\ m^{-1}\ K^{-1}$)
Fat	13	0.07	200	900	3500	0.21
Muscle	69	0.70	300	1000	3500	0.642
Bone	16	0.06	100	1600	1000	0.436
Target (=cervix)	69	0.70	800	1000	3500	0.642
Bladder	24	0.29	150	1000	3500	0.6
Heart	99	0.70	600	1000	3500	0.642
Intestine	108	1.62	500	1000	3500	0.55
Kidney	109	0.77	4000	1000	3500	0.577
Liver	75	0.46	1000	1000	3500	0.64
Lung	35	0.71	200	500	1000	0.2
Myelum	6	0.04	100	1000	3500	0.642
Spleen	101	0.77	600	1000	3500	0.577
Stomach	82	0.89	600	1000	3500	0.577
Uterus	69	0.70	300	1000	3500	0.642
Vagina	69	0.70	300	1000	3500	0.642

The resolution of each CT-slice is 0.1*0.1 cm^2 and the slice thickness is 0.5 cm. This is resampled to 0.2*0.2*1 cm^3, and then tissues are defined. Generally, a patient model is

based on 140 CT-slices, covering 70 cm of the patient, approximately from breast to knees.
From this segmented CT, a tetrahedral grid of patient and applicator is defined. This grid typically consists of 250,000 tetrahedra with edge lengths between 0.3 and 2.5 cm. This spatial resolution is commonly considered to be satisfactory for reliable SAR and temperature predictions and comparable to other studies, published on HTP using Sigma Hyperplan [100, 113].

2.3 Results

2.3.1 Literature survey

Table 2.3: Quality indicators found in literature with a short explanation of their functionality.

Indicator	Formula	Unit
1	P_{targ}	[W]
2	$P_{ratio1} = P_{targ} / P_{tot}$	[-]
3	$P_{ratio2} = P_{targ} \Big/ \sum_{i=1:10} SAR_{max,i}$	[kg]
4	$P_{ratio3} = P_{targ} \Big/ \left[\int_{V \setminus targ} SAR^2 dV \right]^{1/2}$	[kg m$^{-1.5}$]
5	$P_{ratio4} = P_{targ} \Big/ \left[\int_{V \setminus targ} \left(SAR / w_b \right)^2 dV \right]^{1/2}$	[kg m$^{-4.5}$s^{-1}]
6	$P_{ratio5} = P_{targ} \Big/ \sum_{i=1:10} \left(SAR / w_b \right)_{max,i}$	[m^{3}s^{-1}]

7	$P_{square\text{-}ratio} = P^2{}_{targ} / P_{tot}$	[W]
8	$STH_{ratio} = SAR^2{}_{targ} / SAR_{hotspot}$ With STH the Square Target Hotspot ratio	[W/kg]
9	SAR_{targ}	[W/kg]
10	$SAR_{ratio} = SAR_{targ} / SAR_{tot}$	[-]
11	$10gSAR_{max}$, SAR IEEE-1529 Peak Spatial SAR	[W/kg]
12	$10gSAR_{max\,ratio} = 10gSAR_{\max} / \overline{SAR}_{tot}$	[-]
13	$x\%SAR_{max}\ \ coverage = V_{x\%SARmax} / V_{targ}$ with $V_{x\%\ SARmax}$ the volume enclosed by the x% SAR isosurface.	[-]
14	$HC = V_{75\%SAR\,targ\,max} / V_{25\%SAR\,targ\,max}$ with HC the homogeneity coefficient	[-]
15	$SAR_{10max} = \sum_{i=1}^{10} SAR_{\max,i}$ with $SAR_{max,i}$ the i^{th} highest SAR-value	[W/kg]
16	$SAR_{hs-targ\ ratio} = \frac{\mathrm{SAR1}_{region}}{\mathrm{SAR50}_{target}}$ with $SARx_{region}$ the SAR exceeded in x% of a region.	[-]

The indicators describing SAR in target and/or hotspots as found in the literature survey are listed in table 2.3. In addition, a brief description is given per indicator, providing a basic overview of the reported quantity.

P_{targ} :the power absorbed in the target [79].

P_{ratio1}: ratio of target power to the total power absorbed in the patient [79-81].

P_{ratio2}: target power divided by the sum of the 10 maximum SAR locations [81].

P_{ratio3}: target power divided by the volume integral over the squared SAR in normal tissue, which gives a penalty to high SAR peaks [81].

P_{ratio4}: target power divided by the volume integral over the squared SAR in normal tissue expanded with the blood perfusion. Instead of SAR, the SAR-perfusion quotient is used. The addition of perfusion corrects for a major bias between temperature and SAR modeling [81].

P_{ratio5}: target power divided by the sum of the10 maximum SAR-perfusion quotients. Again, the addition of tissue perfusion provides a better view of heating on basis of deposited energy [81].

$P_{square\text{-}ratio}$*:* ratio of the squared target power and the total power in normal tissue. The squared target power gives more weight to the target power [79].

STH_{ratio}*:* ratio of squared SAR_{targ} (the volume averaged target SAR) and hotspot SAR: the accumulated SAR in the 10 highest power points per antenna. The square in nominator gives more weight to target SAR [79].

SAR_{targ}*:* volume averaged SAR in the target. Used as objective function in Paulsen et al. [82] with constraint $SAR_{tot} \leq 1\ \mathrm{W/kg}$. Constraints of the form $SAR(x) \leq 1\ \mathrm{W/kg}$ lead to less satisfactory results. In Sandrini et al. [83], more generally defined as power deposited in a region divided by region volume, as dosimetric indicator [78, 82-83].

SAR_{ratio}*:* ratio of average SAR in the target and the average SAR in the patient [82, 84-86]. In Kuster et al. [87], more generally defined as ratio of Average SAR in a region and Average SAR in the patient.

Maximum average SAR over 1 or 10 grams of tissue, defined in IEEE-1529 [88]. Used as dosimetric unit to define for example maximal doses of electromagnetic field [83, 89-91]. Also mentioned in ICNIRP-guidelines [92].

Maximum average SAR in 1 or 10g relative to average SAR in patient, reported in Bernardi et al. [91] as measure for maximal SAR relative to whole body average SAR.

Part of volume enclosed by *x%* SAR_{max}. According to Meyerson et al. [93] and Lee et al. [94]. *25%*SAR_{max} *coverage* is a potential, prognostic factor, characterizing the particular SAR distribution in the target. In Neumann et al. [141] and Johnson et al. [142] SAR

coverage is used to asses the quality of heating by a superficial heating system. Also mentioned in Paulides et al. [74] and De Bruijne et al. [123].
Ratio of the volume enclosed by the $75\%SAR_{targ\ max}$ isoSAR and the volume enclosed by $25\%SAR_{targ\ max}$ isoSAR. Gelvich et al. [95] used this quality indicator and found it suitable for applicator characterization.(see figure 3b)
SAR_{10max} is defined as the sum of the 10 highest SAR spots [79].
Ratio of the SAR exceeded in 1% of a region's volume and the median target SAR. In Kroeze et al [86] this indicator is used to asses the quality of heating in deep hyperthermia. In Van de Kamer et al [96], a similar definition of $SAR0.1_{tot}/SAR_{targ}$ is used.

Table 2.4: Heuristic evaluation of the quality indicators from table 2.3

	Criterion A	**Criterion B**			**Criterion C**		**Criterion D**	
Indicator	Independency of SAR_{max}	**SAR in target**	**SAR in target relative to normal tissue**	**Homogeneity in target**	**Hotspot SAR level**	**Hotspot SAR level relative to target SAR**	**Maximization of target SAR or power**	**Minimization of hotspot SAR or**
1	Y	N	N	N	N	N	Y	N
2	Y	N	N	N	N	N	Y	N
3	N	N	N	N	N	N	Y	Y
4	Y	N	N	N	N	N	Y	N
5	Y	N	N	N	N	N	Y	N
6	N	N	N	N	N	N	Y	Y
7	Y	N	N	N	N	N	Y	N
8	N	N	N	N	N	Y	Y	Y
9	Y	Y	N	N	N	N	Y	N
10	Y	N	Y	N	N	N	Y	N
11	Y	N	N	N	N	N	N	Y
12	Y	N	N	N	N	N	Y	Y
13	N	N	N	N	N	N	Y	N
14	N	N	N	Y	N	N	Y	N
15	N	N	N	N	Y	N	N	N
16	Y	N	N	N	N	Y	Y	Y

2.3.2 Evaluation of SAR quality indicators as found in literature

As explained in the Methods section, a SAR quality indicator has to meet certain criteria in order to achieve maximum utility. Table 2.4 gives an overview whether the criteria are met (Y/N) for each indicator.

From table 2.4, for target related characterization of SAR distributions, two indicators appear to be most useful: SAR_{targ} *(9)* and SAR_{ratio} *(10)*. They cover the absolute and relative effectiveness of a heat treatment, respectively. Additionally, $x\%SAR_{max}$ *coverage(13)*, considering the coverage of the target with sufficient SAR, has been reported to be useful in the literature. Modifications of this indicator are needed however, to remove dependency on SAR_{max} (see Methods section).

In our opinion, the *Homogeneity Coefficient (14)* appears also a reasonable indicator for describing the distribution of target SAR, but is also dependent on SAR_{max}. In the next paragraph, improvements for both $x\%SAR_{max}$ *coverage (13)* and *HC (14)* are suggested.

For hotspot related characterization of SAR distributions, only a few indicators were found, and only one of them sufficiently meets the formulated heuristic criteria (see table 2.4). Here again we consider the SAR_{max} dependency a disadvantage. Only $SAR_{hs\text{-}targ\ ratio}$ *(16)* is an indicator that clearly relates SAR in hotspots to the target SAR. Furthermore, it is difficult to predict a hotspot (which is defined by a temperature-volume threshold) from a SAR indicator, because there is a complex dependency on the exposed volume, the perfusion, and the specific thermodynamics of the surroundings. However, if the SAR is low, it certainly will not cause a hotspot in well perfused normal tissue.

Finally, most of the indicators are possible objective functions for optimization. P_{ratio2} *(3)* and P_{ratio5} *(6)* satisfy both criteria formulated for optimization (see table IV). However, they only take into account the top 10 SAR-values as hotspots, which makes them potentially sensitive for model inaccuracies for the reasons as mentioned for SAR_{max} in the criteria section. Also, the STH_{ratio} *(8)* depends on SAR_{max}. A good candidate for a goal function is $SAR_{hs\text{-}targ\ ratio}$ *(16)*. This function relates the hotspots to the target without being dependent on SAR_{max}. An alternative to the goal functions mentioned above is SAR_{ratio} *(10)*, which scores quite well according to the formulated general criteria and meets one of the two optimization criteria (see table 2.4). Additional constraints should be applied to suppress hotspots.

We recommend defining all volume related indicators relative to the patient volume inside the applicator. Since the part of the patient that is included in the model often differs between patients and institutes, patient volume inside the applicator is an

unequivocal measure (at least for the BSD2000 Sigma 60 applicator), allowing comparisons between different patients, institutes and systems.

We conclude from our literature survey that, especially for target characterization, most criteria are sufficiently covered by the existing Indicators. Only sensitivity for model inaccuracies due to SAR_{max} dependence is considered less satisfactory.
For hotspot characterization however, not all criteria are matched and an additional set of indicators is proposed for this purpose.

2.3.3 Suggested new or modified indicators

Table 2.5 summarizes our suggestions for modifications and new formulations of indicators to complete the spectrum of quality indicators and SAR-optimization objective functions.

Table 2.5: Suggested modified and new quality indicators for characterization and SAR-optimization

Indicator	**Formula**	**Unit**
13-m	$SAR5_{tot}\ coverage = \frac{V_{targ}(SAR > SAR5_{tot})}{V_{targ}}$ with V_{targ} the target volume, and $SAR5_{tot}$ the SAR exceeded in 5% of the total volume.	[-]
14-m	$HC_{new} = \frac{SAR75_{targ}}{SAR25_{targ}}$ with SARn_{targ} the SAR exceeded in n% of the target volume.	[-]
16-m	$SAR_{hs-targ\,\text{ratio new}} = \frac{SAR(V1)}{SAR_{targ}}$ With SAR(V1) the average SAR in *V1*. *V1* is defined as 1st volume percentile.	[-]
17a	$\rho_{hs}\left(\vec{x}\right) = \frac{1}{4/3\pi \cdot 0.05^3} \cdot \int\limits_{\vec{x}\in\left\lvert\vec{y}-\vec{x}\right\rvert<0.05} dV_{hs}\left(\vec{y}\right)$ With V_{hs}=*V1*	[-]
17b	$I_{hs}(\vec{x}) = SAR_{hs}\left(\vec{x}\right) \cdot \rho_{hs}\left(\vec{x}\right)$ with SAR_{hs} the SAR values inside *V1*.	[W/kg]
17c	$I_{hs\ region} = \frac{\sum_{region} I_{hs}(n) \cdot V(n)}{V_{region}}$ with V(n) the volume of an element n inside a region.	[W/kg]
17	$I_{hs\ ratio\ region} = \frac{I_{hs\ region}}{SAR_{targ}}$	[-]
18	$SAR_{targ-compl\,\text{ratio}} = \frac{SAR_{targ} - SAR_{complaint\_region}}{SAR_{tot}}$	[-]

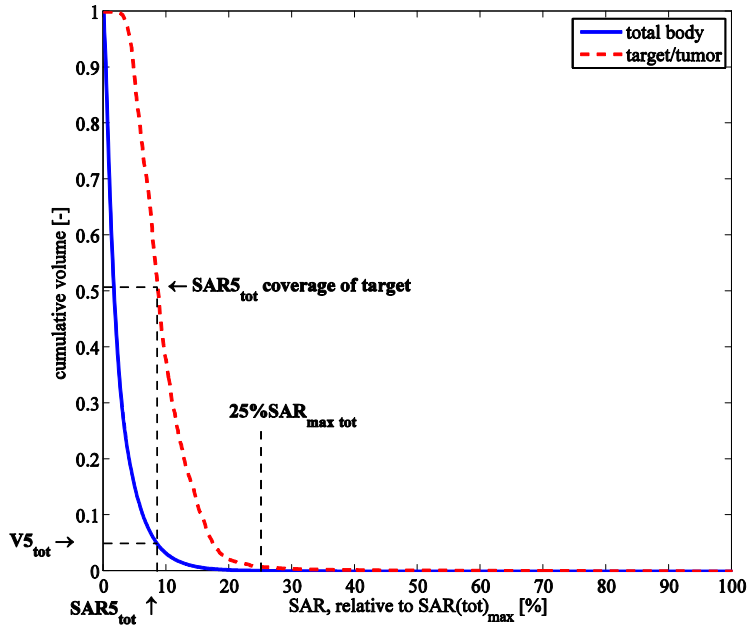

(a)

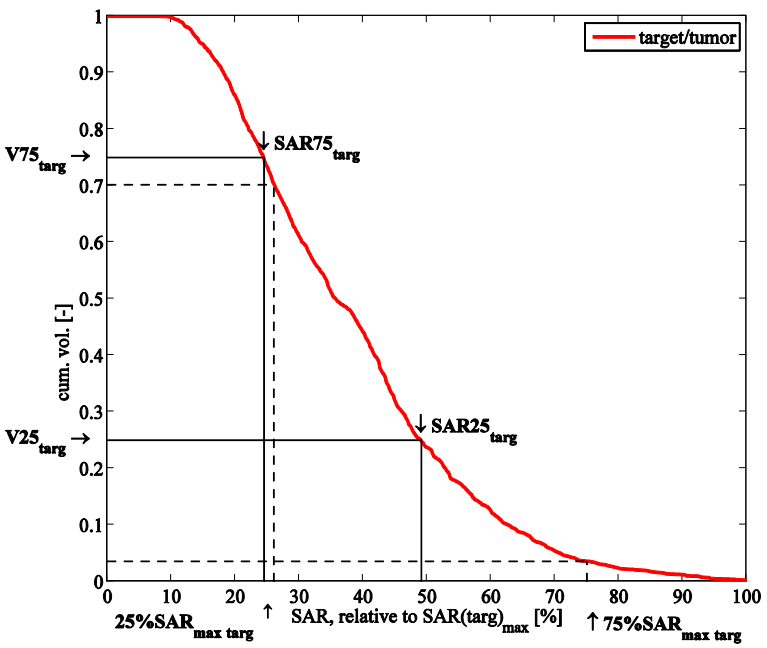

(b)

Figure 2.3: Illustration of SAR_5 definition: $SAR(tot)_5$ covers a substantial part of the target (a), and of $25\%SAR_{targ\ max}$ and $75\%SAR_{targ\ max}$ definition versus $SAR25_{targ}$ and $SAR75_{targ}$ definition (b). Both histograms are averages of 10 patient models.

In the paragraphs below, the rationale and function of the modifications and new indicators are explained:

13-m: $SAR5_{tot}$ coverage

First, *$x\%SAR_{max}$ coverage (13)* is dependent on SAR_{max}. Furthermore, this indicator was originally introduced in superficial hyperthermia, where the tumor is heated more directly: SAR_{max} is almost always located in the target area. In deep hyperthermia though, $25\%SAR_{max}$, i.e. 25% of the maximum SAR in the patient, covers almost no target volume at all, because of a small volume with very high SAR values. In figure 2.3a, this is illustrated in a cumulative SAR histogram, where the target and total body SAR are depicted, averaged over 10 patients. Therefore, we introduce the volume dependent $SAR5_{tot}$ *coverage* (the SAR which is exceeded in 5 % of the total volume). $SAR5_{tot}$ *coverage* is defined as the part of the target where the SAR exceeds $SAR5_{tot}$. This is illustrated in figure 2.3a, which shows that V5 covers approximately 50% of the target volume. This volume dependency, instead of SAR_{max} dependency, should provide a less sensitive indicator. From the average of 10 patient models in figure 3a, we deduced the measure of 5% of the total volume. The 5^{th} volume percentile appears to cover the target exactly as much as needed for a sensitive indicator, since the $SAR5_{tot}$ value is situated on the steep part of the target SAR histogram. Therefore, higher or lower volume percentages would reduce the value of this indicator. Therefore, we presume that $SAR5_{tot}$ is a good measure for target coverage of the part of the patient with the highest SAR and is sensitive for differences between patients. This indicator produces the same sort of information as the *$x\%SAR_{max}$ coverage (13)*, but is independent of SAR_{max} and more suitable for the deep hyperthermia practice.

14-m HC_{new}

The homogeneity coefficient *HC(14)* is also dependent on $SAR_{targ\ max}$. Therefore, a similar improvement based on the volume dependent $SAR75_{targ}$ and $SAR25_{targ}$ is introduced. In figure 3b, the rationale of this new approach is depicted in a cumulative volume-SAR histogram of the target. This histogram again is an average of the calculated target SAR in 10 patient models. Values of $SAR75_{targ}$ and $SAR25_{targ}$ appear to be less different from each other than $25\%SAR_{targ\ max}$ and $75\%SAR_{targ\ max}$, as can be seen in figure 2.3b. However, the modified indicator HC_{new} provides information about the steepness of the target dose-volume-histogram and thus about the homogeneity. Therefore, it provides the same information as the original HC but is less sensitive to $SAR_{targ\ max}$ changes.

16-m: $SAR_{hs\text{-}targ\ ratio\ new}$

Ratio of hotspot SAR and target SAR. Hotspot SAR is defined as the average SAR in *V1*. *V1* is the volume of normal tissue where SAR>$SAR1_{tot}$. This function is only slightly modified. Averages instead of medians are used because they provide a more direct relationship with the absorbed powers.

17a: ρ_{hs}

Besides the SAR value in the 1st percentile, we assume that the density of hotspots determines the local risk to induce any kind of discomfort. A single small hotspot may not become clinically relevant, because of the high cooling effect of the surroundings. On the contrary, extended hotspots, or multiple hotspots close together are more likely to cause complaints. In order to quantify this, we defined a new indicator, namely: *hotspot density,* ρ_{hs}. A density must be evaluated over a certain volume. Therefore, we choose an averaging volume of a sphere with a 5cm radius. Although the exact size of 5 cm is an arbitrary choice, the rationale is that the radius is on one side smaller than the patient volume. On the other hand, the volume must be considerably larger than the average tetrahedron/voxel volume to be able to obtain a density.
The hotspot density at a certain point in the patient evaluates the hotspot volume in a sphere of 5 cm radius around that point. *Hotspot density* is a helper function to evaluate the clinical significance of a hotspot.

17-b: I_{hs}

I_{hs}, the Hotspot intensity, the product of ρ_{hs} (*17-a*) and the absolute SAR level, is considered to provide the most predictive value to estimate the clinical relevance of a single hotspot.

17c: $I_{hs\ region}$

By averaging over a certain volume, the $I_{hs\ region}$, the local average hotspot intensity is introduced. This description is equivalent with SAR_{targ} *(9),* and is useful for absolute intra- and inter-patient comparison.

17: $I_{hs\ ratio\ region}$

$I_{hs\ ratio\ region}$ is the ratio between $I_{hs\ region}$ and whole body average SAR. This indicator is particularly useful in model studies, if relative SAR distributions have to be compared (and the absolute power level is not known).

18: $SAR_{targ\ compl\ ratio}$

As an objective function for SAR-optimization, we propose $SAR_{targ\ compl\ ratio}$. This essentially is the SAR_{ration} *(10)* that is constrained when patient complaints occur. This function is

relatively insensitive to peaks in SAR and minimizes hotspots by taking into account relative SAR in all regions where hotspots occur.

2.4 Quantitative evaluation of all quality indicators

Indicators to characterize the SAR distribution and their correlation to temperature increase.

In figure 2.4, the correlations between all SAR indicators and $T50_{targ}$ are displayed. Each indicator is individually evaluated in its own graph, which has the number that is also used in table 2.3, table 2.4, and table 2.5.
For all indicators, except the HC indicators, their correlation to the $T50_{targ}$, the median target temperature, has been calculated. In every temperature calculation, the input power was increased up to maximum patient tolerance (i.e. until the temperature in normal tissue reaches 44^{o}C).
The homogeneity coefficients, HC (14) and HC_{new} (14-m), are correlated to an equivalent temperature homogeneity expression of $T75_{targ}/T25_{targ}$, since these two indicators are not meant to provide information about median temperatures, but instead about temperature homogeneity.

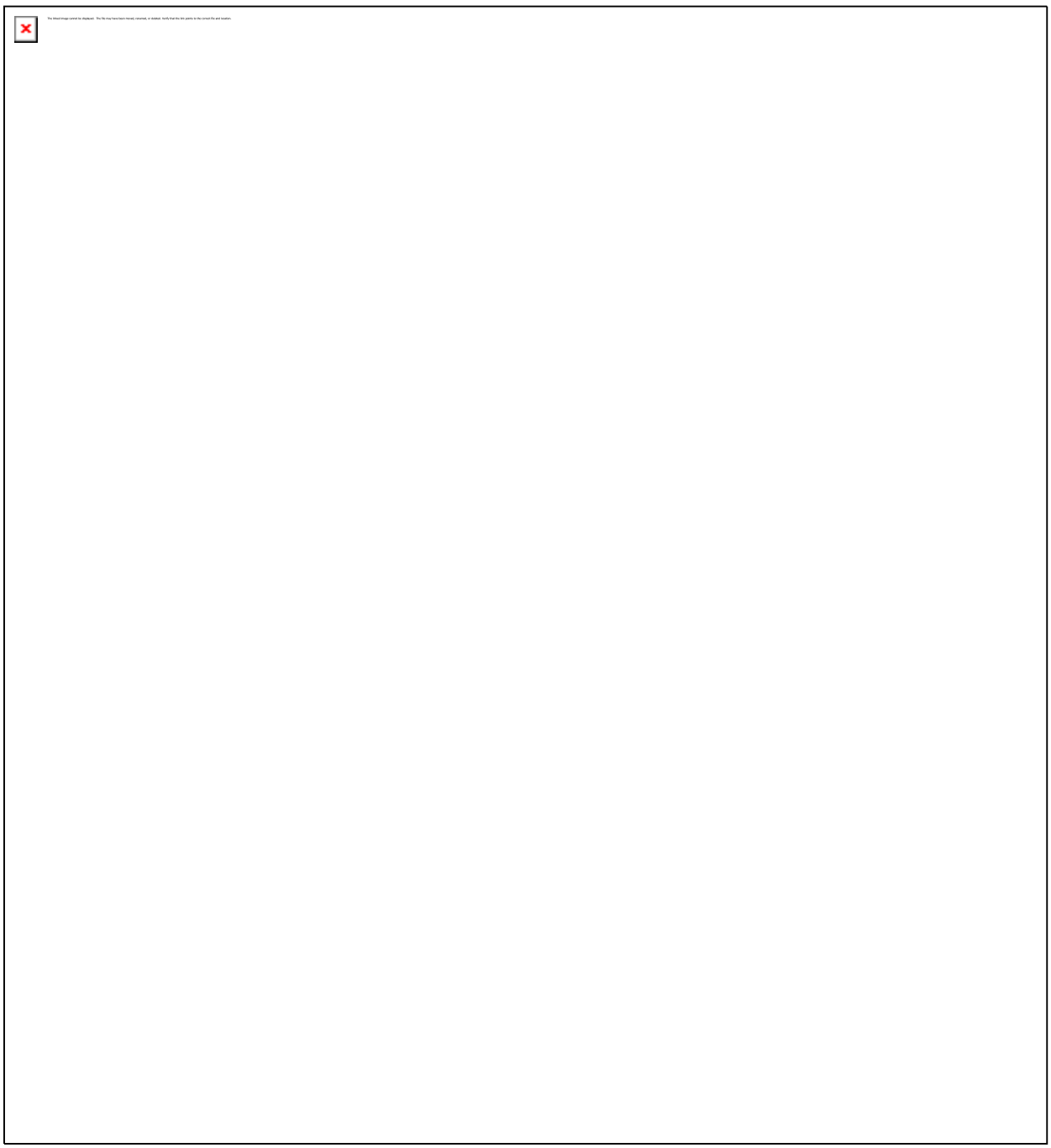

Figure 2.4: Correlation of all indicators with target temperatures. Each indicator is individually plotted in a separate subfigure. Above each subfigure, the indicator number is depicted. R^2 correlation coefficients in each subfigure indicate the amount of correlation between the respective indicator and the corresponding $T50_{targ}$ value.

Indicators 1 to 7 are all power-related. However, target and patient volumes are not taken into account. This causes the correlation coefficient to be very low.
The SAR-related indicators 8 to 10 therefore have a much better correlation coefficient that is > 0.5. Indicator 18, which is derived from indicator 10, has approximately the same R^2 value as indicator 10.
Indicators 11 and 12, the 10g average SARmax and SARmax ratio, again have almost no correlation with temperature. This can be understood by the fact that only the hotspot part is taken into account by these indicators, while the target SAR is left out.
Indicators 13 and 14 correlate poorly with temperature. However, their modified version 13-m and 14-m do. This confirms the benefit of our decision to remove SAR_{max} dependency from the indicators, and turn this into a volume related term.
Indicator 15 is again SAR_{max} dependent, and is correlating poorly with temperature.
Indicator 16 on the other hand, correlates very well, which slightly improves when modifying $SAR50_{tot}$ to average SAR (indicator 16-m).
The idea of multiplying SAR with a hotspot density does not appear to lead to a better correlation: indicator 17 does correlate, but worse than its SAR-only counterpart 16-m.
Helper functions 17a, 17b, and 17c are not evaluated, since they describe a whole distribution over multiple tetrahedra, and thus are hard to summarize in a single number.

Ability of indicators to achieve the optimal temperature distribution.

For a SAR-indicator to be suitable for optimization of the SAR distribution in an individual patient, it is not absolutely necessary to have a predictive value for temperature over a range of patients. An optimization indicator should only have a predictive value within a single patient, i.e. optimization using the indicator as a goal function should lead to an optimal $T50_{targ}$. Therefore, we used each indicator as a goal function for optimization in the same 36 patients. Just as in the previous correlation calculations, calculation of the temperature distribution is performed for each indicator with $T50_{targ}$ at the maximum patient tolerance (i.e. using the optimized phase and amplitude settings, power is increased until normal tissue temperature reaches 44^{o}C). Figure 2.5 shows the $T50_{targ}$ value, averaged over the 36 modeled patients, with standard errors added.
For optimization modeling, it can be derived from figure 2.5 that $SAR_{hs\text{-}targ\ ratio}$ *(16)* and its modified version (16-m) are the most suitable indicators for optimization, according to the calculated optimized $T50_{targ}$ values. They are the only indicators with a target T50 above 42^{o}C. Also the P_{ratio}'s (4 and 5) with a squared SAR in the denominator, P_{targ} (1), $P_{square\ ratio}$(7), STH_{ratio}(8), SAR_{targ}(9), and $SAR5_{tot}$coverag(13-m) lead to good optimization results, i.e. they are not significantly different ($p>0.05$) from indicator 16-m, as shown

with a 2 sample t-test. Indicators 11, 12, and 15, which are not related to the target, obviously lead to very poor results. The *25%SAR$_{max}$ coverage* (13) is, as stated in figure 3a, generally not covering any target at all, and therefore also does not lead to a good result. The homogeneity coefficients (14 and 14-m) are not very suitable as goal functions because they only relate SAR-values within the target. The modification of *SAR$_{max}$* related parameters appears to be beneficial also in optimization. The practical value of the objective function is currently assessed in a clinical study.

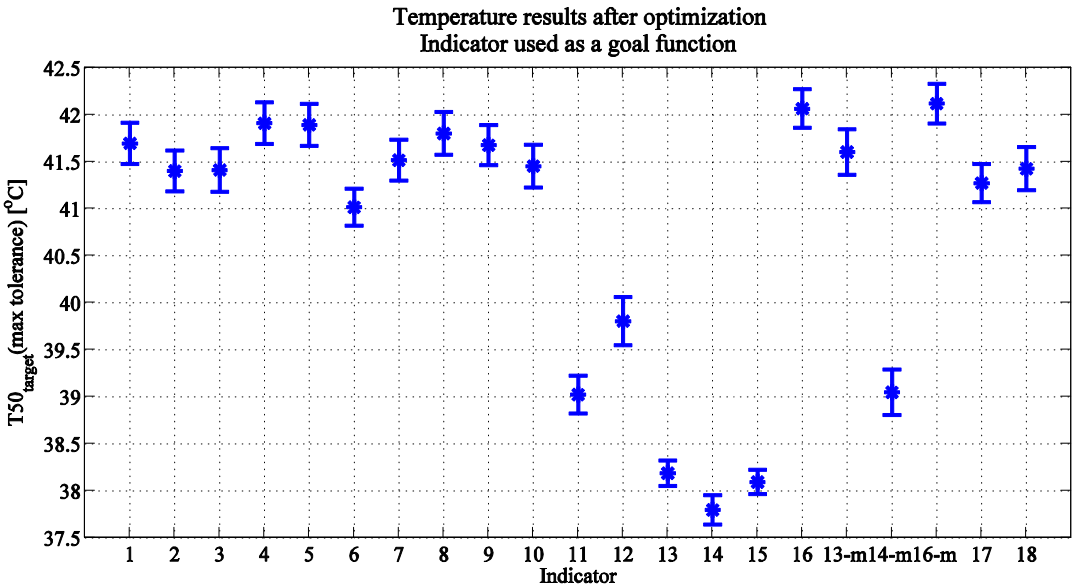

Figure 2.5: T50$_{targ}$ at the maximum patient tolerance, after optimization with each indicator. The average T50$_{targ}$ over 36 patients is shown, together with SE of means as error bars.

2.5 Discussion

2.5.1 The scope of this study

All modeling presented in this study was done with a Sigma Hyperplan model of the BSD2000 Sigma 60 [139, 143]. However, we believe that the result of this study can be extended more generally, and is applicable to all deep hyperthermia treatments applied by a phased array system. In every calculated SAR distribution for deep hyperthermia, the same effects will play a major role: power absorption (and heating) of the target and hotspot reduction. Therefore, regardless of the chosen applicator, we believe that

characterization and optimization in deep hyperthermia in the lower pelvic region will benefit from the proposed set of standard indicators to optimize and to compare SAR-distributions.
Additionally, the focus on cervical cancer patient models limits the variety of locations of the tumor over the 36 patient models. However, we expect that the results found in this study are also valid in patients with other tumor locations, although the correlation between temperature and SAR-indicator may differ.

2.5.2 SAR vs temperature modeling, pro's and contra's

With Sigma Hyperplan, both SAR and temperature distributions can be simulated. In many modeling studies, temperature is used as the main quality indicator. This approach has the advantage of a direct link between modeling outcome and temperature measurements during treatment. Predicting temperature accurately is, however, a difficult task. The easiest approach is the solution of the bio-heat equation [40]. This equation consists, among others, of a power related term and a blood perfusion related term. The blood perfusion related term is only approximately known in a specific patient [144]. Moreover, blood perfusion is a dynamic process that changes in time during the heat treatment, depending on both power and heating time. Obviously, an incorrect assumption of perfusion would lead to significant errors in the temperature predictions. The discrete vasculature model [43, 145] is another approach for calculating temperature. Although this model has a number of appealing features, its application in clinical practice is still focusing on relatively small volumes, due to the required detailed knowledge of the vessel anatomy. The same limitation with regard to accurate flow values exists. Furthermore, modeling packages provide only steady state solutions and neglect the dynamic behavior of blood flow.
Instead of temperature, the SAR distribution might be considered as a prognostic factor. The *25%SAR$_{max}$ coverage* (i.e. coverage of the tumor with at least 25% of maximum SAR) was found to be an important prognostic factor in earlier studies on superficial hyperthermia [93-94]. Meyerson et al. [93] demonstrated in 1990 for a group of 60 patients that coverage of the tumor by *25%SAR$_{max}$* was the most important factor predicting treatment outcome. Later, Lee et al. [94] confirmed these findings in a different group of 151 patients with 196 lesions of recurrent breast cancer of the chest wall. They both found the complete response rate and the local tumor control to be significantly higher if the tumor was covered by *25%SAR$_{max}$*.

The interaction of the radiated electromagnetic field with several tissues having different permittivities and conductivities results in a power deposition pattern.

The calculated SAR distribution in a model strongly depends on these constants, but has only minimal sensitivity for changes in blood flow. This is an advantage of SAR as a prognostic factor.

From the extensive HTP as performed in this study, it may appear that the target SAR values are quite low in comparison to, for example, the SAR values in muscle. However, this corresponds to what we see during a treatment. The average temperature found in 444 deep hyperthermia patients was approximately 40.5^{o}C [117]. The treatment limiting hotspots are expected to be approximately 44^{o}C when causing complaints. Hence, other regions are indeed often more heated than the target. This is an effect that is inherent to the use of interfering electromagnetic sources for heating the patient. Currently, work is in progress to improve targeting SAR to the tumor by using applicators with more antennas or higher frequencies.

At present, the most pressing problem concerns the translating of HTP from the monitor to the clinical application in the patient [122, 146]. For SAR this is due to a variety of causes, such as cross-coupling between antennae, inaccurate positioning of the patient, etc, for which currently clear efforts are undertaken to reduce their impact. For temperature prediction, also a more fundamental problem has to be solved such as integration of discrete vasculature in large models and the inclusion of the thermal dose dependent behavior of blood flow. In our opinion, especially the last argument demonstrates a need for good SAR optimization algorithms. Later on, the gathered experience can be used to quickly proceed with temperature optimization algorithms.

2.5.3 Validity of the electromagnetic models

In this study, all model calculations are performed in Sigma Hyperplan. A critical factor in the accuracy of electromagnetic modeling is the correct number of tetrahedra. At the start of this study, we increased the number of tetrahedra from 100,000 to as much as 900,000, and checked at which number a stable solution was reached. We found that 200,000 Tetrahedra is enough to reach a reliable solution of the finite element method model, which is in line with other studies [39, 100, 113]. Using more tetrahedra would require more computing time without providing a more accurate prediction. Especially when using HTP and optimization in the clinic, the computing time is limited. We consider

that on-line optimization during a patient treatment must be less than 2 minutes, putting clear restrictions on the number of tetrahedra.
More generally, there is sufficient literature available supporting the validity of current available electromagnetic models used in HTP. A number of studies have demonstrated excellent subjective and objective performance of electromagnetic models to predict the SAR distribution in homogeneous phantoms [62, 100, 107, 136, 147].
De Bruijne et al. [107] demonstrated a dose-difference of 2% and a distance to agreement of 2 mm between predicted and measured SAR distributions, which is equivalent to performance of modeling in radiotherapy.

2.5.4 Most suitable indicators

The results as shown in figure 2.4 and figure 2.5 both identify 16m as the most favorable quality indicator. With respect to the other indicators the objective evaluation for the generic and the patient specific do not identify the same indicator sequence, although the same metric for evaluation is used, namely $T50_{targ}$. This is mainly because of the approach per individual patient model in optimization, in contrast to the general, i.e. all patient, approach for characterization indicators.
For both characterization and optimization, $T50_{targ}$ is used as the main metric for evaluation. The use of $T50_{targ}$ as an evaluation indicator has the advantage that it is not sensitive to possible temperature outliers that may disturb the evaluation, contrary to average target temperature. Other temperature indicators or thermal dose parameters derived form the whole data-set and insensitive for outliers may also be used.
From figure 2.4, the indicators that are most useful for characterization, i.e. the indicators that correlate best with target temperature ($T50_{targ}$), can be derived.
The correlations lead to the following list of most suitable indicators, listed in terms of their function:
Characterization of SAR distributions: Target
For target characterization-modeling, $SAR_{hs\text{-}targ\ ratio}$ *(16-m)* and SAR_{targ} *(9)* are the most useful indicators for relative or absolute SAR in target characterization-modeling. SAR_{targ} *(9)* is most useful for absolute SAR value comparison, while $SAR_{hs\text{-}targ\ ratio}$ *(16-m)* provides a generator power independent understanding of target SAR in relation to hotspots. Additionally, the redefined *HC (14-m),* that provides valuable additional information about SAR-distribution within the target, should be added.
Characterization of SAR distributions: Hotspots
For hotspot characterization, the most useful indicator is $SAR_{hs\text{-}targ\ ratio}$ *(16-m).* This

indicator is very useful to compare the parts of the normal tissue with the highest SAR-levels to the target SAR. Indicator 17, based on hotspot density appears to have less value for predicting temperatures. The correlation with $T50_{\,targ\ max\ tolerance}$ of $I_{HS\ ratio}$ *(17)* is not an improvement in comparison to $SAR_{hs\text{-}targ\ ratio}$ *(16-m)*.
For optimization modeling, $SAR_{hs\text{-}targ\ ratio}$ *(16-m)* is the most suitable hotspot indicator. This indicator on one hand maximizes the target SAR, while on the other hand the SAR in the most absorbing parts of the patient is minimized. The optimization results of indicators 1, 4, 5, 7, 8, 9, 13-m, and 16 are not significantly different from indicator 16-m.

2.6 Conclusions

We formulated subjective heuristic criteria and assessed the predictive value as a basis for selecting a set of quality indicators, useful in hyperthermia treatment planning for characterization as well as optimization of the SAR distribution during deep hyperthermia applied with the BSD2000 Sigma 60 applicator. Preferably the selected indicators are independent of the input power, target volume, and patient anatomy, and allow intra- as well as inter-patient comparison of results. Importantly, the selected indicators also facilitate comparison between institutes or systems. Such comparisons are, in our opinion, highly relevant to improve quality of heating widely.
Useful indicators for target SAR analysis are SAR_{targ} *(9),* SAR_{ratio} *(10)*, $SAR_{hs\text{-}targ\ ratio}$ *(16-m),* and HC_{new} *(14-m).* For hotspot analysis $SAR_{hs\text{-}targ\ ratio}$ *(16-m)* is the most suitable indicator. For optimization, the best option for an objective functions is the $SAR_{hs\text{-}targ\ ratio}$ *(16-m)*. This objective function attempts to increase average SAR_{targ}, while the SAR in a selected hotspot region decreases. Indicators 1, 4, 5, 7, 8, 9, 13-m, and 16 can be considered also for optimization.
This survey is a first step towards a more standardized set of quality indicators in characterization and optimization of SAR distributions. Undoubtedly, future research will lead to better quality indicators and goal functions in this area.

3 Complaint adaptive PD-optimization as a tool for HTP-guided steering in deep hyperthermia treatment of pelvic tumors

This chapter was published as:

Canters RAM,Franckena M, Van der Zee J, Van Rhoon GC. Complaint adaptive PD-optimization as a tool for HTP-guided steering in deep hyperthermia treatment of pelvic tumors. Phys Med Biol, 2008. 53(23): 6799-820.

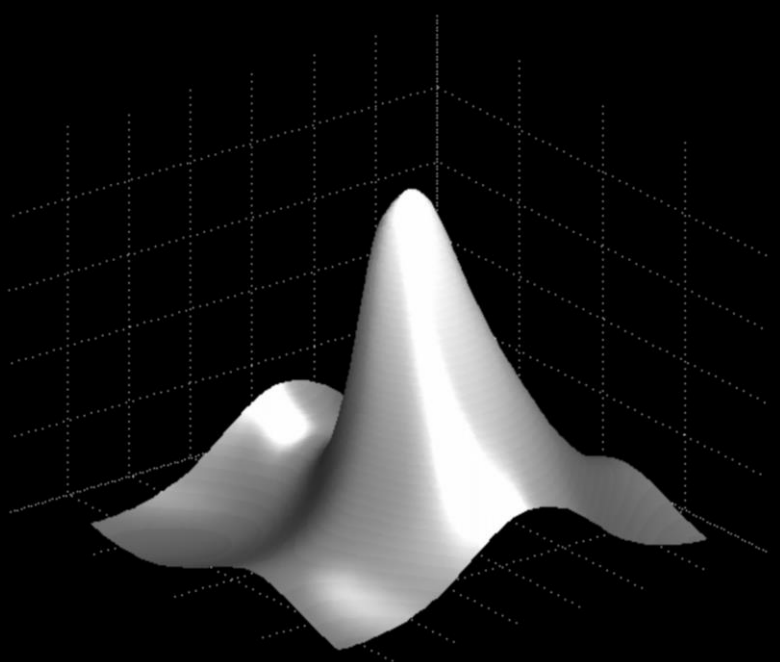

Abstract

Purpose: For an efficient clinical use of HTP (Hyperthermia treatment planning), optimization methods are needed. In this study, a complaint-adaptive PD (power density)-optimization as a tool for HTP guided steering in deep hyperthermia of pelvic tumors is developed and tested.
Methods: PD distribution in patients is predicted using FE-models. Two goal functions, Opt1 and Opt2, are applied to optimize PD distributions. Optimization consists of three steps: initial optimization, adaptive optimization after a first complaint, and increasing the weight of a region after recurring complaints. Opt1 initially considers only target PD whereas Opt2 also takes into account hot spots. After patient complaints though, both limit PD in a region. Opt1 and Opt2 are evaluated in a phantom test, using patient models and during hyperthermia treatment.
Results: The phantom test and a sensitivity study in 10 patient models, show that HTP-guided steering is most effective in peripheral complaint regions. Clinical evaluation in two groups of five patients shows that time between complaints is longer using Opt2 ($p=0.007$). However, this does not lead to significantly different temperatures [T50's of 40.3(Opt1) vs. 40.1^{o}C (Opt2) ($p=0.898$)].
Conclusion: HTP-guided steering is feasible in terms of PD-reduction in complaint regions and in time consumption. Opt2 is preferable in future use, because of better complaint reduction and control.

3.1 Nomenclature

Table 3.1: nomenclature of all used symbols

Unit	Explanation
V_i [m^3]	i-th percentile of the patient volume inside inpplicator, i.e. i-th percentage with the highest PD
V_i (n)	i-th percentile of the volume of region n, i.e. i-th percentage with the highest PD
PD [W/m^3]	Power density
PD_i [W/m^3]	PD exceeded in i% of the patient volume
$PD(V_i)$ [W/m^3]	Average PD inside V_i
PD_i –coverage [-]	Part of the target that is covered by at least PD_i
PD_{target} [W/m^3]	Average PD in target volume
PD_{tot} [W/m^3]	Average PD in patient volume
PD_{target_ratio} [-]	Ratio of PD_{target} and PD_{tot}
$PD_{target\_ratio\_0}$ [-]	Optimized PD_{target_ratio}
$PD_{ratio}(n)$ [-]	Ratio of PD in region n and PD_{tot}
$PD_{targ\_hs\_ratio}$ [-]	Ratio of $PD(V_1)$ and PD_{target}
$PD_{targ\_hs\_ratio\_0}$ [-]	Optimized $PD_{targ\_hs\_ratio}$
$PD_{targ\_hs\_ratio}(n)$ [-]	Ratio of $PD(V_1(n))$ and PD_{target}
Homogeneity Coefficient [-]	Measure for the homogeneity: ratio of PD_{75} and PD_{25}
Hotspot Volume [m^3]	Volume where $PD>PD_{target}$
Hotspot Volume ratio [-]	Ratio of Hotspot Volume and Patient Volume

3.2 Introduction

Hyperthermia, i.e. heating of the tumor, is used as an adjuvant modality to radiotherapy or chemotherapy in the treatment of various cancer types. Since 1990, hyperthermia treatments of pelvic tumors in the Erasmus MC (Rotterdam, The Netherlands) are carried out using a BSD 2000 system [34]. The vast majority of pelvic tumors are treated in the Sigma 60 applicator [140] that contains a single ring of 8 dipole antennas. Antennas are coupled in pairs into 4 independent channels. Phase and amplitude of each channel can be controlled.

Intuitively, a higher power input is expected to lead to higher temperatures inside the tumor. In a recent study, Fatehi et al [117] confirmed this expectancy. For individual patients a positive correlation of average target temperature and the total power delivered into the patient was found. At the same time this study reported that increasing the power input to the patient is often limited by painful hot spots. This emphasizes the need for a better understanding of the power distribution inside the patient and its dependency on amplitude and phase settings.

Commonly, phase and amplitude of the antennas are empirically adapted to modify the absorbed energy distribution in reaction to patient complaints. In Rotterdam, the strategy for patient complaints in deeper situated tissues, is to change phase settings to move the focus away from the complaint region. Amplitude is used to respond to superficial complaints. This steering strategy is further referred to as empirical steering [135]. A serious shortcoming of this empirical steering protocol however, is the inability to predict the effects of the steering actions.

Fortunately, the currently available HTP (hyperthermia treatment planning) systems provide excellent opportunities to improve the understanding of both power and temperature distribution. HTP may also be beneficial for steering during treatment, since it has the potential to predict the effects of the steering actions. Sigma Hyperplan [39, 100], a HTP system, is capable of calculating PD (power density) and temperature 3D distributions. Temperature distribution however, is very sensitive to the selected blood perfusion values, which vary between patients and over time, limiting the practical reliability of predicted temperature distributions. Although PD does not provide a direct picture of heating, it provides a time- and perfusion- independent indication of power absorption in the patient. Therefore this study focuses on PD optimization with amplitude and phase as variables.

Calculating optimized starting settings is becoming common practice in HT. However, a role of HTP controlled PD optimization to reduce PD in a complaint region is highly

desirable. This is likely to lead to a more controlled treatment quality. This second step is further referred to as HTP-guided steering. In this study, the tools necessary for HTP-guided steering, using the Sigma 60 applicator, are developed and the sensitivity of HTP-guided steering is tested pre-clinically in a phantom and in 10 patient models. Next, the feasibility of HTP-guided steering is evaluated clinically in a small group of 10 patients.

3.3 Methods

The methods section is subdivided in the subsections Sigma Hyperplan model and hyperthermia equipment (3.3.1), Optimization method (3.3.2), Phantom test setup (3.3.3), treatment protocol for clinical testing (3.3.4) and Model sensitivity study, clinical treatment and statistical methods (3.3.6).

3.3.1 The Sigma Hyperplan model and the hyperthermia equipment

From CT-scan to patient model

In this study, for each patient included a CT-based anatomic model is made in Sigma Hyperplan. The CT is segmented into the tissues named in table 3.2, where also dielectric properties of the tissues are presented [48-49] at 77 MHz. This is the standard treatment frequency used in Rotterdam. Given the relatively large confidence interval with which the dielectric parameters are currently known, the temperature dependency of ε_r and σ is neglected.

Table 3.2: Used tissues and their electrical properties at 77 MHz [48-49]

Tissue	ε_r	σ [S/m]
Fat	13	0.07
Muscle	69	0.70
Bone	16	0.06
Rod	1	0
Target	69	0.70
Bladder	24	0.29
Heart	99	0.70
Intestine	108	1.62
Kidney	109	0.77
Liver	75	0.46
Lung	35	0.71
Myelum	6	0.04
Spleen	101	0.77
Stomach	82	0.89
Uterus	69	0.70
Vagina	69	0.70

After segmentation a tetrahedral grid of patient and Sigma 60 applicator is created. Models on average consist of 220,000 tetrahedra, with edge length between 0.3 and 2.5 cm. The E-field is calculated as described in Gellermann et al [100]. The coordinate system used in the models is the following: X is the lateral (left-right) direction, Y the ventral-dorsal direction and Z the caudal-cranial direction.

Definition of regions for HTP-guided steering

To respond to patient complaints during HTP-guided steering, different regions need to be defined a priori. The size of these regions reflects the precision of complaint localization by the patient and the technical ability to adapt the PD distribution. Each region can be constrained in HTP-guided steering to reduce PD in that region after complaints occur.

Existing tissue types are used as a basis for the definition of these regions. Steering of the Sigma 60 is effective in the XY-plane in the pelvic region. Most pelvic tissue types are either restricted to a limited volume or have intrinsic low energy absorption, like for

example bone. Only fat and muscle tissues occur throughout the whole XY-plane. Therefore in the pelvic region fat and muscle tissue are each divided into five separate regions: left, right, top middle and bottom. In figure 3.1 an axial slice of a patient model is shown with all defined regions

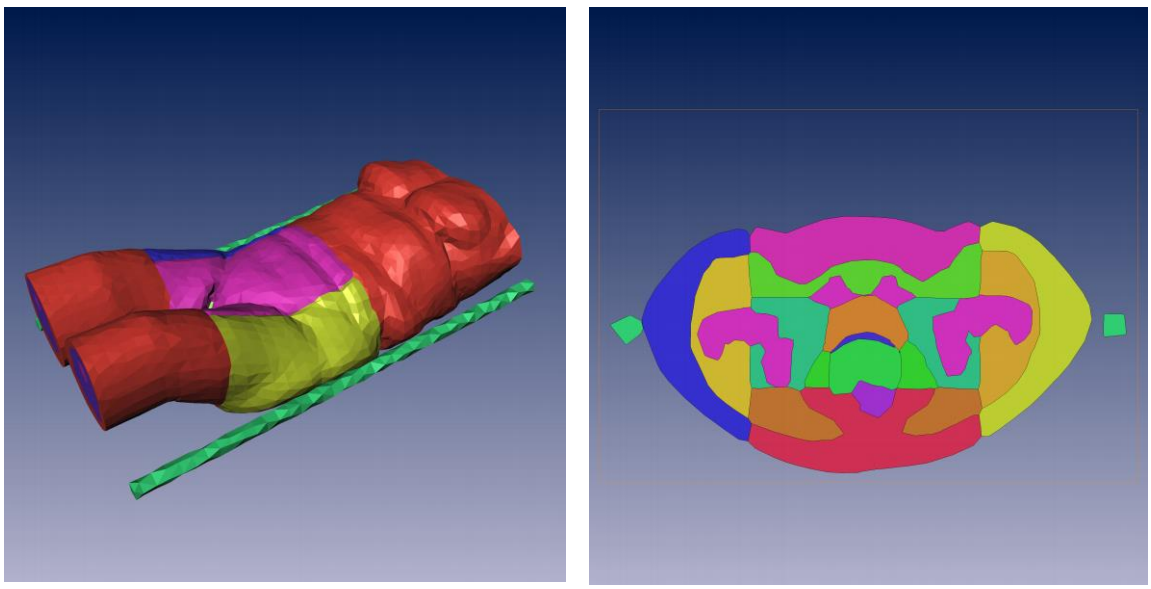

Figure 3.1: Regions defined in model. The slice (right) shows muscle and fat are divided into 5 regions: top, mid, bottom, left and right.

The hyperthermia equipment

All patients presented in this study were treated for cervical cancer in the BSD Sigma 60 [140] . This applicator has a diameter of 60 cm and a length of 50 cm. Furthermore, it consists of a ring of 8 dipole antennas that are coupled in 4 channels of two antennas each, which is schematically depicted in figure 3.2. Amplitudes and phases of each of these channels can be controlled independently. The optimization methods in this study use amplitudes and phases as optimization variables, i.e. amplitudes and phases of each channel is adapted to create an optimal PD-distribution.

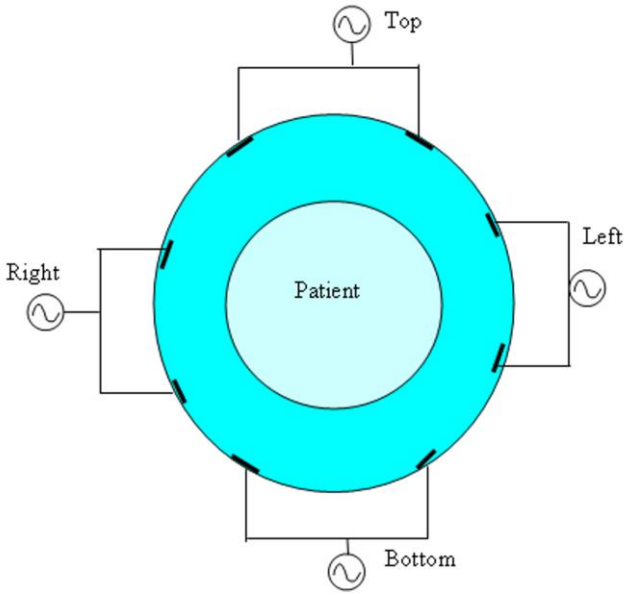

Figure 3.2: Axial view from the caudal direction of the Sigma 60 applicator, with the four channels, each connected to two antennas

3.3.2 Optimization method

HTP-guided steering has to meet the following demands to be advantageous above empirical steering. First, PD in the tumor area has to be maximized. Second, HTP-guided steering requires the possibility to impose constraints upon a priori defined complaint regions. A patient's complaint triggers a steering action. Constraining the optimization after complaints is expected to lead to a better balance in maximization of tumor PD and minimization of PD in the complaint region. Third a weight factor proportional to the severity of the complaint is given to the imposed constraints. With this weight factor the balance in optimization is shifted between tumor and complaint region, dependent on the intensity of the complaint.
Two possible goal functions for HTP guided steering are proposed in this study. The first goal function maximizes target PD and reduces PD in hot spots only after complaints and is commonly known from literature [82, 85]. The second goal function maximizes PD, while minimizing hot spots a priori, and is derived from a previous study [45]. On complaints, hot spots in the complaint region are further reduced. The two goal functions are further referred to as Opt1 and Opt2. In both strategies an optimization in three steps

is used: an initial optimization to obtain starting settings for a treatment, addition of a complaint-region related term to the goal function if a patient complaint occurs, and an increase of the weight of the complaint-related term if another complaint occurs.
Both goal functions are optimized in Matlab using the 'fmincon' function to find a global minimum of the goal function varying amplitude and phase. Amplitude has an upper bound of 1 logically, and a lower bound of 0.5, because of BSD amplifier stability reasons [148-149]. Phase has no upper or lower bounds.

3.3.2.1 Goal functions in optimization

Opt1: maximizing target PD

The first step in Opt1 is an initial optimization. In this first step, the goal function has the following form:

$$\max\left(\overline{PD}_{\text{targ\_ratio}}\right) = \max\left(\frac{\overline{PD}_{\text{target}}}{\overline{PD}_{\text{tot}}}\right) = \overline{PD}_{\text{targ\_ratio\_0}} \qquad \textbf{3.1}$$

In Seebass *et al* for example, similar objective functions were used [80]. $\overline{PD}_{targ\_ratio\_0}$ considers only target behavior and no hot spots. $\overline{PD}_{\text{targ\_ratio\_0}}$ is the result of this optimization.
The second step is initiated after a complaint occurs during a treatment. A second term is added to equation 3.1 to minimize PD in a complaint region. This results in equation 3.2.

$$\max\left[\left(\frac{\overline{PD}_{\text{targ\_ratio}}}{\overline{PD}_{\text{targ\_ratio\_0}}}\right) - \sum_{n\in regions} 0.25\cdot w(n)\cdot\frac{\overline{PD}_{\text{ratio}}(n)}{\overline{PD}_{\text{ratio\_0}}(n)}\right] \qquad \textbf{3.2}$$

Hot spots are now taken into account by using the full goal function equation 3.2, with w(n) set to one for the complaint region n. The first term in equation 3.2 is equal to the goal function of step 1, normalized on the outcome of the initial optimization equation 3.1. The second, complaint induced term of equation 3.2 consists of $\overline{PD}_{ratio}(n)$, the PD-ratio in region n, defined as:

$$\overline{PD}_{\text{ratio}}(n) = \frac{\overline{PD}(n)}{\overline{PD}_{\text{tot}}} \qquad \textbf{3.3}$$

and is also normalized on the outcome of step 1.

The third step in optimization is induced by a recurrent complaint in a region. In that case the weight of the complaint induced term of equation 3.2 is increased by adding one to w(n) (the weight factor) for complaint region n. The maximum value for the sum of w(n) is chosen to be four. From our experience with empirical steering we expect four steering steps to be sufficient during treatment. A larger number would either reduce the influence per step too much or over-increase the influence of the hot spot part of equation 3.2. To ensure that the maximum value of this hot spot part of equation 3.2 is always smaller than the target part, the weight factor has to be multiplied by 0.25. (an equivalent approach would be to range the weight factors from 0 to 1 in steps of 0.25)

Opt2: maximizing the ratio of target PD and hot spot PD

Opt2 is, like Opt1, divided in three steps. The first step, the initial optimization, is a minimization, chosen equivalently to a goal function [81] and has the following form:

$$\min\left(\overline{PD}_{\text{targ\_hs\_ratio}}\right) = \min\left(\frac{\overline{PD}(V_1)}{\overline{PD}_{\text{target}}}\right) = \overline{PD}_{\text{targ\_hs\_ratio\_0}} \qquad \textbf{3.4}$$

with $\overline{PD}(V_1)$ the average PD within V_1. V_1 is the 1st volume percentile of the patient that is enclosed by the applicator (see figure 3.3). $\overline{PD}_{\text{targ\_hs\_ratio\_0}}$ is the result of the optimization.

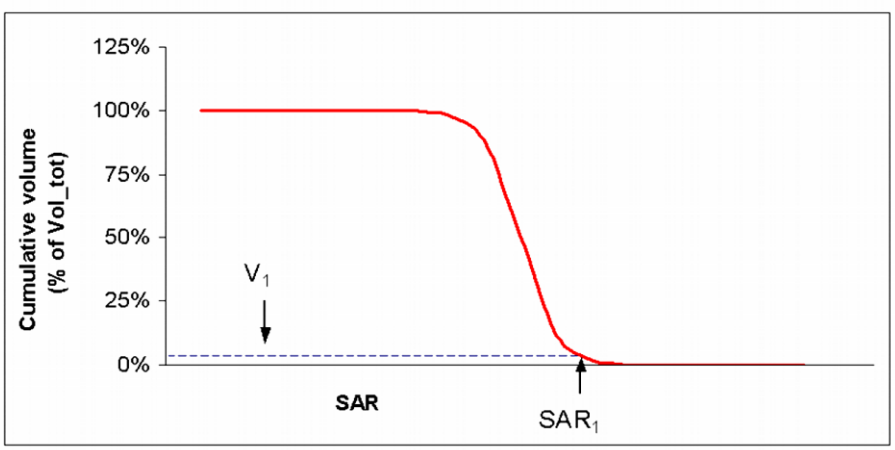

Figure 3.3: Definition of V_1. A cumulative SAR histogram is depicted to illustrate the V_1 definition. V_1 is defined as the 1st percentile. PD_1 is defined as the PD exceeded in 1% of the volume, thus the PD enclosing V_1.

The second step is initiated after a complaint occurs during a treatment, adding an additional hot spot term to the goal function, changing it to equation 3.5, with w(n) set to one for region n.

$$\min\left[\left(\frac{\overline{PD}_{\text{targ\_hs\_ratio}}}{\overline{PD}_{\text{targ\_hs\_ratio\_0}}}\right)+\sum_{n\in regions}0.25\cdot w(n)\cdot\frac{\overline{PD}_{\text{targ\_hs\_ratio}}(n)}{\overline{PD}_{\text{targ\_hs\_ratio\_0}}(n)}\right] \qquad \textbf{3.5}$$

Equivalently to Opt1, the second part of the goal function equation 3.5 is a hot spot related term, normalized on it's initial value $\overline{PD}_{targ\_hs\_ratio\_0}(n)$. $\overline{PD}(V_1(n))$ is the average PD within $V_1(n)$. $V_1(n)$ is the 1st percentile of region n where PD exceeds $PD(n)_1$.
The third step, increasing the weight of the second term in equation 3.5 after recurrent complaints, is equivalent to Opt1.

$$\overline{PD}_{\text{targ\_hs\_ratio}}(n)=\frac{\overline{PD}(V_1(n))}{\overline{PD}_{\text{target}}}, \qquad \textbf{3.6}$$

3.3.3 Phantom test setup

Before the optimization routine can be used as HTP-guided steering tool during clinical treatments, it is tested in a phantom setup for its effectiveness in steering. We used a 2g/l NaCl saline water phantom as described by Van Rhoon *et al* [140]. Subsequently a model of the phantom is made, in which a number of possible complaint regions are defined (figure 3.4).

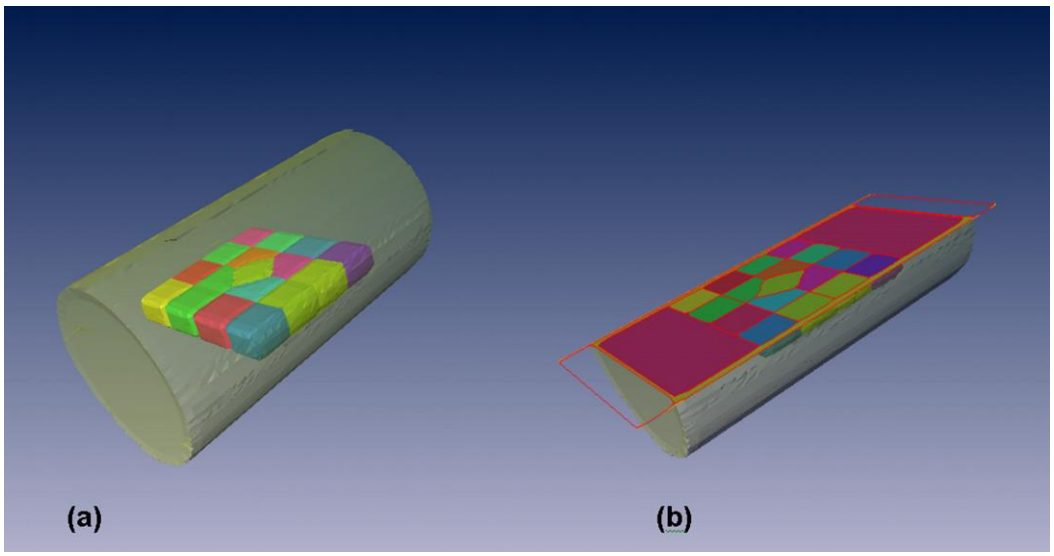

Figure 3.4: Regions defined in the phantom (a) and the XZ-plane, in which measurements take place (b)

We measured the reduction of PD in the constraint region when a weight factor is applied using E-field sheets with Schottky diodes [140, 150], placed in the XZ-plane. Diode positions are depicted in figure 3.5.

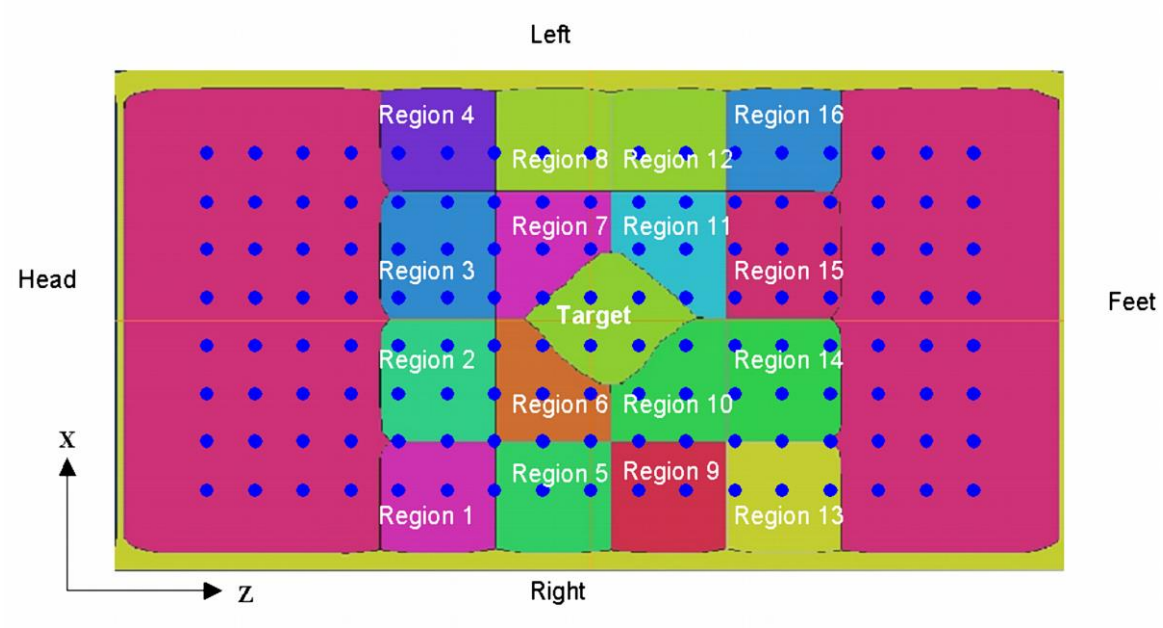

Figure 3.5: Regions defined and diode positions in the XZ-plane

The square of the diode voltage output is proportional with PD. The average PD in a region can be calculated as follows:

$$\overline{PD}(region)_{\text{measurement}} = \frac{\sum_{n \in region} |E(n)|^2}{nr\_of\_diods(region)} \quad \textbf{3.7}$$

in which E(n) is the E-field at diode n. The E-field sheets measure only in the XZ-plane (see figure 3.5). However, since the regions are only small in Y-direction we assume that equation 3.7 is a valid approximation for average PD in a region. PD is normalized on PD_{tot}, which is derived from $P_{forward}$-$P_{reflected}$. This is further referred to as:

$$PD_{ratio}(region)_{measurement} = \frac{\overline{PD}(region)_{\text{measurement}}}{\overline{PD}_{\text{tot\_measurement}}} = \frac{\overline{PD}(region)_{\text{measurement}}}{(P_{\text{forward}} - P_{\text{reflected}})/V_{\text{tot}}} \quad \textbf{3.8}$$

To compare measurements with the model, PD-values are extracted from the model exactly at the diode spots. $\overline{PD}_{\text{model}}(region)$ can then be calculated similar to $\overline{PD}_{\text{measurement}}(region)$. $\overline{PD}_{\text{tot\_model}}$ is defined as total absorbed power calculated by the model divided by total volume. Thus $PD_{ratio}(region)_{model}$ is defined as:

$$\frac{\overline{PD}(region)_{\text{model}}}{\overline{PD}_{\text{tot\_model}}} \quad \textbf{3.9}$$

For comparison of model and measurement, the PD-ratio is normalized to the maximum PD-ratio measured with zero phase and amplitude 1 on all channels. This is necessary because $PD_{measurement}$ is based on a measured E-field, which can only qualitatively be interpreted.

3.3.4 The phantom test

First, Opt1 and Opt2 are optimized for both a centrally positioned target as well as a target positioned more peripheral (in region 5 of figure 3.5) to check their performance in optimization. Next, the effects of HTP guided steering actions are evaluated in case of complaints in a specific region (experiment nr 1-4, table 3.3), recurring complaints in a specific region (experiment nr 5-8, table 3.3) and in case of complaints in multiple regions on the same or opposite side of the phantom (experiment nr 9-11, table 3.3).

Table 3.3: Experiments in the phantom test, varying complaint regions and value of the weight factors

Experiment number	Experiment
1	Complaint in region 1, weight factor = 1
2	Complaint in region 5 weight factor = 1
3	Complaint in region 2, weight factor = 1
4	Complaint in region 6, weight factor = 1
5	Complaint in region 1, weight factor = 4
6	Complaint in region 5, weight factor = 4
7	Complaint in region 2, weight factor = 4
8	Complaint in region 6, weight factor = 4
9	Complaint in region 1 and 5, weight factor = 1 in both regions
10	Complaint in region 1 and 8, weight factor = 1 in both regions
11	Complaint in region 1 and 16, weight factor = 1 in both regions

In the tests with a single complaint region, (i.e. experiment 1 to 8), attention is focused on region 1, 2, 5 and 6, all situated in one quadrant of the phantom. This is representative for the other regions due to symmetry of the phantom. Measuring reductions for weight factors 1 and 4 tests also the effect of increasing the weight factors. To simulate the occurrence of multiple complaints, 3 additional distributed complaint regions are chosen, located both at the same side of the phantom as region 1(region 5) and opposite to region 1 (regions 8 and 16).

3.3.5 Treatment protocol for HTP-guided steering

In figure 3.6, the treatment protocols for both empirical steering and HTP-guided steering are highlighted. In all treatments, both with empirical steering and HTP-guided steering, the patient is the indicator of his/her tolerance for heating. We instruct the patients before treatment to indicate if any discomfort is occurring. Of course the tolerance for heat is different per patient, but this is inherent in the hyperthermia treatment. Since thermometry is only done in the different lumina of the patient, the largest part of the pelvic area is not covered by thermometry. Therefore the patient as an indicator of temperature is absolutely necessary. If however, a patient does not complain in case of discomfort, this becomes quickly visible by increased heart rate or observed unrest of the patient. In both cases, the operator communicates with the patient to find out what is

causing the discomfort, and adapts settings according to the information received from the patient. An indication of discomfort is further referred to as 'complaint' in this study. In the empirical steering protocol [135], a treatment is started with (0,0) target settings (i.e. balanced amplitudes and phases). If no complaint occurs, power is increased with 100 W per 5 minutes. If however a complaint occurs, the focus of the EM field is shifted away from the complaint region, by adjusting the phases.

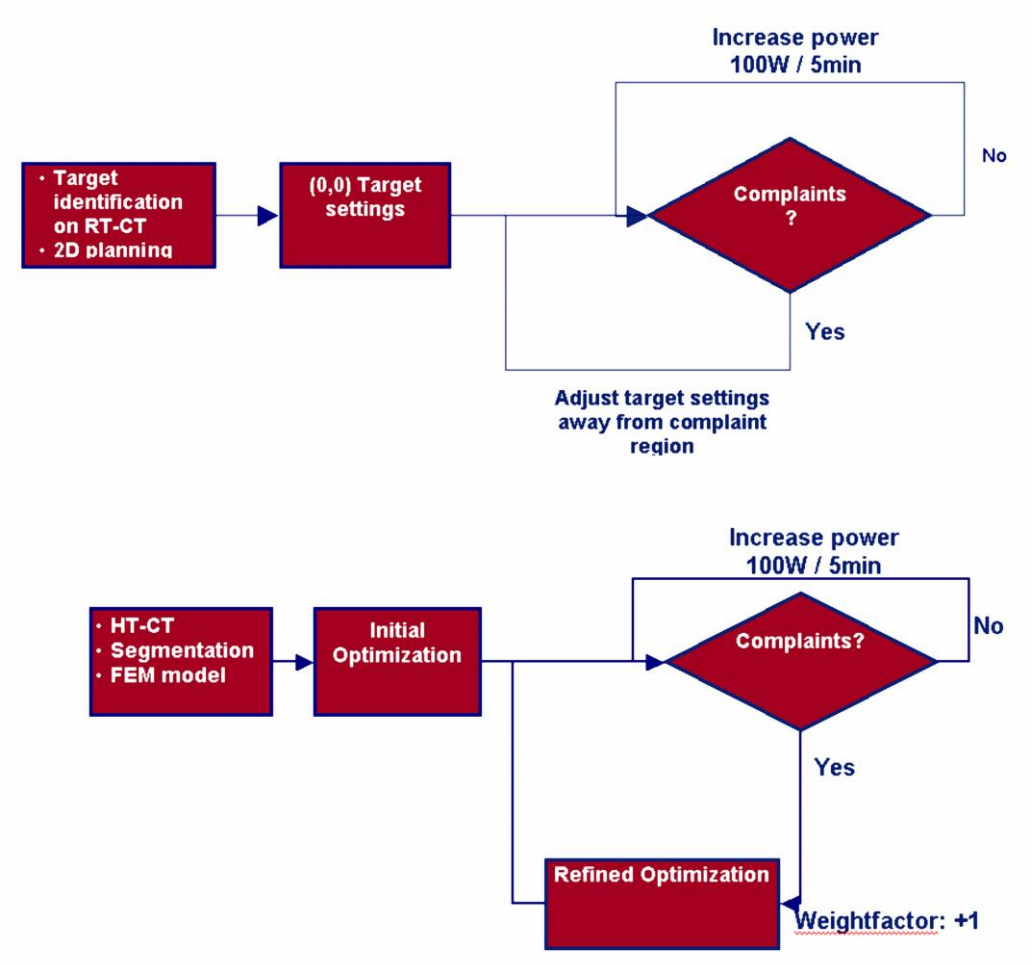

Figure 3.6: Flowchart for empirical (top) and HTP (Hyperthermia Treatment Planning) guided (bottom) steering

A new treatment protocol for HTP-guided steering is developed to provide optimized treatment settings for the start of treatment and in case of hot-spot-related complaints. Treatment is started with optimized settings for phase and amplitude, obtained from the

first step in the optimization routine. As before, input power is increased by 100 watts after every 5 minutes interval without complaints, indicative of hot spots.
After a complaint, a constraint is put on the matching region with weight factor 1, and the second optimization step is calculated. If the response time is long, power is temporarily lowered by 50 watts for the duration of the calculation. When the new settings are available, power is increased again by 50 watts and calculated settings are put into effect. To reduce response time, amplitude and phase settings are precalculated for a number of common complaints. Again, after 5 minutes without complaints, power is raised by 100 watts. Besides complaints, also temperatures from intraluminal measurements in healthy tissue exceeding 43^{o}C, are a reason for putting a constraint on the matching region.
The moment a new complaint occurs, a weight factor of 1 is added for the new complaint region as long as the sum of all weight factors is less than 4.
After a complaint occurs while the sum of weight factors is already 4, but the sum of weight factors in the complaint region is below 4, one weight factor is added to the complaint region. At the same time for the region most distant from the complaint region a weight factor is subtracted.
If a complaint occurs in a region where the sum of weight factors is already 4, we assume that amplitude and phase steering are not sufficient. In that case, a frequency change is applied, similarly to our empirical protocol, after which the PD is re-optimized using the previous weight factors. Given the total treatment time of 90 minutes, we have chosen to apply a maximum of 2 frequency changes.
If none of the above steering actions reduce complaints (or temperatures in healthy tissue exceeding 43^{o}C) to an acceptable level, we assume that the maximum possible heating is reached. All amplitude and phase settings are kept at the same level, after which power is reduced in steps of 50 watts until complaints (or temperatures in healthy tissue exceeding 43^{o}C) disappear.

3.3.6 Sensitivity study, clinical treatment and statistical methods

A sensitivity study was performed for 10 patients. Equivalently to the phantom test initial optimization and reduction in possible complaint regions is evaluated. Besides PD_{target} various other quality indicators are evaluated:
PD_5 coverage of the target (the part of the target exceeding PD_5)
homogeneity coefficient (ratio of PD_{25}(targ) and PD_{75}(targ))
$PD(V_1)/PD_{targ}$ (see section 3.3.2)
hot spot volume ratio (part of the patient above 2 times PD_{targ}).

For the same patients, HTP-guided steering using Opt1 and Opt2, is tested during actual treatment, each in a group of five patients. Opt 1 and Opt2 are compared on complaint frequency and obtained temperatures. In table 3.4, patient characteristics are summarized.
Results obtained from the treatments, are compared statistically between Opt1 and Opt2, using a χ^2 test in case of percentages, and a two sample t-test in case of number of complaints and time between complaints.
Patient characteristics of the 10 patients are depicted in table 3.4.

Table 3.4: Patient characteristics

patient characteristics		
	mean Opt1 (range)	mean Opt2 (range)
age (y)	59 (45-82)	65 (55-84)
WHO	0	0
length (cm)	162 (158-171)	168 (161-176)
weight (kg)	60 (51-73)	68 (50 -80)
diameter AP (cm)	20 (19-22)	23 (18-26)
diameter lat-lat (cm)	37 (36-40)	40 (34-44)
tumor size (cm3)	116 (57-184)	96 (46-184)

Figo stage	# Opt1	# Opt2
Ib	1	1
IIb	2	2
IIIb	2	0
IVa	0	1
IVb	0	1

3.4 Results

3.4.1 Phantom measurements

Initial optimization (step1)

Both Opt1 and Opt2 lead to approximately similar PD distributions in a cylindrical phantom with central (0,0) target settings and optimization. Figure 3.7a shows the shape of measured PD-ratio for Opt1 and Opt2 in X-direction at Z=0 (center of phantom is at the

center of the Sigma 60 applicator). However for both optimization routines the maximum seems to be shifted slightly to the left, probably due to positioning uncertainties. To get more insight in the performance of the two optimization routines, the target region is shifted from the center to the peripheral region 5, after which new treatment settings are calculated using both optimization routines. The measured PD_{target}-ratio of both optimization routines for an off-center target is presented in figure 3.7a. In figure 3.7b and figure 3.7c results predicted by Sigma Hyperplan for the off-center target situation using respectively Opt2 and Opt1 are presented to illustrate the measurements in figure 3.7a and to provide a 3D overview.
In the off-center target situation there is a clear difference between Opt1 and Opt2. The width of the focus in z-direction is longer for Opt1, while the width in X-direction is smaller.

Reduction in complaint regions (step 2 and 3)

The results of the tests (mentioned in table 3.3) for Opt1 and Opt2 are presented in figure 3.8. For both optimization routines, the PD-ratio in regions more peripheral with respect to the target is easier reduced (regions 1 and 5) than in regions adjacent to the target (regions 2 and 6) (see experiment 1-4). For Opt2 this effect is stronger and with weight factor one almost no reduction takes place in the regions (regions 2 and 6) adjacent to the target. For all steering actions, reduction in PD-ratio of the complaint region is larger than the reduction in the target, which means that all experimentally tested steering actions are effective in terms of complaint reduction and PD-maximization.

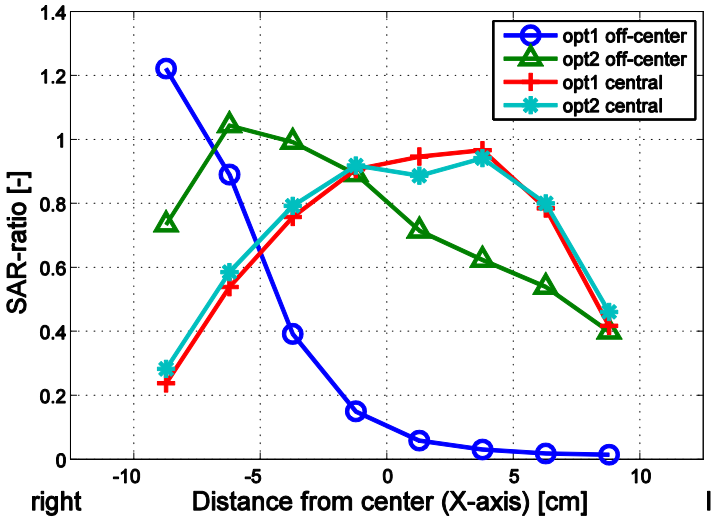

(a)

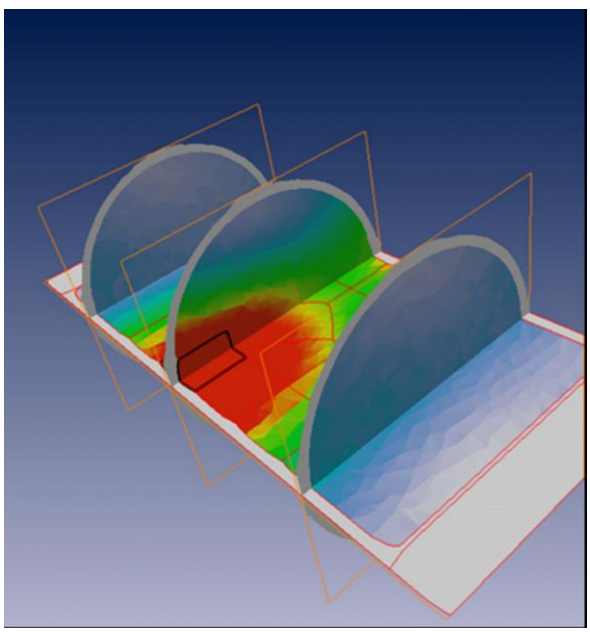

(b)

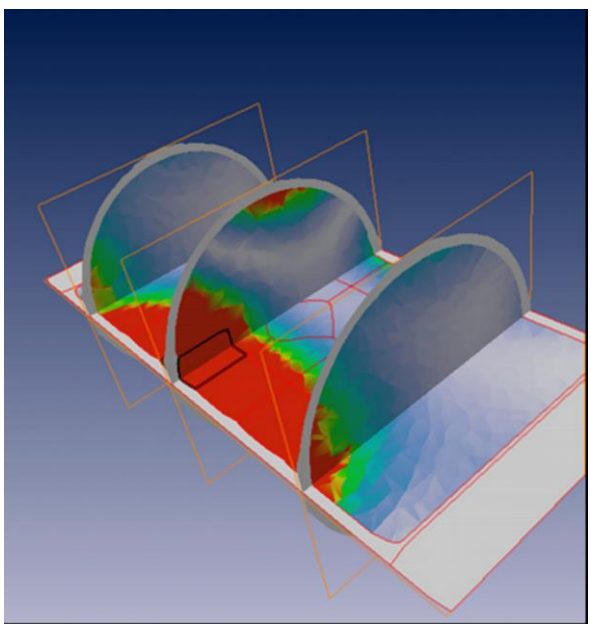

(c)

Figure 3.7: a) Measured normalized PD-profile along the x-axis at z=0 for both optimization methods in a central target and an off-center target, b) PD-distribution in off center target using Opt2 and c) off center target using Opt1 .

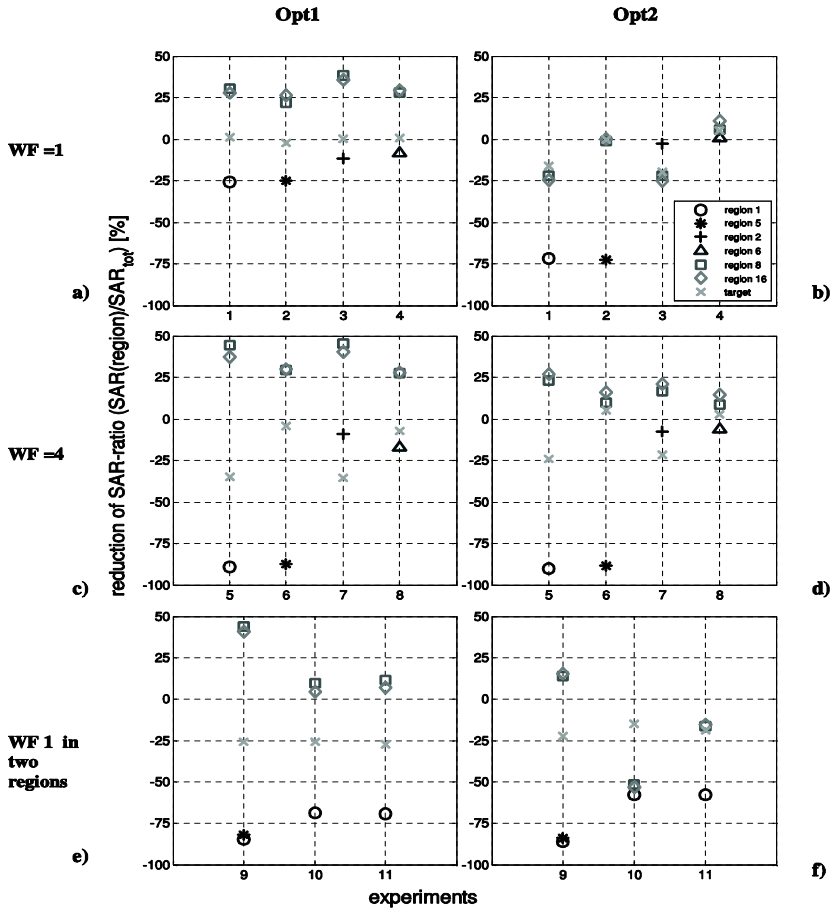

Figure 3.8: Results of the phantom test: Measured reduction on using weight factors with Opt1 (left) and Opt2 (right). Experiment numbers refer to the following experiments:

Experiment number	Experiment
1	Complaint in region 1, weight factor = 1
2	Complaint in region 5 weight factor = 1
3	Complaint in region 2, weight factor = 1
4	Complaint in region 6, weight factor = 1
5	Complaint in region 1, weight factor = 4
6	Complaint in region 5, weight factor = 4
7	Complaint in region 2, weight factor = 4
8	Complaint in region 6, weight factor = 4
9	Complaint in region 1 and 5, weight factor = 1 in both regions
10	Complaint in region 1 and 8, weight factor = 1 in both regions
11	Complaint in region 1 and 16, weight factor = 1 in both regions

4	8	12	16
3	7	11	15
2	6	10	14
1	5	9	13

T

Increasing the weight factor to 4 (experiment 5-8) increases the reduction of PD-ratio in peripheral regions for both Opt1 and Opt2. The regions adjacent to the target appear to be less influenced by increasing the weight factor. Adding weight factors to two complaint regions (experiment 9-11) reduces the PD-ratio in both complaint regions using Opt2. Opt1 reduces the PD-ratio's in both regions when on the same side of the phantom (regions 1 and 5). However, when opposite to region 1 (regions 8 and 16), a reduction is more difficult to achieve. Still though, in the regions opposite to region 1 (region 8 and 16), PD-ratio is lower than in experiment 1 (only a weight factor on region 1).

Accuracy of amplitude and phase settings and Monte Carlo analysis

The clinical value of HTP guided steering is highly dependent on the accuracy of the equipment, i.e. the accuracy of the BSD amplitude and phase settings. Using a vector voltmeter , during the phantom test we measured an average deviation of amplitude of -0.01 with a standard deviation of 0.02. The average deviation of phase measured was -5^{o} with a standard deviation of 5^{o} (phases of channel 1 are set to 0 as reference). The 95% confidence interval of the amplitude and phase deviation then is approximately [-0.05, 0.03] and [-15^{o}, 5^{o}].
To test how this deviation influences tumor PD in a calculated optimum, a Monte Carlo analysis is conducted on both Opt1 and Opt2. 100,000 Random phase-amplitude combinations are generated, distributed uniformly around the optimum amplitude-phase combination within the found confidence intervals. For each amplitude-phase-combination, PD_{target}-ratio is calculated.
For Opt1 the calculated distribution of PD_{target}-ratio is within 2.5% of the optimum, while for Opt2 a distribution of PD_{target}-ratio within 2.9% of the optimum was found.

3.4.2 Results in patient models for Opt1 and Opt2

For the 10 patients treated using HTP-guided steering, the effectiveness of steering actions in different regions is theoretically evaluated using Sigma Hyperplan, and optimized settings were calculated using both Opt1 and Opt2. The results of modeling for both optimization routines are presented in figure 3.9, where PD-levels of Opt1, Opt2 and a central focus are compared, relative to PD_{tot} (figure 3.9a) and PD_{target} (figure 3.9b). In figure 3.9c, various other quality indicators are depicted.

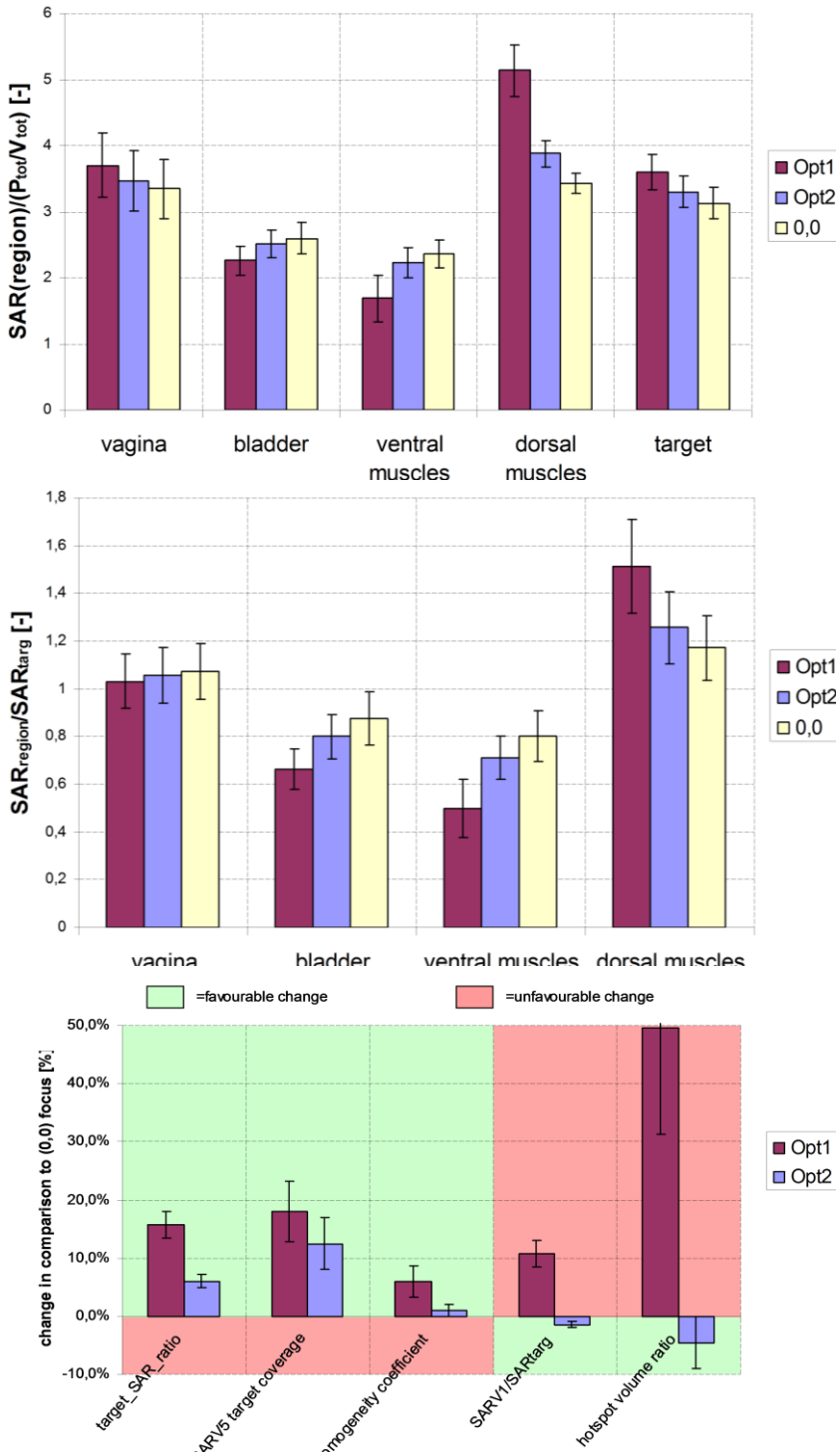

Figure 3.9: (a) PD in regions normalized PDtot, (b) PD normalized on PDtarget and (c) increase of various quality indicators with respect to central target settings.

Figure 3.9a and figure 3.9b show that PD levels are more equally distributed in Opt2 than when using Opt1, both absolute as well as relative to target PD. A central focus however, seems to lead to even more equally distributed PD-levels. Taking into account figure 3.9c, though, makes clear, that Opt2 is nevertheless advantageous over the central settings. PD_{target} is higher, $PD(V_1)/PD_{target}$ equation 3.4 is lower, a substantially larger part of the target is covered by the PD_5 contour, hot spot volume is smaller and homogeneity of the target is slightly higher. Opt1 has also some advantages over central focus, for example an increase of 16% in target PD compared to (0,0) settings. A serious drawback for this optimization routine, though, is the 50% higher hot spot volume. However, since hot spots in initial optimization of Opt1 are not taken into account, this is not surprising.

Table 3.5: measured difference in amplitude(A) and phase(φ) between Opt1 and Opt2

	A(left)	A(bottom)	A(right)	A(Top)	φ (left)	φ (bottom)	φ (right)	φ (top)
difference								
Opt1- Opt2	0.01	0.14	-0.12	-0.32	8	27	11	3
SD	0.06	0.06	0.04	0.08	7	5	7	4

Using a vector voltmeter [151], we measure on average higher amplitudes in the top antennas and higher phase in the bottom antennas in Opt1 (see table 3.5). This confirms the PD distribution from the model in figure 3.9, where PD is shifted more to dorsal in Opt1

Patient-specific models showed that reduction of PD-ratio in a complaint region is effective, which means that reduction in the region is larger than reduction in the target (see figure 3.10). Similar to the phantom measurements , PD in dorsal- and ventral abdominal muscles (peripheral) was relatively well reduced using weight factors, while the vagina region (adjacent to target) was less reduced. Opt1 generally reduced PD better than Opt2. However, reductions in Opt1 as well as Opt2 were in the same range when PD is normalized to PD_{target}. Moreover, Opt1 reduced PD_{target} with approximately 20%, while Opt2 hardly reduced PD_{target}. This is consistent with the findings in the phantom test. Finally, an increase of weight factors always led to an increased reduction in the complaint region.

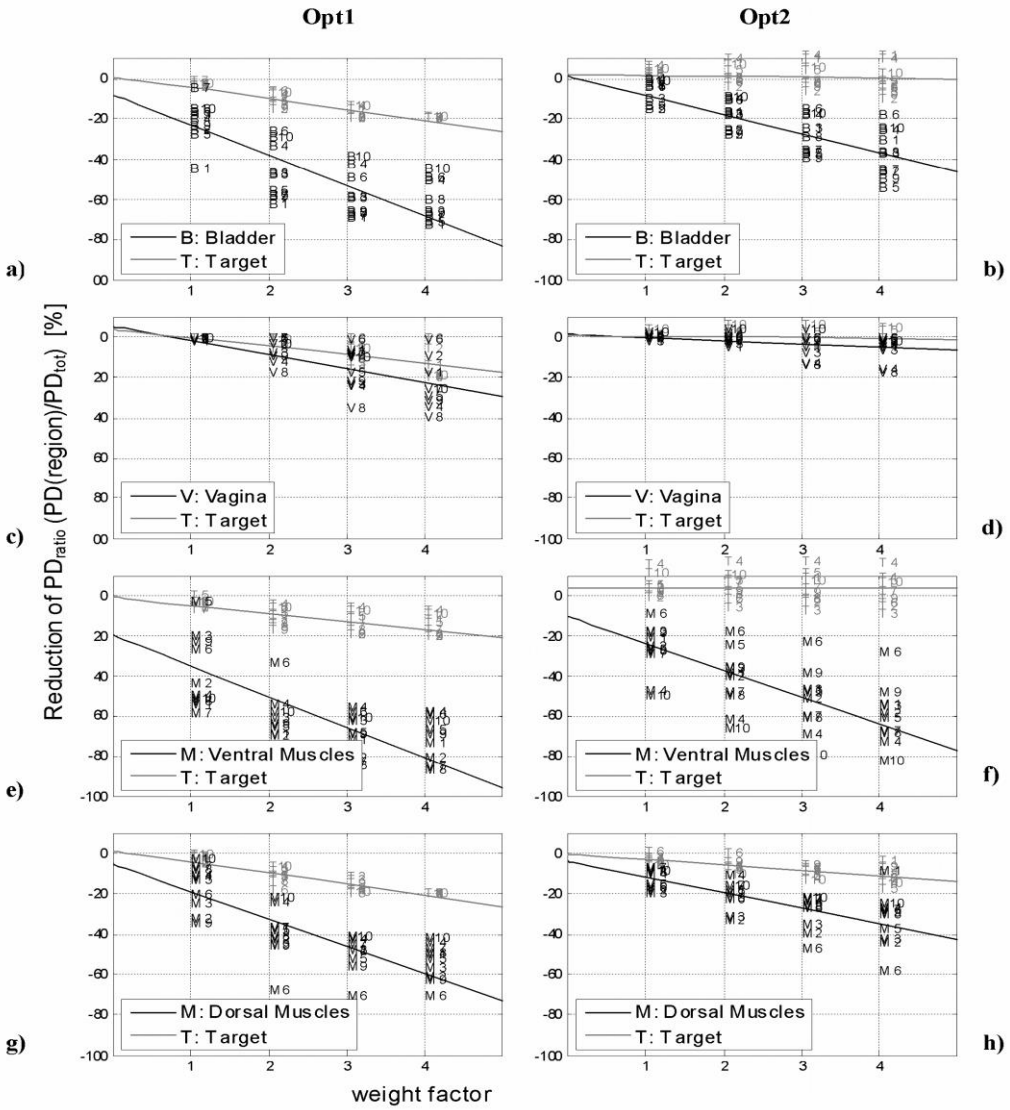

Figure 3.10: Results from the patient model sensitivity study. Reduction on complaints in Bladder(a and b), Vagina(c and d), ventral muscles(e and f) and dorsal muscles (g and h) for Opt1 and Opt2

3.4.3 Treatment outcome and feasibility

Since the results of the phantom experiments were satisfactory, we also tested both Opt1 and Opt2 in clinical practice. Five patients were treated using Opt1 and another five using Opt2.

Using a number of precalculated settings for the most common complaints, a real-time response to complaints is possible. For rarely occurring complaints, settings are calculated

during treatment, which takes approximately one minute. Treatment characteristics are represented in table 3.6.

Table 3.6: Treatment characteristics of the two groups of 5 patients treated using either Opt1 or Opt2.

Evaluation criteria	**Opt1 (±s.e.)**	**Opt2 (±s.e.)**	**p**
Time between complaints [min]	4.8±0.4	6.3±0.4	0.007
# of complaints during treatment	14±1	11±1	0.128
Complaint disappears for ≥ 10 min [%]	12±3	20±4	0.109
Complaint disappears for ≥ 5 min [%]	53±5	67±5	0.041
Location of complaints			
Dorsal muscles [%]	45±5	57±5	0.089
Ventral muscles [%]	36±5	37±5	0.799
Dorsal and ventral muscles [%]	5±2	3±2	0.579

For both Opt1 and Opt2, complaints mostly occur in the dorsal muscles, followed by the ventral muscles. All the rest of the regions are responsible for less than 15% of the complaints. Generally complaints disappear for a significantly longer time (p=0.007) using Opt2. Temperatures turn out to be generally well within the range (see table 3.7), we normally obtain in DHT of patients with cervical carcinoma [117]. However, no significant differences between Opt1 and Opt2 are measured.

Table 3.7: Temperature outcome for the two groups of 5 patients treated with respectively Opt1 and Opt2

Temperature averaged over all lumina	**Opt1 (±s.e.)**	Opt2 (±s.e.)	**P(Opt1-Opt2)**
T90	39.3±0.2	39.5±0.2	0.167
T50	40.3±0.2	40.1±0.2	0.898
T20	40.9±0.2	40.6±0.2	0.609

An analysis of the powers during the steady state of the treatments (see table 3.8) shows that average powers, maximal powers, the time of $P_{max,}$ and the power difference between begin and end of steady state, do not differ significantly between Opt1 and

Opt2. Also the number and the total time of off-switches is not significantly different between Opt1 and Opt2. The variation in power level during the steady state however, is significantly larger for Opt1.

Table 3.8: Power during the steady state of the treatment for both Opt1 and Opt2

	Opt1(±s.e.)	**Opt2(±s.e.)**	**P(Opt1-Opt2)**
Unit	**mean**	**mean**	
P-mean [W]	801±38	797±49	0.94
Variation in power during steady state (SD) [W]	58±7	31±4	0.004
P-max [W]	885±32	854±51	0.61
Time P-max [min]	63±5	61±6	0.88
P_{begin}-P_{end} [W] steady state	-93±32	-47±25	0.26
'# off-switches'	18±2	16±1	0.35
'Total time off'	11±1	9±1	0.45

3.5 Discussion

In this study HTP-guided steering has shown to be applicable in clinical treatment optimization. This study is a first step in introducing HTP-guided steering during treatment. The results obtained in this study are quite specific, in terms of using one single applicator and a single frequency. However, in our opinion, the feasibility of this way of optimization can be extrapolated to all phased array applicators, used for loco-regional heating in the pelvic region. Regardless of the fact that other applicators may have different numbers of antennas and other frequency ranges, the optimization procedure presented in this study should lead to an optimized distribution of powers. For applicators that use incoherent EM-waves (e.g. the superficial lucite cone applicators for superficial heating [107], other optimization variables might be needed with more emphasis on for example the power level of the different antennas.
Although the validation of the Sigma Hyperplan model is mostly qualitative so far, it has been shown to be reliable. The research, reported in several studies [39, 62] showed good correlations between the Sigma Hyperplan model and measurements. The number

of tetrahedra used in this study is in the same order as comparable studies [113]. When refining the model, we found that this number of tetrahedra was sufficient to converge to a correct solution. Furthermore, using more tetrahadra would lead to clinically unacceptable long calculation times.
The initial optimization routines were derived from the functions used in several studies by other institutes [79, 81-82, 85, 152]. An advantage of this approach is the possibility of solving the optimization analytically, as an eigenvalue problem [78, 153]. This leads to short calculation times. However, this approach causes problem when using upper and lower bounds of amplitude. The initial optimization function (equation 3.4) for Opt2 has similarities to the functions reported by other studies [79, 81-82]. For practical reasons V_1 is chosen as a measure for hot spots, since the in Wust *et al* [81] defined hot spot definition makes the goal function highly non linear. The complaint-induced part of the goal function is introduced equivalently to Opt1.
Hot spots contain a varying number of tetrahedra at different amplitudes and phases. This makes it impossible to solve the goal function of Opt2 analytically. Therefore a SQP (sequential quadratic programming) [154] optimization method was used, that is far more time consuming than analytical solving. However, when using the Sigma 60, optimization is still fast enough for use in clinical situations. Future research should investigate other optimization methods like genetic algorithms for possibilities in speed improvement. Also a deeper look into multi-objective optimization may offer benefits, using Pareto optimal sets to visualize the effect of using weight factors in advance.
For both optimization routines weight factors are used to change the goal function on complaints, instead of using fixed constraints. Fixed constraint steps of 10% in a region per weight factor was tested and appeared to over-constrain the optimization easily, especially when facing complaints in more regions. We assume that optimization of the PD-distribution and a subsequent increase of power as long as patient comfort is not endangered, provides maximum treatment results. A change of phases after adaptation of the optimization, could lead to a small change in applicator efficiency, i.e. the total absorbed power in the patient changes. However, based on patient complaints, the power is increased or decreased to constantly remain at the maximum that the patient can tolerate. Therefore, this change of applicator efficiency during treatment should not influence the treatment quality. Including frequency in the optimization would be beneficial. However, with the current version of Sigma Hyperplan, this requires an E-field calculation for each frequency, which is at present too time consuming in clinical practice.
In the phantom test setup, Schottky diode sheets were used to measure the E-fields. These sheets provide only a limited spatial resolution and measure E-field only in the z-

direction. Considering the wavelength (approximately 45 cm at 77 MHz) however, the 2.5 cm interval of the diodes is sufficient to display the behavior of the E-field.
The results of the phantom test clearly show that steering actions are effective in both optimization routines. Both routines reduce PD in complaint regions effectively if necessary. However, regions more peripheral to the target show a larger reduction of PD than regions adjacent to the target. In peripheral regions, Opt2 caused more PD-reduction in complaint regions than Opt1, while target PD was reduced less. In regions close to the target, Opt1 caused more PD-reduction in a complaint region than Opt2, but in most cases target PD was also reduced more in Opt1. For other regions than the complaint region or the target, Opt2 is generally more beneficial, since it prevents an increase of these regions that is larger than Opt1. This makes the net effectiveness of steering actions better for Opt2.
The phantom test also showed that deviations of amplitude and phase from the set value are similar to deviations found in Kongsli et al [149]. A Monte Carlo analysis showed that the influence of these deviations is only small.
The sensitivity study of 10 patients showed that Opt1 clearly has a disadvantage in terms of hot spot volume (see figure 3.9c). The high value of PD in the dorsal muscles and the substantially larger hot spot volume while using Opt1, raised the question whether to use this optimization in clinic. However, in figure 3.9b the difference in PD in dorsal muscles between Opt1 and Opt2 is not significant, and we expect hot spot volume to be efficiently reduced after possible complaints. In terms of reduction after complaints, the findings in the sensitivity study confirm those of the phantom test, i.e. PD reduction is better in peripheral regions than in regions adjacent to the target for both Opt1 and Opt2. For Opt1 in most regions PD reduction is larger than for Opt2. The most likely cause of this difference is the fact that Opt1 shifts the focus regardless of hot spots elsewhere in the patient, thus being able of larger reductions in the complaint region. However, normalized to PD_{target} both Opt1 and Opt2 perform more or less equally. Often, it may be hard to achieve the power increase needed to compensate for reductions in PD_{target}, since steering may induce new complaints. Opt2 has less possibilities of reduction, since new hot spots would immediately increase the goal function. This leads to more moderate reductions that are beneficial to PD_{target}. From these patient-specific models therefore Opt2 seems preferable above Opt1.
The results of the clinical treatments confirmed the result of the sensitivity study. Using Opt1, the majority of complaints appeared to occur in the dorsal muscles, closely followed by the ventral muscles, and was not easily solved with steering. Using Opt2, complaint locations again were situated mostly in the dorsal muscles, followed by the

ventral muscles. Average time between complaints was significantly higher in Opt2 [6.3 vs. 4.8 minutes, p=0.007]. Both Opt1 and Opt2 led to tumor temperatures within the therapeutic range with T50's of 40.3^{o}C and 40.1^{o}C, and both were equally feasible in terms of calculation times. An analysis of the powers used during steady state shows that only the variation in powers during steady state is larger in Opt1. The difference between Opt1 and Opt2 in the clinical settings is considered rather small, compared to the results we obtained in the phantom test. Only the complaint interval was found to be significantly different. On one side this can be caused by the small number of five patients in each group and a difference in the patient characteristics [117]. On the other hand, during treatment there were other variables that are yet to be controlled better, like for example patient positioning. This transition from HTP to clinic has to be controlled better, which current research is aimed at. However, considering the lower hot spot PD in the sensitivity model study and the longer complaint interval in the treatments, Opt2 is the best choice for HTP-guided steering.
In a currently running study, patients with primary cervical carcinoma are treated in the Sigma 60 applicator, using HTP-guided steering with Opt2 to test effectiveness of HTP-guided steering.

3.6 Conclusion

HTP-guided steering has proved to be feasible in terms of calculation times and effectiveness of PD-reduction in complaint regions. Moreover, tumor temperatures achieved in treatments using HTP guided steering are well within the therapeutic range. The performance of the optimization routines tested in clinical practice, indicate that Opt2 is more effective than Opt1. The effectiveness of HTP-guided steering in terms of ability to improve tumor temperatures must be demonstrated in a specifically designed clinical study.

4 Patient positioning in deep hyperthermia: influences of inaccuracies, signal correction possibilities and optimization potential

This chapter was published as:

Canters RAM, Franckena M, Paulides MM, Van Rhoon GC. Patient positioning in deep hyperthermia: influences of inaccuracies, signal correction possibilities and optimization potential. Phys Med Biol, 2009. 54(12): 3923-36.

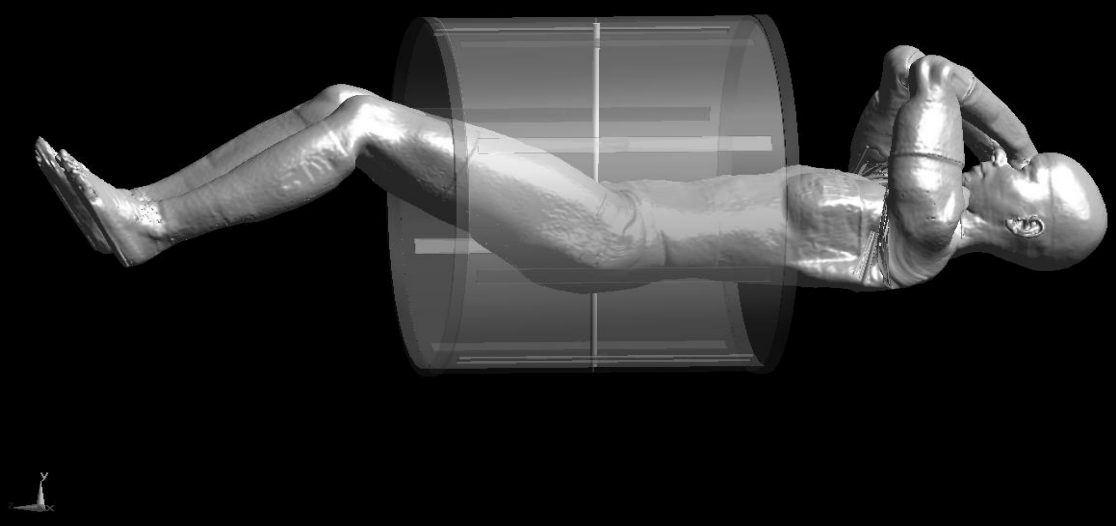

Abstract

Purpose: In this deep hyperthermia study, the robustness of SAR (specific absorption rate) patterns to patient-position variations is assessed, as well as the possibilities to correct for an improper positioning and the benefits of non-standard positions.
Methods: With a finite element model the SAR distributions were predicted for ten patients on 33 positions. Position sensitivity is assessed for both SAR-focus steering, i.e.settings based on a calculated focus in a cylindrical patient representation, and HTP(hyperthermia treatment planning)-guided steering, i.e. model based optimization of the SAR distribution.
Results: Position inaccuracies of less than 1 cm do not significantly affect SAR patterns. For SAR-focus steering, the SAR-maximum is not always at the desired focus location, especially in Y (anterior/posterior) and Z (axial) directions. For a maximum shift of 5 cm in all directions, both SAR-focus steering and HTP-guided steering are suitable to correct for improper positioning up to the level that none of the investigated positions appears preferable. Current positioning precision is sufficient in the X (right-left)-direction but precision measurements are needed to reach the desired accuracy in the Y-direction. In the Z-direction, a cranial shift of the applicator is predicted to be beneficial.
Conclusions: If position is known accurately, correction of the treatment setting is possible without loss of heating efficiency. Additionally, no preferable positions exist.

4.1 Introduction

At present in the Netherlands , hyperthermia as an additional treatment to radiotherapy is considered a regular part of the Dutch healthcare. After the publication of the Dutch Deep Hyperthermia Trial (DDHT) [4] in 2000, radiotherapy (RT) plus loco-regional deep hyperthermia (DHT) has become an accepted treatment for locally advanced cervical cancer. More recently, Franckena et al. [155] reported the follow-up of the DDHT over a period of 12 years and found that survival in the radiotherapy (RT)+hyperthermia (HT) arm remains stable at twice the level of the RT-alone arm. Fatehi et al [117] showed that good reproducible heating is achieved with the BSD-2000 Sigma-60 [139] over the years. However, in their retrospective temperature analysis of 444 patients, they also demonstrated that intraluminal temperatures are relatively low, on average 40.5 ^{o}C. Combined with the existing literature on thermal dose effect relationships [26-31], it needs no explanation that there is a strong need to improve our ability to prescribe the thermal dose of a hyperthermia treatment. The latter is even more emphasized by the recent paper of Franckena et al., in which the value of thermal dose as independent prognostic parameter for treatment outcome was demonstrated specifically for patients with advanced cervical cancer treated with RT+HT [33].
In the past, several studies have been conducted by our group to improve control of treatment quality [107, 131-132, 156]. However, the impact of patient positioning on the hyperthermia treatment quality, a potentially important parameter, has not been evaluated yet. Therefore, in this study we addressed the relation between patient position and the specific absorption rate (SAR) distribution in the tumor volume. In our regular treatments, DHT is applied using settings from an empirical steering protocol [135].This empirical steering protocol basically consists of: 1) focusing the electromagnetic (EM) field at the tumor site, 2) steering this focus away from deeply located complaints and 3) ,in case of superficial complaints, lowering the amplitude on the complaint side.
In most hyperthermia centers, the settings for steering the focus are determined by the rather basic approach of analytically calculating the location of maximal interference of the electromagnetic field in the XY plane, i.e. the focus, approximating the patient by a homogenous - patient sized - ellipsoid. For example, if a focus of (5,-2) is desired, $phase_{left}$=5*n, $phase_{right}$=-5*n, $phase_{top}$=-2*n, and $phase_{bottom}$=2*n, with n the nr. of degrees phase shift per cm focus shift . Steering of the focus in this manner ,using phase shifts, is a standard option in the BSD2000 Sigma 60 operator software [Turner *et al* 1989]

and is called SAR-focus steering. A second option is hyperthermia treatment planning (HTP) guided steering, which is based on simulation and optimization of the SAR distribution in a 3D patient model [47, 157-158]. Upon complaints, the SAR distribution can be re-optimized to reduce heating by applying a constraint at the complaint region.
In this study, three main research topics have been addressed, both for SAR-focus- and HTP-guided SAR steering, using patient models of cervical cancer patients:
The sensitivity of the SAR distribution for errors in patient positioning.
Especially for HTP-guided steering, the position in the HTP model should accurately resemble the position during the clinical application in order to obtain predictive value. When using a steering protocol, errors and inaccuracies in patient positioning may lead to suboptimal SAR patterns, resulting in a lower treatment quality.
The possibility to electronically correct for improper patient positioning.
To assess if a correction for improper patient positioning is possible, it should be known how accurate the SAR focus can be shifted to the tumor center (TC) by phase and amplitude steering. An example of such SAR steering occurs when the patient's position is changed to improve comfort by reducing water bolus pressure. Alternatively, tumors located non centrally require a specific setting of amplitude and phase in order to have the SAR distribution focused at the tumor center.
Optimal patient position in longitudinal, lateral and anterior-posterior direction.
Following the results of the previous questions, the possibility of an optimal patient position is investigated, i.e. are there specific positions that, combined with HTP-guided steering using a correctly shifted patient model, lead to better SAR patterns. This question is an important extension of the more commonly addressed question of how to optimize the SAR distribution, by phase and amplitude modification. The outcome of this part of the study may lead to prescribing a specific patient-applicator position.
The overall potential benefit of HTP guided steering over SAR-focus steering is assessed using the results as obtained by the sub-studies to answer the formulated three questions. Ultimately, these final analyses of the data will result in appropriate protocols in order to achieve the required accuracy in patient positioning.

4.2 Materials and methods

4.2.1 Equipment

In this study, the effects of positioning on the SAR-pattern in a patient model, and the possibilities of electronic correction are studied using an EM-model implementation of the most frequently used DHT applicator, the BSD Sigma 60 [34, 140, 143] (BSD medical

corporation, Salt Lake City, USA). Amplitudes and phases of the signals, which are fed into each antenna, can be modified to control the interference pattern of the RF (radiofrequency)-field. The Sigma 60 applicator consists of a ring of 8 dipole antennas that are coupled in 4 channels of two antennas each. Because the antennas in the Sigma 60 applicator are situated in one ring in the XY-plane, steering is restricted to the lateral (X) and ventral-dorsal (Y) directions. (In figure 4.1, a patient model and the coordinate system are depicted) In addition, moving the Sigma 60 applicator in the Z-direction provides a third degree of freedom to control the SAR pattern.

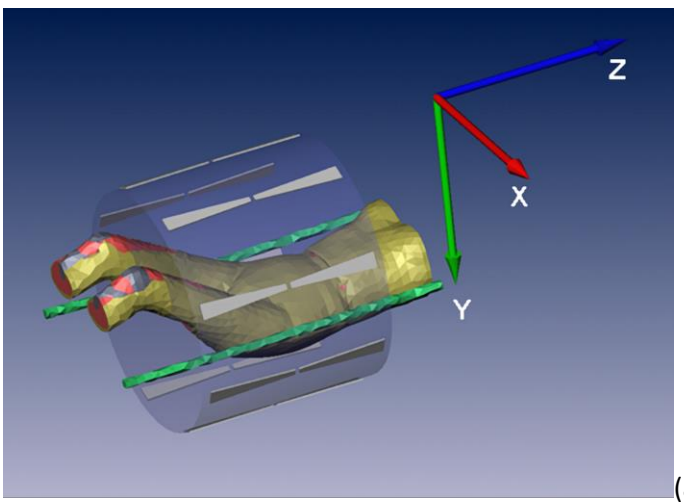

(a)

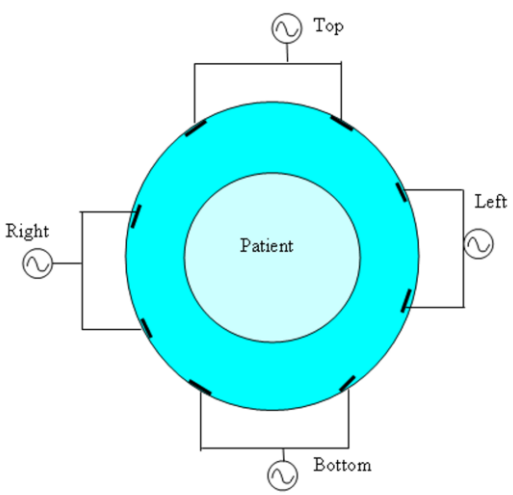

(b)

Figure 4.1: Patient model plus the BSD Sigma 60 applicator with coordinate axes as shown in the graphical user interface of Sigma Hyperplan. The eight dipole antennas are visible. (a) Axial view from the caudal direction of the Sigma 60 applicator, with the four channels, each connected to two antennas (b)

4.2.2 SAR-focus steering vs. HTP-guided steering

Generally, two methods are used to optimize amplitudes and phases for focusing the RF-field at the requested location during deep hyperthermia: SAR-focus steering [74, 135] and HTP guided steering [47]. As explained before, SAR-focus steering is the current standard steering method in the clinic whereas HTP-guided steering only became feasible after the development of advanced EM models.
HTP-guided steering is a well-defined method to determine the optimal phase and amplitude settings for the DHT-treatment, using EM-models. Numerical optimization is used in HTP-guided steering, and as goal function we selected the ratio of tumor SAR to the hotspot SAR: HTQ (hotspot tumor quotient). After a complaint, the weight of the corresponding complaint region in the goal function is increased, and new settings are obtained through re-optimization. This is described in further detail in Canters et al [47].

4.2.3 Patient position measures

In this study, the origin of the coordinate system is defined at the center of the tumor volume: TC (tumor center). If a patient is positioned such that the AC (applicator center) is in the same position as the TC, this is further referred to as the central applicator position (i.e. $X_{AC}=Y_{AC}=Z_{AC}=0$). A position shift is defined as the AC shifting in X, Y, or Z direction. This is illustrated in figure 4.2.

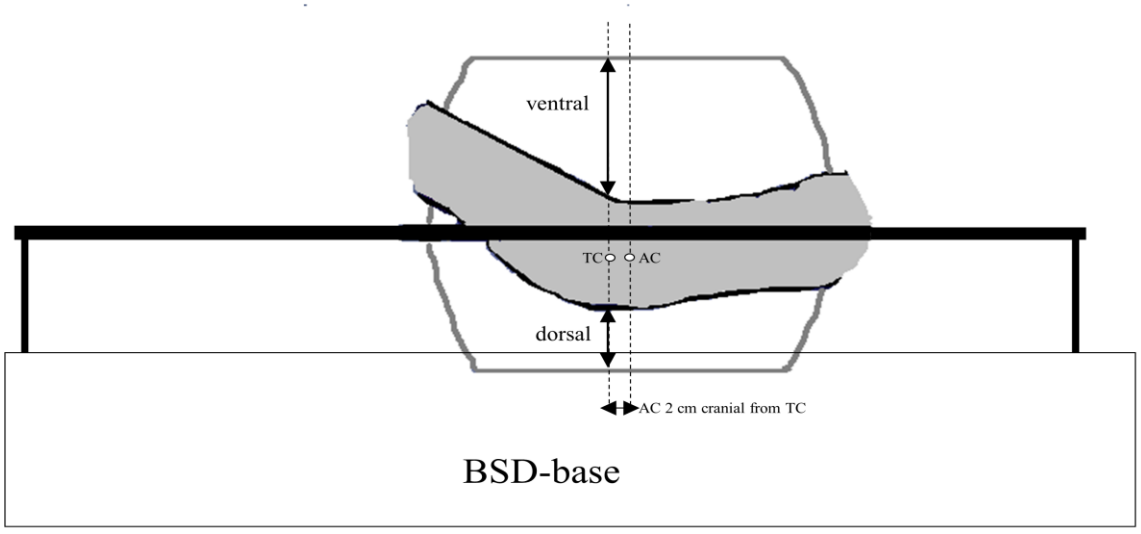

Figure 4.2: Illustration of patient position in Y- and Z-direction, including a shift of 2 cm in cranial direction (referred by Z=2).

4.2.4 Patient and applicator modeling using the Sigma Hyperplan software

The study is performed on 10 representative patient EM models of patients with cervical cancer. EM calculations for 3D patient models are performed using the finite element method (FEM) of Sigma Hyperplan (Dr. Sennewald Medizintechnik GmbH, München, Germany). The workflow for this modeling is extensively described in Sreenivasa *et al* [39] and Gellermann *et al* [100].

On average our models consisted of 220,000 tetrahedra, with edge lengths of the tetrahedra between 0.3 and 2.5 cm, with the grid the most dense near the antennas, and in the pelvic area. Other studies using Sigma Hyperplan [39, 100, 113] reported similar numbers of tetrahedra and support our selection. The antenna coupling is taken into account in the models.

Setups were created where each of the ten patient models were shifted along X-, Y- and Z-axis, in steps of 1cm, ranging from –5 cm to +5 cm from the central tumor position (see figure 4.3). Hence, we arrived at 31 positions per patient model and 310 different setups in total.

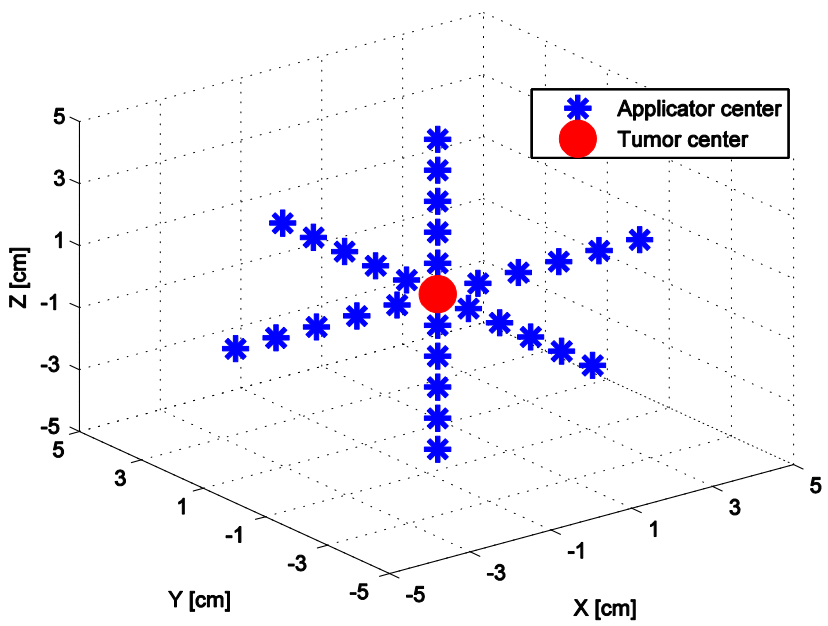

Figure 4.3: For each patient, 31 positions of the applicator center (AC) are modeled. For all calculations the tumor center (TC) is located at the origin.

Table 4.1: dielectric and thermal properties of tissues at 77 MHz [39, 49, 113]

Tissue	ε_r	σ [S/m]	Perfusion (ml/100g/min)	ρ(kg/m^3)	Heat capacity (J kg^{-1} K^{-1})	Conductivity (W m^{-1} K^{-1})
Fat	13	0.07	20	900	3500	0.21
Muscle	69	0.70	30	1000	3500	0.642
Bone	16	0.06	10	1600	1000	0.436
Hammock support rods	1	0	0	1000	N/a	N/a
Tumor (=cervix)	69	0.70	8	1000	3500	0.642
Bladder	24	0.29	15	1000	3500	0.6
Heart	99	0.70	60	1000	3500	0.642
Intestine	108	1.62	50	1000	3500	0.55
Kidney	109	0.77	400	1000	3500	0.577
Liver	75	0.46	100	1000	3500	0.64
Lung	35	0.71	20	500	1000	0.2
Spinal cord	6	0.04	10	1000	3500	0.642
Spleen	101	0.77	60	1000	3500	0.577
Stomach	82	0.89	60	1000	3500	0.577
Uterus	69	0.70	30	1000	3500	0.642
Vagina	69	0.70	30	1000	3500	0.642

To quantify the quality of the SAR distributions, we used the hotspot SAR to tumor SAR quotient (HTQ), which is formulated as:

$$\mathrm{HTQ} = \frac{SAR(V_1)}{SAR_{tumor}} \qquad 4.1$$

$SAR(V_1)$ is the average SAR in the 1st SAR percentile (highest SAR values) in the normal tissue and SAR_{tumor} is the average SAR in the tumor region. HTQ is also used as the goal function for optimization of the SAR distribution in HTP-guided steering. Hereto we created a custom-made add-on to Sigma Hyperplan, running in a Matlab environment. This goal function is used to effectively maximize tumor SAR while minimizing SAR in potential hotspots [47].

4.2.5 Model calculations

For each of the patients and all 31 positions, the results of the model calculations are used to answer the questions as mentioned in the introduction.

The sensitivity of the SAR distribution to errors in patient positioning

For both SAR-focus steering and HTP-guided steering, we varied patient positioning and examined the resulting SAR distributions. For SAR-focus steering, a central focus with balanced amplitudes (A =1,1,1,1) and phases (phi=0,0,0,0)), i.e. the initial settings for a treatment of centrally located tumors (AC=TC) is used. In contrast, for HTP-guided steering the initial settings are the amplitude and phase settings optimized for an AC=TC position. The same settings are maintained, while the AC is moved along the 31 different positions and a new HTQ value is calculated for that position. From these calculations, the required accuracy in positioning during clinical hyperthermia can be determined

The possibility to electronically correct for improper patient positioning

The ability to correct for position shifts is assessed differently for SAR-focus steering as for HTP-guided steering. Again, 31 positions per patient are evaluated. However, this time not a single amplitude and phase setting is used, but for each position a correction for the position shift is applied. For SAR-focus steering, the position shift is corrected for by a focus shift in X- or Y-direction corresponding to the applicator (thus AC) shift. For HTP-guided steering, the position shift is corrected for by calculating a novel position-specific optimized setting.

Optimal patient position in longitudinal, lateral and anterior-posterior direction

As mentioned before, from the results of all previous simulations with HTP guided steering, it is possible to deduce what the optimal position to treat the patient is. If so, this position will lead to a better HTQ and therefore the most optimal SAR distribution. Finally, a comparison of the results of all previous simulations will provide an overview of the potential benefit of HTP-guided steering in comparison to SAR-focus steering.

4.2.6 Temperature calculations

A clear objective criterion is required for a sound assessment of the required position accuracy. As thermal dose is related to treatment outcome [26, 29-31], we consider that this criterion has to be derived from the maximum allowed temperature decrease. For this analysis, we define a decrease in temperature $\geq 0.2^{o}$C (±5% of the average temperature increase above 37 °C) as clinically relevant. In order to correlate a change in

tumor temperature with a change in HTQ, we performed temperature calculations for a subset of positions, i.e. temperatures for X_{AC}=0, 3, 4 and 5 cm are calculated for all 10 patients. For both central focus and optimization, a temperature distribution was calculated using the thermal settings reported in table 4.1. Input power was increased until temperatures in healthy tissue reach 44^{o}C, to asses the maximum feasible temperature in the tumor. From this data, a correlation between change in HTQ and temperature change is established.

4.3 Results

4.3.1 Correlation tumor T50 change with HTQ change

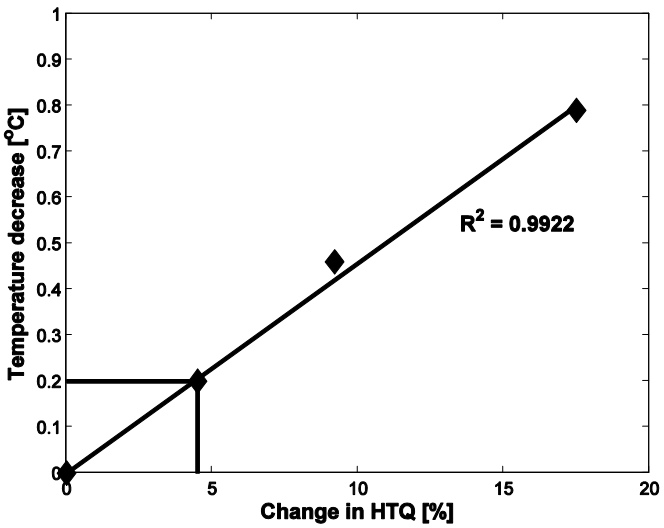

Figure 4.4: Correlation between a change in HTQ and the corresponding decrease in T50.

For 3 patient models, it was physically not allowed to position the applicator at X_{AC}= 5cm and for two also X_{AC}= 4 cm was not possible because, for these positions, parts of the patient were closer to the applicator wall than accepted by our treatment protocol (< 5 cm). Optimized phase and amplitude settings were applied for all positions. In figure 4.4, the results of these calculations are presented.
The T50-decrease appears to be highly correlated (R^2=0.9922) with the change in HTQ. As stated before, we consider a decrease by 0.2^{o}C in T50 as relevant and therefore we conclude a HTQ increase by 5% is required to obtain a meaningful improvement in the SAR distribution.

$$\Delta T50 = \Delta HTQ \cdot 4.81 \qquad \textbf{4.2}$$

4.3.2 Results of the SAR calculations

I. Sensitivity of the SAR distribution for errors in patient positioning.

In figure 4.5, the average HTQ values as calculated for all 10 patient models are presented per X_{AC}, Y_{AC}, Z_{AC} position, with the standard error over the 10 different patients depicted as error bars. The HTQ-values are normalized at the HTQ-value of position 0,0,0. For all calculations, the tumor center remained fixed at the TC position 0,0,0. Data is shown for both SAR-focus steering (solid line) and HTP-guided steering (dashed line).

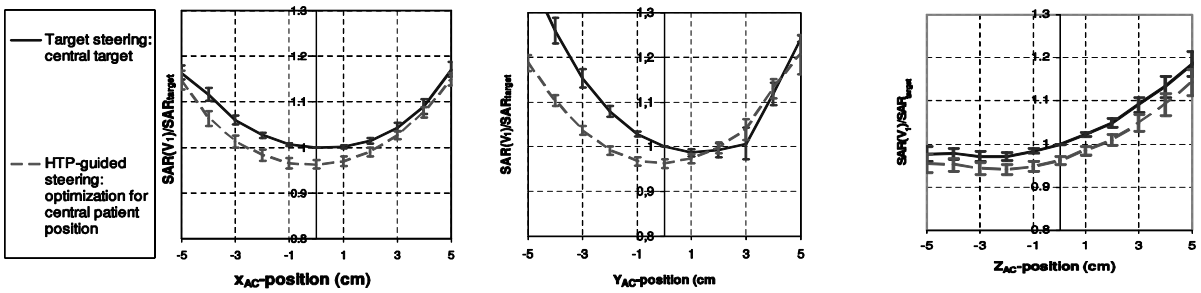

Figure 4.5: Sensitivity of the HTQ value (=SAR(V1)/SARtumor) for position shifts of the applicator center in X, Y, and Z direction. The center remained at 0,0,0 for all calculations. The error bars represent the standard error over the results per position for the 10 patients.

Overall, figure 4.5 demonstrates a similar behavior for both empirical and HTP-guided steering. More detailed, the following aspects are shown:

SAR-focus steering: central focus with balanced amplitudes and phases

For X_{AC}-positions the central position, i.e. X_{AC}=0, is clearly the most beneficial. When compared to each other in a two sample T-test, position deviations with respect to X_{AC}=0 are significantly smaller than 5% ($p<0.05$), if $-2 \leq X_{AC} \leq 2$ cm. In Y-direction, the most optimal position is located at Y_{AC}=1cm. Position deviations with respect to Y_{AC}=1 are significantly

smaller than 5%, if $0 \leq Y_{AC} \leq 2$ cm. In Z-direction, Z_{AC}=-2 cm appears to be the optimal position for heating a patient. Position deviations with respect to Z_{AC}=-2 cm are significantly smaller than 5%, if $Z_{AC} \leq 0$ cm. Generally, this means that position inaccuracies smaller than or equal to 1 cm, do not significantly affect heating of the patient in the empirical steering approach. Further, position deviations in negative Z-direction do not lead to significant changes in HTQ.

HTP-guided steering: optimized amplitude and phase settings for central applicator positioning

For both X_{AC} and Y_{AC}-position, the optimum in this case is, of course, situated at the 0 cm position since the SAR pattern was optimized for a central tumor position, i.e. TC=AC. For Z_{AC}-position, the optimum appears to be situated at Z_{AC}=-2 cm, equivalent to the SAR-focus steering. Position deviations from the (0,0,0) position, that cause changes in HTQ significantly smaller than 5%, are $-1 \leq X_{AC} \leq 1$ cm , $-1 \leq Y_{AC} \leq 1$ cm, and $Z_{AC} \leq 0$cm. So again, position inaccuracies smaller than or equal to 1 cm, do not significantly affect heating of the patient.

II The possibility to electronically correct for improper patient positioning by SAR steering

In figure 4.6, the HTQ value is plotted after a SAR focus steering and HTP-guided steering correction for the shift in the X, Y and Z-direction.

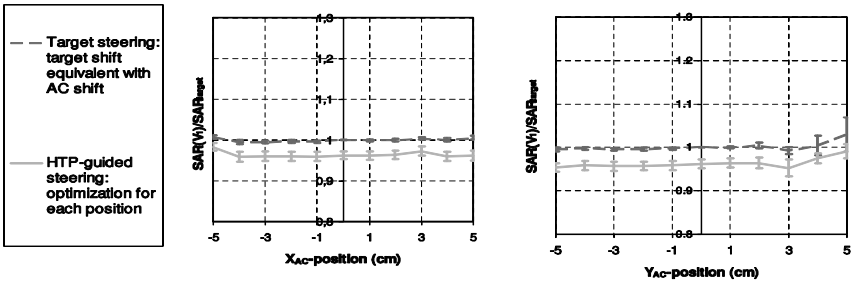

Figure 4.6: HTQ values (=SAR(V_1/SAR_{tumor}) after correction for position shifts in X and Y-direction. The error bars represent the standard error of the means. In SAR-focus steering, the position-shift correction of the phases is based on the simple elliptical model. In HTP-guided steering a new set of optimized amplitude and phase settings are calculated for the shifted antenne-patient configuration.

The following aspects are shown in figure 4.6:

SAR-focus steering: Focus is placed on the TC position
For X_{AC}-position, all tested positions moving the SAR focus to the TC as indicated by the homogeneous elliptical approach result in a HTQ that is not significantly different from the X_{AC}=0 position. At X_{AC}=0, HTQ obtained with SAR-focus steering, is also not significantly different from the HTQ using a central focus. For all Y_{AC}-positions, HTQ is also not significantly different from the Y_{AC}=0 position. Together this means that, for all except one X_{AC}- and Y_{AC}-positions, it was possible to correct for positioning inaccuracies and reach the same level of HTQ as obtained for the central position and using a central focus. Only for the Y_{AC} position, the HTQ change cannot be satisfactory corrected by redirecting the SAR focus. In Z-direction, correction for position shifts is not possible, because the antennas are arranged in a single ring in the XY-plane, i.e. SAR focus steering in the Z-direction is impossible with the Sigma applicator.
Generally, at 77 MHz, the wavelength is approximately 40cm. Each cm of focus shift would typically require a phase change of 9^{o}.
HTP-guided steering: optimized amplitude and phase settings for each position.
Applying position-specific optimization for every X_{AC}- and Y_{AC}-direction position-shift results in equal HTQ values for all positions except one: only for the Y_{AC}=5 position, the HTQ-value changes by >5%. Hence, also with HTP-guided steering it is possible to fully correct for position-shifts in X and Y-direction. Again, correction is not possible in the Z-direction.

III Optimal patient position in longitudinal, lateral and anterior-posterior direction.
The results in figure 4.6 show that, if the misalignment of the patient with the intended position is known, both SAR-focus steering and HTP-guided steering provide adequate tools to obtain a HTQ value equal to the intended original position. Hence, both figures demonstrate that there is no preferred X_{AC} or Y_{AC} position, when using HTP guided steering and the exact position is known.
However, any steering in the Z-direction is not possible with the Sigma 60 applicator. The sensitivity of the HTQ-values, as shown in figure 4.5, indicate that a substantial improvement in heating quality might be obtained by selection of the proper Z-position, i.e. Z=-2 cm. Over the investigated range of Z-positions the HTQ-value changes by 20%.

4.4 Discussion

Theoretical models lend themselves perfectly for parameter studies like the one performed for this paper. A major point of concern is often how the results can be

transferred into the clinical practice. With regard to this particular parameter study, there are no reasons to be concerned. Research reported in previous studies [39, 62] showed a good correlation between Sigma Hyperplan modeling and related measurements. Although the absolute value might not be validated, there exists sufficient literature supporting the qualitative validation of the Sigma Hyperplan model [80, 159]. In our opinion, the Sigma Hyperplan is an excellent tool to exploit the effect of the variation in a specific parameter and we are convinced that the clinical application of hyperthermia will greatly benefit from the outcome of such studies.
The HTQ goal function is considered an efficient function, both for evaluation and for optimization of SAR distributions. In a previous study, we have evaluated optimization of various SAR goal functions by their temperature model outcomes, and the HTQ appeared to perform the best [45]. Additionally, previous research has shown the feasibility and effectiveness of using HTQ in HTP-guided steering in a clinical situation [47]. This study showed that model generation, optimization, and HTP-guided steering during treatment are feasible. However, a limitation of the HTQ as a goal function is the lack of information about the systemic heating of the patient. In the extreme case of homogeneous heating of the patient, the HTQ value is one, which would be considered quite well. However, in targeted heating with phased arrays this situation is highly unlikely to occur.
The results as reported in this study show that positioning is an important aspect in achieving maximal treatment quality in hyperthermia treatments. Overall, the sensitivity of the SAR distribution in the patient to exact positioning shows an identical behavior for SAR-focus steering as well as HTP-guided steering. This means that the required positioning accuracy is the same for both methods of steering. However, as is shown in figure 4.5a-c and figure 4.6a,b, applying HTP-guided steering: with optimized phase and amplitude settings for each individual patient, provides a small but consistently better (i.e. 3-5% lower) HTQ-value as compared to SAR-focus steering. Hence, this study indirectly promotes the standard use of 3D hyperthermia treatment planning as a tool to improve hyperthermia treatment quality. At the same time, the study indicates that precise positioning is mandatory for high quality HT-treatments.
In this study into position effects, the theoretical modeling addressed three major issues, for which the relevance on current practice and their impact on our future treatment protocol design is discussed consecutively hereafter.

Sensitivity of the SAR distribution for errors in patient positioning.

In treatments using SAR-focus steering, position inaccuracies in X-direction are likely (at least in our experience) to be relatively small in practice. Movement in X-direction is effectively limited by the hammock on which the patient is lying during treatment. Therefore, we anticipate that any position error in X-direction falls within the acceptable range of X_{AC}=[-2,2], for which the change in HTQ is less than 5%. For the Y-direction, the hammock does not provide a similar constrainted positioning. Hence, a good position verification protocol is required to assure that the final position of the patient is within the acceptable range of Y_{AC}=[0,2]. Unexpectedly, the most favorable position, when applying SAR-focus steering, was not at Y=0 cm. Modeling results indicate that, for SAR-focus steering, a 1 cm shift of the AC in dorsal direction results in a slightly better value of HTQ, i.e. 3% lower. The asymmetry of the patient, which is more pronounced in the Y-direction, is probably the reason for this decentral optimum.
In Z-direction, positioning-error related HTQ increases are low for Z_{AC}<=0 but they grow worse rapidly for each additional 1 cm z-shift for Z_{AC}>0. The most favorable AC position is located at Z_{AC}=-2 cm: both for SAR-focus steering and HTP-guided steering. Z_{AC}=-2 cm means a slightly caudal position of the AC. This positioning has the additional advantage that the SAR patterns are only slightly sensitive (±2%) to positioning errors for Z_{AC} ranging from -5 to 0.
Together, the demonstrated sensitivity of the HTQ-value on X, Y and Z-positioning leads to a required accuracy in patient positioning of 1 cm. However, this demand should be applied most strictly in the Y-direction.

<u>Possibility to electronically correct for improper patient positioning by SAR steering.</u>

For both X- and Y-positioning, the use of SAR-focus or HTP-guided steering to correct for a position shift does not produce HTQ values that are significantly different of those from the (0,0,0) position. Therefore, as long as correction for the precise TC position is possible, there is no theoretical difference in treatment quality between different positions. Hence, both SAR-focus and HTP-guided steering are effective methods to correct for non-central TC positions.

<u>Optimal patient position in longitudinal, lateral and anterior-posterior direction.</u>

The use of SAR-focus - of HTP-guided steering for optimizing the SAR distribution to each specific patient position and to correct for misalignment demonstrates also that there is no clear favorable position in X- and Y-direction. This absence of preference from a quality assurance point of view means that the most convenient position for the patient

can be used (for minimizing discomfort) as long as the registration accuracy remains at 1 cm. Therefore, X and Y-position shifts should not be used as optimization variable.
As mentioned earlier, the results in figure 6c show that there is a benefit of a roughly 5% lower HTQ value only for the Z-direction when the center of the Sigma 60 applicator is placed 2 cm below the tumor center. In our current patient positioning protocol, Z_{AC}=2cm is used as a standard position. The reason to select Z_{AC}=2cm as a preferred position goes back to our clinical experiences with deep heating using the Sigma 60 applicator in the early 1990's. In our first treatment of patients with advanced cervical cancer, we frequently found preferential heating at the introitus. In a personal discussion, a similar observation was reported to us by Gibbs [160]. This discussion, together with the results reported by Jia *et al* [103] in their paper comparing measured and computed SAR distributions as induced by the Sigma 60 applicator in the Utah phantom (a simplified heterogeneous phantom of the female pelvic), made us decide to position the center of the Sigma 60 applicator 2 cm cranial from the tumor center.
More recently Gellermann et al [113] also studied the influences of positioning on the temperature pattern in presacral tumors using an anatomy based phantom. In their study, they found a similar dependency on positioning in the X-direction as reported here. Similarly, in the Y-direction, they also found an optimum for Y_{AC}=1cm. In contrast with our study, the optimum in Z-direction was found at Z_{AC}=0cm and not at Z_{AC}=-2 cm. For tumors located in the lower pelvis, Gellermann et al also found that moving the applicator center in cranial direction away from the tumor center reduces the preferential energy deposition (i.e. heating) in the perineal region. The different favorable position in z-direction from the three studies is, in our opinion, caused by the differences in the tissue geometries used: Jia et al [103] used a simplified heterogeneous muscle-fat pelvic phantom, Gellermann et al used an anatomy based phantom (muscle tissue with the pelvic bones included) and we used real 3D patient models. Also, Gellermann et al used the Sigma Eye applicator in stead of the Sigma 60 applicator. Additionally, our study quantifies the variation that can be expected between patients, using patient specific models. In summary, we believe that our results are most predictive for the clinical setting.
From the current findings, two clear reasons can be deduced to adapt our current patient positioning protocol. Firstly, at Z_{AC}= 2cm the HTQ-value is quite sensitive to position changes, which largely disappears at Z_{AC}= -2cm. Secondly, Z_{AC}= 2cm is 4 cm from the most favorable position. As a consequence, we have started a clinical study to confirm this theoretical finding by comparing tumor temperatures in two successive treatments in the same patient with Z_{AC}= 2cm or Z_{AC}= -2cm in subsequent treatments.

4.5 Conclusions

In this study we investigated the influence and optimization-potential of patient-positioning on the SAR patterns obtained during loco-regional deep heating of advanced cervical cancer using the Sigma 60 applicator. We found that the position of a patient has a relevant influence on the quality of heating and positioning errors should not exceed 1 cm for a maximum SAR deviation of 5% in hotspot SAR to tumor SAR quotient (HTQ). In X-direction, the hammock already provides sufficient fixation, while in Y-direction, specific measures should be used to obtain positioning to this accuracy. Currently, ultrasound distance measurements are introduced in the clinic to obtain a sufficiently positioning accuracy of 1 cm. In Z-direction, Z_{AC}=-2cm (i.e. the applicator center shifted in caudal direction) is expected to provide the best HTQ. This shift in Z-direction has the additional advantage of making the SAR pattern less sensitive to position shifts. Currently, a laser positioning system is introduced to accurately define the Z-position. Using SAR-focus or HTP-guided steering, it is possible to fully correct for off-center positioning in X and Y direction. Because the Sigma 60 applicator has only one antenna ring, corrections in Z-direction are not possible.

SAR focus steering or HTP guided steering is only effective if the patient position in the applicator matches the position in the model. Therefore, accurate positioning is of great importance. We recommend that positioning in DHT is performed with an accuracy of +/- 1 cm. The technology to achieve this positioning accuracy is currently implemented in our clinic. No preferred position exists in X- or Y-position, whereas a position of the applicator center is advised to be at Z= -2cm (i.e. 2 cm below the TC). Finally, the SAR-calculations show that using the HTP results in an improvement of HTQ by approximately 5% on average. Therefore, we consider the use of HTP-guided steering as a relevant and significant tool, which is clinically feasible, when applying local regional deep heating with the Sigma 60 applicator.

6 Clinical implementation of hyperthermia treatment planning guided steering: a cross over trial to assess its current contribution to treatment quality

This chapter was published as:

Franckena M, Canters RAM, Termorshuizen F, Van der Zee J, Van Rhoon GC. Clinical implementation of hyperthermia treatment planning guided steering: a cross over trial to assess its current contribution to treatment quality. Int J Hyperthermia, 2010; 26:145-157.

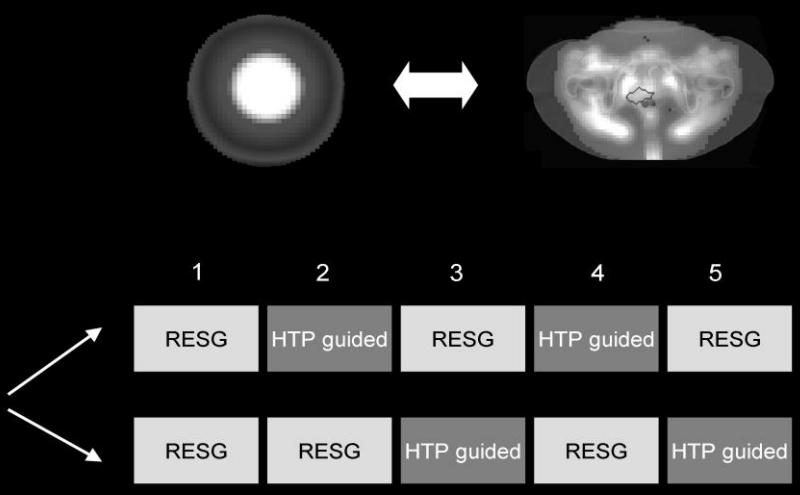

Abstract

Purpose: To assess the current feasibility and its contribution of online hyperthermia treatment planning guided steering (HGS) to treatment quality in deep hyperthermia for locally advanced cervical cancer in a cross over trial.
Materials and methods: 36 patients were randomized to receive either their 2nd and 4th (arm A) or their 3rd and 5th (arm B) hyperthermia treatment of the series with the aid of HGS. The other treatments were conducted according to our empirical steering guidelines (RESG or Rotterdam Empirical Steering Guidelines).
Results: During period I (2nd and 3rd treatment of the series) similar results were found for HGS and RESG with a slight, non-significant difference found in favor of HGS. However, during period II (4th and 5th treatment of the series) HGS performed less well, with significant lower thermal dose parameters, minimum, mean and maximum intraluminal temperatures, acute toxicity measures and net integrated power.
Conclusion: We found that the procedure of online treatment planning guided steering is feasible. For maximal exploitation of its possibilities, however, better control and understanding of several patient, tumor and technical parameters is required. This study has been very helpful in identifying some of the challenges and flaws that warrant further investigation in the near future, such as patient positioning and the prevention of hotspot- related complaints. With the progress that has been made during this study, we hope to perfect the principle of hyperthermia treatment planning guided steering in the near future.

6.1 Introduction

In the Netherlands, combined radiotherapy (RT) and deep hyperthermia (DHT) is part of regular health care for patients with locally advanced cervical cancer (LACC) since 1996. Several randomized trials showed that the addition of DHT to RT improves local control and survival for these patients and most recently we demonstrated a 5-year local control rate of 53 %.[4, 9, 155, 168-172] Not withstanding this encouraging result in a group of patients with relative poor prognosis, i.e. large primary tumors, there is still ample room for further improvement of treatment outcome and we should continue to search for better treatment strategies.[118-119]

In this perspective, the finding of a significant correlation between the thermal dose delivered during treatment and patient outcome in a group of 420 patients with LACC treated with RT+DHT clearly opens a window for further research.[33] This thermal dose-effect implies that better results should be obtained when higher thermal dose levels can be delivered. Obviously, the most elegant possibility to increase the thermal dose delivered is to aim for more tumor-selective and patient-specific heating than is currently achieved.

At present, most DHT treatments are applied empirically, i.e. experience and dedication of the treatment team plays a major role in the final treatment quality. In general, the occurrence of hotspots, or areas of discomfort to the patient due to uncomfortable temperatures locally, limit temperatures achieved during hyperthermia.

Commonly, the strategy to manage hotspots is to apply a short break in the power applied, followed by adjustment of phase and amplitude settings to the antennas in order to steer the energy away from the hotspot. The precise approach of this strategy and thereby its effectiveness varies from center to center. Of course, a more objective approach would be preferable as it would allow a more systematic strategy and would also enable transfer of knowledge between centers and education of new staff. If the clinical application of such a systematic strategy were useful and effective, it would mean a major step forward. For the first time in the history of hyperthermia standardization, improvement of treatment quality, a priori assessment of potential quality of treatment and better treatment quality in centers new to the field can be expressed as an objective quality index. For these reasons a hyperthermia treatment planning (HTP) system is considered a great aid as HTP can help us better understand the effects of phase and amplitude adjustments on power and temperature distribution and even predict the effect of the adjustments during treatment.[39, 100, 123, 135] Consensus exists that the

combination of HTP with optimization of treatment settings to maximize power deposition in the tumor and minimize hotspots, will improve temperatures in DHT.[81] The use of a HTP is becoming common practice in hyperthermia, but for its use during treatment an optimization routine is necessary that not only optimizes power deposition in the tumor, but also reduces deposition in a complaint-related area (HTP-guided steering).[39, 47, 81, 100, 113, 123-124, 135, 173] Although not yet demonstrated in a clinical situation, the development of HTP-guided steering for standardization and improvement of treatment quality is a very important step in the further development of hyperthermia. Such a strategy would promote uniformity of treatment quality and comparison of treatments among the various institutes applying DHT. On the other hand, the preparation process is time-consuming and labor intensive and our current treatment approach (i.e. following the Rotterdam Empirical Steering Guidelines or RESG) proved its effectiveness in several clinical trials.[135] Further, the RESG are based on decades of clinical experience and it will be difficult to improve its results with a new technique that has never been used in a clinical setting before. As a first step, we designed a clinical trial to compare the two treatment approaches in terms of temperatures achieved during treatment, thermal dose delivered and acute toxicity. This study provides us with an assessment of the current status and performance of HTP-guided steering in a clinical situation and show how clinical results compare to our golden standard of the RESG.

6.2 Materials and methods

6.2.1 Clinical background

For patients with LACC, 5 hyperthermia treatments of 90 minutes each are planned for each patient during the period of external beam radiotherapy. For all hyperthermia treatments in this study, the BSD-2000 3D system (BSD Medical Corporation, Salt Lake City, Utah, USA) was used with the Sigma-60 applicator.[62, 140, 143] The standard operating frequency of the Sigma-60 is 77 MHz. The treatment is started at a power output of 400 Watts and was increased with steps of 100 Watts for every 5 minutes as long as the patient has no hotspot-related complaints or normal tissue temperatures do not exceed 43 ^{0}C. In case of hotspot-related complaints or normal tissue temperature > 43 ^{0}C, the power is briefly turned off until the discomfort subsides or temperature is below 43 ^{0}C, and phase, amplitude or frequency settings are adjusted to prevent recurrence. The further increase of power is not resumed until a complaint-free period of

5 minutes has been established. These principles were maintained over all treatments in this study. For a detailed description of the procedure and its rationale we refer to the paper of Van der Wal et al[135].

6.2.2 Study design

For this study, all patients with LACC and an indication for DHT were eligible if thermometry could be performed in bladder, vagina and rectum. After informed consent, patients were randomized to receive either the 2^{nd} and 4^{th} or the 3^{rd} and 5^{th} hyperthermia treatment with HTP-guided steering (HGS). A cross-over design was chosen because interpatient variation was observed to be larger than the intrapatient variation as we learned from previous data.[119] Further, as the effect of a hyperthermia treatment on intraluminal temperatures is short lived, it is unlikely that the outcome of a previous treatment influences the outcome of a consecutive treatment (i.e. probably no carry over effect). To account for the influence of progression of the treatment series on patient tolerance, both treatments were repeated per individual patient.The first treatment was excluded from the study in order to allow the patient to get acquainted with the principles of the hyperthermia treatment and equipment.
Primary endpoints for this study were temperature, thermal dose and treatment-limiting hotspots. For temperature, we chose to use the T20 (the temperature exceeded by 20% of monitored sites per patient in bladder, vagina and rectum), T50 (temperature exceeded by 50% of monitored sites per patient in bladder, vagina and rectum) and T90 (temperature exceeded by 90% of monitored sites per patient in bladder, vagina and rectum). For thermal dose, we chose CEM43T90 (cumulative equivalent minutes of T90 at 43 ^{0}C as described by Fatehi et al.) and TRISE (a custom made thermal dose parameter based on T50 and the duration of heating).[174] This second parameter has been shown retrospectively to correlate very well with treatment outcome in our patient group.[33]
For treatment-limiting hotspots, we chose the number of off-switches (NOS), the total duration of off-switches (DOS) and the time from start of treatment to first complaint (TTFC) as measures. An off-switch is defined as turning off the power of the BSD-2000 system longer than 20 seconds to reduce a hotspot-related complaint. Shorter off-switches are mostly caused by hyperthermia staff entering or leaving the treatment roo**m.**
Further we chose the net integrated power as described by Fatehi et al. as a secondary outcome measure, because an increase in net integrated power is expected to be accompanied by an increase in target temperature.[81, 117]

6.2.3 Temperature and thermal dose data preparation

For thermometry Bowman probes were placed in the patient's bladder, rectal and vaginal lumen. Thermal mapping was performed every 5 minutes with a step size of 1 cm and a maximum map length of 14 cm. Based on the temperatures measured intraluminally, several treatment parameters were calculated using RHyThM (Rotterdam Hyperthermia Thermal Modulator), which has been described elsewhere in detail.[175]

6.2.4 Current treatment approach using the RESG [135]

Preparation: Currently, all patients are positioned in the same way in the Sigma-60 applicator in the anterior-posterior and lateral directions. The preferred craniocaudal position is derived from the CT (Computed Tomography)-scan made for radiotherapy treatment planning. From this CT-scan the distance from the center of the tumor to a bony landmark, in this case the pubic bone is calculated. The patient is positioned so that the center of the pelvis is in the center of the Sigma-60 applicator. In the craniocaudal direction, the patient is positioned such that the tumor center is located 4 cm caudal to the center of the Sigma-60 applicator. The start-up settings for phase and amplitude are the same for every patient, namely (0,0) for phase and 100% amplitude for all BSD channels.

Optimization during treatment: The RESG state that in case of hotspot-related complaints, the preferred order of steering actions is: phase steering, amplitude steering and finally frequency steering. In addition, phase steering is thought to be more appropriate in case of pressure-like, deep-seated complaints and amplitude steering in case of burning, superficially located sensations. The power is only lowered when phase, amplitude and frequency steering proved ineffective. Besides avoiding and diminishing hotspot-related complaints, we also aim for a homogeneous intraluminal temperature distribution during treatment by means of phase and amplitude steering.[135]

6.2.5 Treatment approach using HTP-guided steering (HGS)

Preparation: Prior to the first hyperthermia treatment, a CT-scan was made of each patient lying in hyperthermia treatment position. All CT-scans were made using a

multislice CT-scanner (Siemens Somatom Sensation Open, Siemens Medical Solutions USA Inc., Malvern, Pennsylvania, United States) with a slice distance of 0.5 cm. The scanned length of the patient had to be at least 80 cm to cover the length of the Sigma-60 cm with 10 cm extra at each end (cranial and caudal). The methods employed for hyperthermia treatment planning have been described elsewhere in detail.[39, 47, 80, 100] After resampling the CT-data to 256 x 256 x 80 pixels, the following tissue types were segmented: tumor, muscle, fat, bone, liver, spleen, kidney, heart, lung, uterus, intestine, stomach, bubbles of air in the bowel system and vagina. Note that we segmented the actual anatomy instead of taking a single permittivity and conductivity as an average for the whole intestine in the pelvic region. The large vessels were not segmented separately but as muscle because of the lack of specific perfusion information and the fact that SAR and not temperature optimization was performed. The permittive and conductive properties assigned to the specific tissue types were derived from Gabriel et al. and are described in table 6.1 [48]. Segmentations were performed by an experienced physician (MF) who did all segmentations in order to promote uniformity. After construction of a tetrahedral model, the SAR distribution inside the patient was calculated using the finite element method (FEM)-module of Sigma HyperPlan (Dr. Sennewald Medizintechnik GmBh, Munich, Germany). Then this SAR distribution was optimized using a custom-made complaint adaptive power density optimization tool providing us with patient-specific optimal treatment settings to start a treatment.[47]

Patient positioning: For patient positioning during HGS treatments, the preferred craniocaudal position was derived from the CT-scan made for hyperthermia treatment planning similar to the currently used method. The anterior-posterior distances of the patient's contour to the water bolus were measured in the Sigma HyperPlan model and, as accurately as possible (preferably <1 cm)[39, 112-113] reproduced in the clinical setting using 2 ultrasound measurement probes integrated in the Sigma-60 ring. Before the first HGS-treatment, an initial SAR optimization was performed, providing us with patient-specific start-up settings for phased and amplitudes.

Optimization during treatment: During the HGS treatments, the actions that were taken upon hotspot-related complaints were not prescribed by the RESG, but the exact amplitude and phase settings were dictated by custom-made optimization software.[47] We needed to define specific hotspot-related regions in the model to allow for the limitation of SAR in that specific region, while still optimizing SAR in the tumor region. In case of a hotspot-related complaint in the abdomen, a constraint was assigned to the ventral abdominal muscles and new treatment settings were calculated with optimal power delivery to the tumor and minimal power to the ventral abdominal muscles.

Homogeneity of measured intraluminal temperatures was not a goal during these treatments.

Table 6.1: Dielectric parameters used for treatment planning[40, 48]

Tissue	ε_r	σ [S/m]	ρ(kg/m^3)
Fat	13	0.07	900
Muscle	69	0.70	1000
Bone	16	0.06	1600
Hammock support rods	1	0	1000
Tumor (=cervix)	69	0.70	1000
Bladder	24	0.29	1000
Heart	99	0.70	1000
Intestine	108	1.62	1000
Kidney	109	0.77	1000
Liver	75	0.46	1000
Lung	35	0.71	500
Spinal cord	6	0.04	1000
Spleen	101	0.77	1000
Stomach	82	0.89	1000
Uterus	69	0.70	1000
Vagina	69	0.70	1000

6.2.6 Statistical analysis

Prior to the start of the study, a power analysis showed that 36 patients would be needed to show a 0.3 ^{0}C difference in temperature measures with this double cross over design with a power (1-ß) of 80 % and a significance level (α) of 95 %.
First, we compared treatment parameters between the arms of the study using a T-test for two independent samples (comparison 1). This was done separately for period I (the 2nd and 3rd treatment) and II (the 4th and 5th treatment). The aim of this analysis was to assess whether a carry-over effect was present. In case no carry-over effect was present (i.e., no difference between the two randomization arms), the data were analyzed according to the cross over design of the study [112]. If a carry-over effect was present,

the data should be analyzed according to a standard parallel group design, i.e. restricted to the first episode of period I cq II.
According to the cross-over design, we compared the patient's first RESG-treatment with the patient's first HGS treatment and the patient's second RESG-treatment to the patient's second HGS-treatment using a paired T-test, disregarding the arm of randomization (comparison 2).
To test whether effect estimates differ between period I and II, a regression model was designed with treatment (RESG vs. HGS), and period (I vs. II) as covariates and an additional term for interaction between treatment and period (comparison 3).[176]
For all statistical analyses, STATA version 10.1 was used (StataCorp, Texas, United States). P-values below 0.05 were considered significant. For comparison 3, the possible correlation between measurements from the same patient in the course of her treatment was taken into account by including a random effect for the intercept in the models. This was done by using the xtmixed regression module of STATA.

6.3 Results

Patient- and tumor characteristics of the 36 patients included in this study are summarized in table 6.2. No significant differences were observed between the 2 arms as assessed using a T-test.
One patient did not receive any HGS-treatments because of a rapid deterioration of her clinical condition during treatment due to gastro-intestinal toxicity. In table 6.3, the model properties for each of the 35 remaining patients are summarized.
In table 6.4, the various outcome measures of this study are reported by type of treatment (RESG or HGS) for periods I and II and for arm A and B separately.

Table 6.2: Patient and tumor characteristic

		Arm A		Arm B	
FIGO stage	IB2	1	(5 %)	3	(19 %)
	IIA	0	(0 %)	1	(6%)
	IIB	6	(30 %)	3	(19 %)
	IIIA	2	(10 %)	1	(6 %)
	IIIB	6	(30 %)	1	(6 %)
	IVA	2	(10 %)	3	(19 %)
	IVB	3	(15 %)	4	(25 %)
WHO performance status	0	12	(65 %)	10	(69 %)
	1	7	(35 %)	5	(18 %)
	2	0	(0%)	2	(13 %)
Nodal status	Nx	9	(45 %)	4	(25 %)
	N0	3	(15 %)	7	(44 %)
	N1	8	(40 %)	5	(31 %)
Age	Mean (range)	60 (30 – 84)		55 (35 – 79)	

Legend: Arm A = 2nd and 4th hyperthermia treatment of the series with the aid of hyperthermia treatment planning guided steering (HGS). Arm B = 3rd and 5th hyperthermia treatment of the series with the aid of hyperthermia treatment planning guided steering. FIGO = International Federation of Gynaecology and Obstetrics

* FIGO IVB includes patients with para-aortic and / or supraclavicular metastasis

WHO = World Health Organisation

Nx = Lymph node status unknown

N0 = No pathological lymph nodes detected

N1 = Pathological lymph nodes detected

Table 6.3: Average model properties for all 35 patients who received HGS treatments

Patient	Number of tetrahedra	Maximum Edgelength of a tetrahedron		Minimum Edgelength of a tetrahedron		Tetrahedron volume	
	'# Tetras'	Mean (cm)	SD (cm)	[Mean (cm)	SD (cm)	Mean (cm)	SD (cm)
1	219262	3.48	1.97	1.81	1.14	4.13	10.18
2	234484	3.63	2.15	1.92	1.25	5.01	12.00
3	212570	3.80	2.14	2.01	1.24	5.31	12.00
4	197587	3.47	1.86	1.82	1.08	3.86	9.47
5	200939	3.51	1.98	1.84	1.15	4.22	10.19
6	198775	3.56	2.00	1.87	1.16	4.37	10.50
7	201501	3.45	1.92	1.80	1.12	3.94	9.69
8	182699	3.47	1.82	1.81	1.06	3.71	8.83
9	206770	3.36	1.83	1.75	1.07	3.58	9.04
10	223556	3.33	1.88	1.75	1.08	3.65	9.36
11	207982	3.26	1.71	1.69	1.00	3.13	8.05
12	200855	3.54	2.00	1.87	1.16	4.36	10.37
13	198907	3.30	1.76	1.72	1.03	3.30	8.33
14	201024	3.44	1.87	1.80	1.10	3.85	9.57
15	207030	3.48	1.96	1.82	1.15	4.15	10.07
16	233736	3.15	1.88	1.64	1.09	3.31	8.79
17	240469	3.25	1.97	1.69	1.15	3.73	9.84
18	353697	2.52	1.65	1.29	0.93	1.98	6.74
19	283914	2.70	1.73	1.38	1.00	2.33	7.17
20	250641	2.89	1.69	1.47	0.99	2.47	7.10
21	204519	3.29	1.80	1.72	1.05	3.38	8.58
22	296232	2.65	1.78	1.37	1.02	2.35	7.43
23	278368	2.95	1.89	1.50	1.10	3.00	8.71
24	266723	2.85	1.77	1.44	1.03	2.58	7.53
25	275863	2.88	1.81	1.46	1.06	2.72	7.97
26	259504	2.98	1.83	1.52	1.08	2.94	8.29
27	268183	2.94	1.80	1.49	1.06	2.80	8.12
28	268499	2.84	1.80	1.44	1.06	2.66	7.81
29	301996	2.87	1.88	1.45	1.10	2.90	8.73
30	366561	2.58	1.75	1.35	0.99	2.30	7.67
31	273816	3.11	1.92	1.58	1.12	3.33	9.35
32	302384	2.64	1.77	1.36	1.01	2.34	7.39
33	269534	2.94	1.76	1.49	1.03	2.71	7.84
34	288728	2.88	1.72	1.46	1.01	2.55	7.66
35	366685	2.62	1.63	1.37	0.92	2.11	7.11

6.3.1 Comparison 1 : Cross over effect

From table 6.2 we can derive that no carry-over effect is present in this study as the differences between arm A and arm B are insignificant.

6.3.2 Comparison 2 : RESG versus HGS effect

When we analyze our data according to arm and period, it becomes clear that HGS performs well in period I, but it performs significantly less well during period II (table 6.4, figure 6.1).
In period I only the duration of off-switches is significantly longer in the HGS-treatments with a difference of 2.1 minutes ($p = 0.03$), indicating less efficient coping with hotspot-related complaints during HGS-treatments. Further, there were favorable trends towards a longer duration of treatment, lesser number of off-switches and higher net integrated power and higher TRISE during HGS-treatments, although these trends were not significant (table 6.4, figure 6.1).
The analysis for period II shows a different picture. The HGS-treatments in the second period show significantly lower thermal dose (figure 6.1, table 6.4). The average CEM43T90 was 0.57 min for the RESG-treatments in period II and 0.38 for the HGS-treatments in that period. For the average TRISE, a similar significant difference was found; 3.26 ^{0}C for RESG-treatments and 2.89 ^{0}C for HGS-treatments in period II (figure 6.1, table 6.4). Further, intraluminal temperatures were significantly lower in period II (T20 with a 0.4 ^{0}C difference, T50 with 0.4 ^{0}C and T90 with 0.3 ^{0}C, figure 6.1). Figure 6.2 illustrates the variation in T50 per period and per patient. Acute toxicity seems less well handled in period II (number of off-switches was increased by 3, duration of off-switches was prolonged with 4,3 minutes) and net integrated power decreased (279 kJ more was administered during RESG-treatments).

6.3.3 Comparison 3 : Differences between treatment period and type of treatment

The interaction between treatment period and type of treatment is significant for TRISE ($p = 0.001$), T20 ($p = 0.002$), T50 ($p = 0.001$) and T90 ($p = 0.001$), suggesting a significant difference in period II compared to period I.

Table 6.4:Estimate (standard deviation) for the outcome measures per arm of the study

Period I					Period II		
Variable		RESG	HGS	**total**	RESG	HGS	**total**
Duration (min)	**Arm A**	88.2 (8.3)	89.5 (1.7)	88.8 (6.0)	88.4 (6.0)	90.0 (0.9)	89.0 (4.3)
	Arm B	86.6 (8.9)	89.7 (1.2)	88.1(6.5) ∞ $^{0.6218}$	86.94 (7.8)	85.9 (13.0)	86.5 (10.5) ∞ $^{0.1626}$
	total	87.3 (8.6)	89.5 (1.6) $^{‡\ 0.1445}$	88.5 (6.2)	87.7 (6.9)	88.1 (8.6) $^{‡\ 0.7508}$	87.9 (7.7)
CEM43T90 (min)	**Arm A**	0.61 (0.80)	0.73 (0.64)	0.67 (0.71)	0.55 (0.53)	0.42 (0.42)	0.48 (0.48)
	Arm B	0.69 (1.10)	0.55 (0.48)	0.62 (0.85) ∞ $^{0.7853}$	0.64 (0.44)	0.33 (0.31)	0.49 (0.41) ∞ $^{0.9826}$
	total	0.64 (0.94)	0.65 (0.57) $^{‡\ 0.9110}$	0.65 (0.77)	0.57 (0.48)	0.38 (0.37) $^{‡\ \mathbf{0.0124}}$	0.49 (0.45)
TRISE (^{0}C)	**Arm A**	3.33 (0.92)	3.40 (0.63)	3.37 (0.78)	3.22 (0.83)	2.97 (0.80)	3.10 (0.81)
	Arm B	2.98 (0.80)	3.22 (0.67)	3.10 (0.73) ∞ $^{0.1493}$	3.34 (0.71)	2.78 (0.73)	3.08 (0.76) ∞ $^{0.9149}$
	total	3.17 (0.89)	3.33 (0.64) $^{‡\ 0.1544}$	3.25 (0.77)	3.26 (0.77)	2.89 (0.76) $^{‡\ \mathbf{0.0044}}$	3.09 (0.79)
T20 (^{0}C)	**Arm A**	40.9 (0.8)	40.9 (0.7)	40.9 (0.7)	40.9 (0.8)	40.6 (0.8)	40.7 (0.8)
	Arm B	40.7 (0.9)	40.8 (0.7)	40.7 (0.8) ∞ $^{0.2741}$	41.0 (0.8)	40.4 (0.7)	40.7 (0.8) ∞ $^{0.9385}$
	total	40.8 (0.9)	40.9 (0.7) $^{‡\ 0.6452}$	40.8 (0.8)	40.9 (0.8)	40.5 (0.8) $^{‡\ \mathbf{0.0006}}$	40.7 (0.8)
T50 (^{0}C)	**Arm A**	40.4 (0.8)	40.4 (0.6)	40.4 (0.7)	40.3 (0.8)	40.0 (0.8)	40.1 (0.8)
	Arm B	40.1 (0.9)	40.2 (0.7)	40.2 (0.8) ∞ $^{0.2499}$	40.5 (0.7)	39.9 (0.6)	40.2 (0.7) ∞ $^{0.6547}$
	total	40.3 (0.9)	40.3 (0.7) $^{‡\ 0.4093}$	40.3 (0.8)	40.4 (0.8)	40.0 (0.7) $^{‡\ \mathbf{0.0009}}$	40.2 (0.8)
T90 (^{0}C)	**Arm A**	39.5 (0.8)	39.7 (0.6)	39.6 (0.7)	39.4 (0.8)	39.2 (0.8)	39.3 (0.8)
	Arm B	39.4 (0.8)	39.5 (0.7)	39.4 (0.8) ∞ $^{0.4203}$	39.7 (0.6)	39.1 (0.6)	39.4 (0.6) ∞ $^{0.5859}$
	total	39.4 (0.8)	39.6 (0.6) $^{‡\ 0.1033}$	39.5 (0.7)	39.5 (0.7)	39.2 (0.7) $^{‡\ \mathbf{0.0051}}$	39.4 (0.7)
NOS	**Arm A**	13.2 (5.2)	15.3 (6.9)	14.2 (6.1)	13.8 (4.9)	16.1 (6.1)	14.9 (5.6)
	Arm B	14.0 (5.5)	14.3 (6.4)	14.1 (5.9) ∞ $^{0.9469}$	14.2 (6.7)	18.6 (6.8)	16.3 (7.0) ∞ $^{0.3528}$
	total	13.6 (5.3)	14.9 (6.6) $^{‡\ 0.2754}$	14.2 (6.0)	14.1 (5.7)	17.1 (6.4) $^{‡\ \mathbf{0.0245}}$	15.5 (6.2)
DOS (min)	**Arm A**	8.4 (3.7)	10.5 (4.9)	9.4 (4.4)	8.9 (3.1)	12.6 (6.4)	10.8 (5.3)
	Arm B	8.8 (3.9)	10.8 (5.8)	9.7 (5.0) ∞ $^{0.7770}$	7.5 (4.1)	12.6 (4.8)	10.0 (5.1) ∞ $^{0.5328}$
	total	8.5 (3.8)	10.6 (5.3) $^{‡\ \mathbf{0.0300}}$	9.6 (4.6)	8.3 (3.6)	12.6 (5.7) $^{‡\ \mathbf{0.0002}}$	10.4 (5.2)
TTFC (min)	**Arm A**	26.4 (11.2)	28.8 (11.1)	27.6 (11.1)	24.9 (10.3)	28.2 (14.7)	26.6 (12.6)
	Arm B	25.6 (13.3)	22.6 (8.9)	24.2 (11.3) ∞ $^{0.2106}$	22.5 (9.7)	20.5 (6.2)	21.5 (8.1) ∞ $^{0.0591}$
	total	26.0 (12.2)	26.1 (10.5) $^{‡\ 0.9890}$	26.0 (11.2)	23.8 (10.1)	24.8 (12.2) $^{‡\ 0.6455}$	24.3 (11.1)
NIP (kJ)	**Arm A**	3028 (651)	2972 (504)	3000 (575)	3051 (486)	2776 (480)	2913 (497)
	Arm B	2890 (692)	3009 (601)	2948 (642) ∞ $^{0.7166}$	2919 (548)	2602 (695)	2766 (633) ∞ $^{0.2741}$
	total	2941 (655)	2988 (539) $^{‡\ 0.6080}$	2977 (601)	2987 (517)	2702 (579) $^{‡\ \mathbf{0.0002}}$	2849 (561)

‡ = p-value for comparison of RESG vs HGS, disregarding the arm of the study

∞ = p-value for comparison of arm 1 vs arm 2, disregarding the number of the treatment

Legend:

Period I = first part of hyperthermia treatment series, ie treatments 2 and 3

Period II = second part of hyperthermia treament sereis, ie treatments 4 and 5

RESG = currently used treatment approach following the Rotterdam Empirical Steering Guidelines [14]

HGS = treatment approach using Hyperthermia treatment planning Guided Steering

Duration = overall duration of treatment

CEM43T90 = cumulative equivalent minutes of T90 at 43 ^{0}C as described by Fatehi et al.[24]

TRISE = a local custom-made thermal dose parameter based on T50 and the duration of heating[11]

T20 = temperature exceeded by 20 % of the monitored sites in bladder, vagina and rectum

T50 = temperature exceeded by 50 % of the monitored sites in bladder, vagina and rectum

T90 = temperature exceeded by 90 % of the monitored sites in bladder, vagina and rectum

NOS = number of off-switches during treatment, indicating the amount of treatment-limiting hot spots

DOS = duration of off-switches during treatment, indicating the severity of treatment-limiting hot spots

TTFC = time to first complaint, or duration from start of treatment until the patient has her first hot spot related complaint, indicating the quality of optimisation

NIP = Net Integrated Power as described by Fatehi et al. [24]

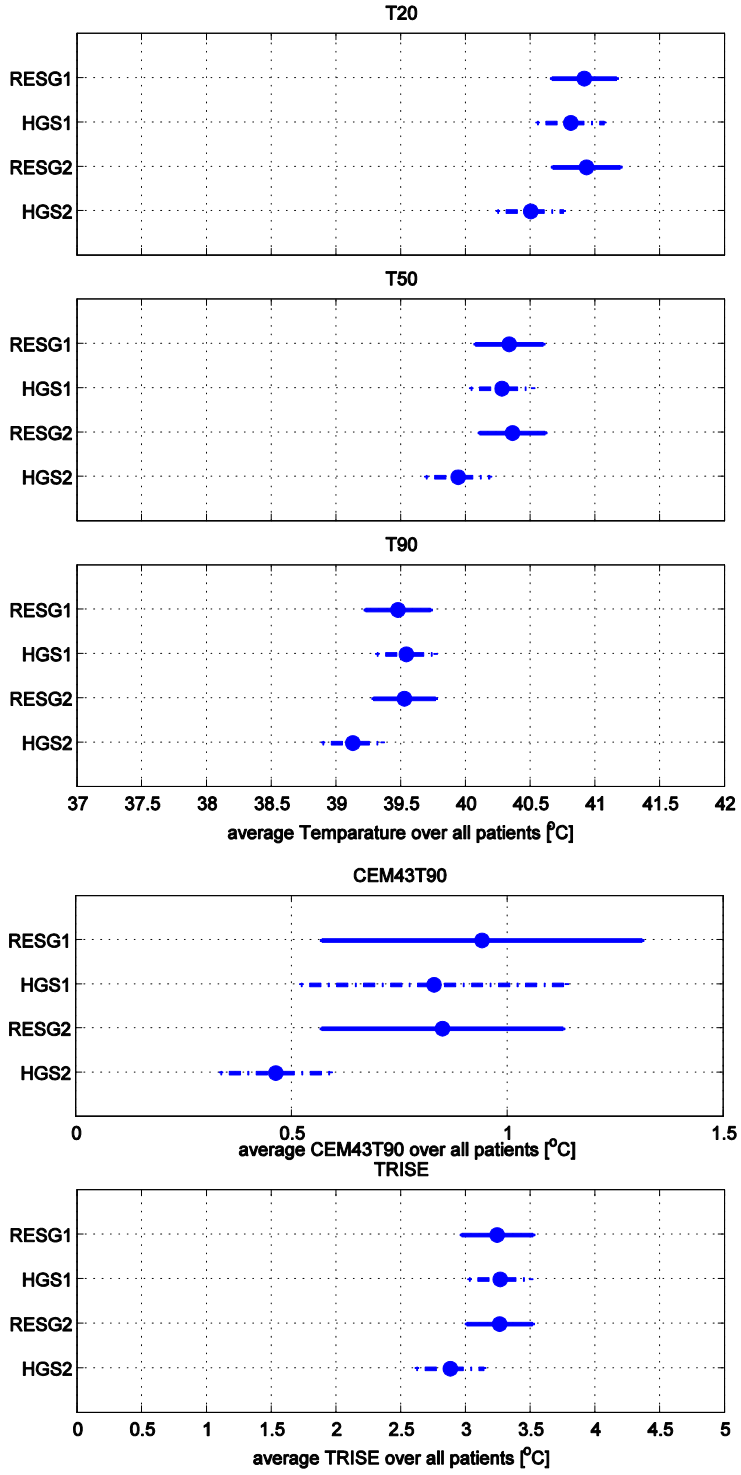

Figure 6.1: Outcome per period and per treatment type (with 95% confidence intervals)

Legend:

Period I = first part of hyperthermia treatment series, ie treatments 2 and 3

Period II = second part of hyperthermia treament series, ie treatments 4 and 5

RESG1 = currently used treatment approach following the Rotterdam Empirical Steering Guidelines[135] during period I,

HGS1 = treatment approach using Hyperthermia treatment planning Guided Steering during period II,

RESG2 = currently used treatment approach following the Rotterdam Empirical Steering Guidelines[135] during period I,

HGS2 = treatment approach using Hyperthermia treatment planning Guided Steering during period II,

CEM43T90 = cumulative equivalent minutes of T90 at 43 ^{0}C in minutes,

TRISE = a local custom-made thermal dose parameter based on T50 and the duration of heating in ^{0}C[11],

T20 = temperature exceeded by 20 % of the monitored sites in bladder, vagina and rectum,

T50 = temperature exceeded by 50 % of the monitored sites in bladder, vagina and rectum,

T90 = temperature exceeded by 90 % of the monitored sites in bladder, vagina and rectum

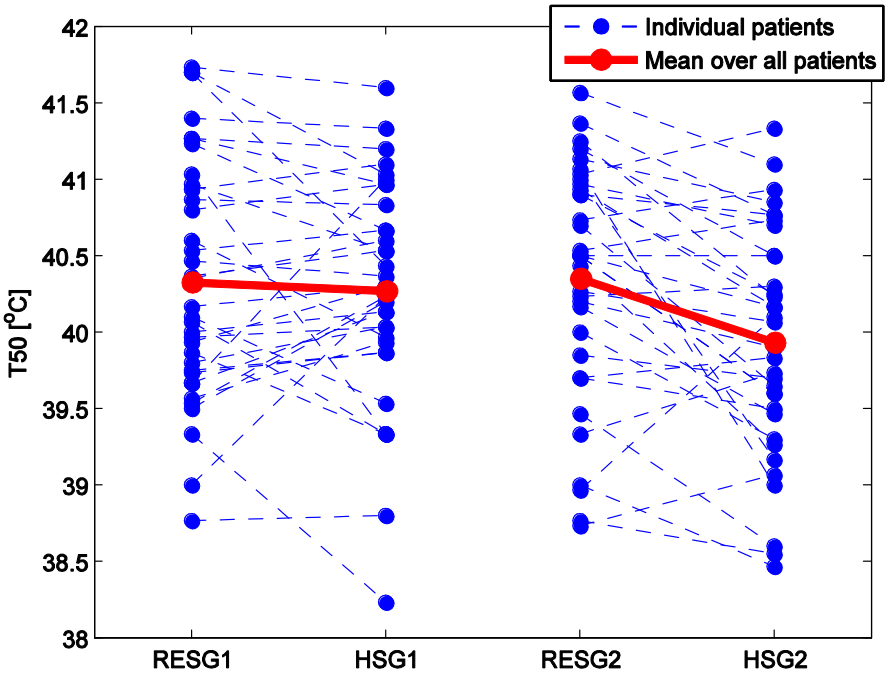

Figure 6.2: T50 per period and per treatment type, interpatient variation

Legend:
RESG1 = currently used treatment approach following the Rotterdam Empirical Steering Guidelines[135] during period I,
HGS1 = treatment approach using Hyperthermia treatment planning Guided Steering during period I,
RESG2 = currently used treatment approach following the Rotterdam Empirical Steering Guidelines[135] during period II,
HGS2 = treatment approach using Hyperthermia treatment planning Guided Steering during period II,
T50 = temperature exceeded by 50 % of the monitored sites in bladder, vagina and rectum

6.4 Learning effects encountered during study

6.4.1 Advanced understanding of applying HTP optimization

During the study it became clear that our primary optimization method (Opt1 from Canters et al.)[20] insufficiently dealt with hotspot-related complaints to allow for a meaningful and swift reaction to clinical situations. We therefore adjusted the optimization method to not only optimize power deposition in the tumor, but also to minimize power deposition in a specific hotspot-related area in the model while maximizing power deposition in the tumor (Opt2 from Canters et al.).[47] As the first

results of Opt2 became known and seemed promising, we switched from Opt1 to Opt2. As a result, the first 5 patients who entered the study were treated using Opt1 during the HGS-treatments. The other 30 were treated using Opt2.

6.4.2 Improved patient positioning

Another problem we encountered during the course of the study was that the accuracy of currently used positioning techniques was somehow inadequate for use in conjunction with a HGS. When trying to reproduce the patient's position from the CT-based computer model to the actual patient position in the Sigma-60 applicator, we encountered problems with patients' legs touching the outer rim of the Sigma-60 when the anterior-posterior position measured in the model was copied to clinical situation. A closer look at our current patient positioning protocol in clinical practice and the protocol used for HTP CT-scans, revealed that most patients were positioned much more cranially during the CT-scan than during treatment. This problem with patient positioning was solved when specific attention was paid to the craniocaudal positioning of the patient in the BSD sling, no more problems were encountered with patient positioning.

6.4.3 Outcome for patients who were correctly positioned

When repeating comparison 2 for patients who were correctly positioned, no differences in outcome measures were observed when comparing them to the results of comparison 2 for the whole group of patients. For period I only the duration of off-switches is significantly longer for HGS-treatments ($p = 0.03$), all other differences were not significant. For period II, again HGS tends to lead to more and longer off-switches, lower thermal dose and lower temperatures compared to RESG. The same outcome we observed in the whole group, namely that results are similar for HGS and RESG for period I, but during period II HGS performs less well, also holds true for this subgroup.

6.5 Discussion

In this article we present our first experience with taking hyperthermia treatment planning guided steering, or HGS, to the clinic. HGS proved to be feasible in every day clinical practice. Early on in a treatment series HGS performs as well as RESG and in view

of the fact that the RESG were developed based on years of clinical experience, this is a very worthwhile result.

During the first part of a treatment series (period I, 2nd and 3rd treatment) only the duration of off-switches, a measure for treatment-limiting hotspots, was significantly longer during HGS treatments. During each hyperthermia treatment, the power is turned off when a patient shows signs or symptoms indicating a hotspot-related complaint. During RESG treatments, the power is turned on again when the patient indicates the complaint has subsided. During HGS treatments, the power was turned on again when the complaint has subsided and new treatment settings were calculated with a custom-made add-on to Sigma HyperPlan.[47] The calculation time required by Sigma HyperPlan could well explain the difference in the duration of off-switches. For thermal dose parameters, maximum temperature and time to first complaint, a slight, non-significant difference in favor of HGS could be found for period I.

The analysis for period II (4th and 5 th treatment of the series) shows a more complicated picture. HGS treatments now show significantly lower power, intraluminal temperatures (T20 with 0.4 ^{0}C, T50 with 0.4 ^{0}C and T90 with 0.3 ^{0}C) and thermal dose (TRISE with 0.37 ^{0}C and CEM43T90 with 0.19 min). Whether these differences have a clinical meaning, remains unsure. Our previous thermal dose analysis showed a significant correlation between thermal dose parameters and treatment outcome, but with great dispersion of the data.[33] For intraluminal temperature measures, no significant relationship was found for various outcome measures. Further, it remains questionable whether intraluminal temperatures represent intratumoral temperatures as well in more tumor-selective heating (HGS) as in the more empirical regional heating that is obtained using the RESG. We must realize that changing heating strategy may cause historical correlations are no longer valid, e.g. Fatehi et al. showed good correlation between intraluminal and intratumoral temperatures, i.e. when treatment settings are adjusted to obtain a homogeneous intraluminal temperature distribution.[174] During HGS treatments, treatment settings are not adjusted to aim for a homogeneous intraluminal temperature distribution, but to obtain maximum SAR in the tumor. If this is done sufficiently selective, this could paradoxally cause a decrease of intraluminal temperatures as a consequence of the more targeted treatment strategy.

In our previous thermal dose analysis it was already apparent that patients become harder to heat as treatment progresses (figure 6.3).[33] A possible explanation for this finding is that as treatment progresses patient tolerance decreases due to the cumulating fractions of radiotherapy administered; acute radiation-induced toxicity and fatigue set in. Also, the applications of brachytherapy are usually administered in the 4th and 5th

week of treatment, greatly increasing the sensitivity and tenderness of a patient's pelvic area. As this previously found difficulty with heating a patient as treatment progresses, is also expected to play a role in this study, we decided to introduce the analysis per period (period I and period II) in order to account for this. The difference between RESG and HGS becomes much more apparent in period II, which could be explained by the fact that RESG is a much simpler optimization model compared to HGS it leaves more room for individual interpretation, making it more flexible and better equipped to deal with deceasing patient tolerance. Another possible explanation could be that somehow patient anatomy changes during treatment. The tumor shrinks, patients may loose weight, and the chemical balance in the intestine may change due to diarrhea. All of these factors can cause changes in the patient and energy- and temperature distribution and are not present in the computer model or the treatment plan. These factors could also explain why HGS performs less well as treatment progresses.

Although the results of this trial show that HGS in its current status can be of merit when applying deep hyperthermia, the 0.3 ^{0}C improvement with HGS this study was designed to detect, could not be found. Since the study closed, we performed a number of theoretical studies that showed that with optimization using the Sigma-60 the maximum SAR improvement that can be reached is within the order of 5 %. Using the bioheat equation, this 5 % SAR should lead to a rise in temperature of 0.2 ^{0}C, an increase that is within the resolution of our currently used thermometry.[40, 48] In retrospect, our estimated 0.3 ^{0}C profit using HTP-guided steering may have been too high a goal with the hyperthermia equipment we used.

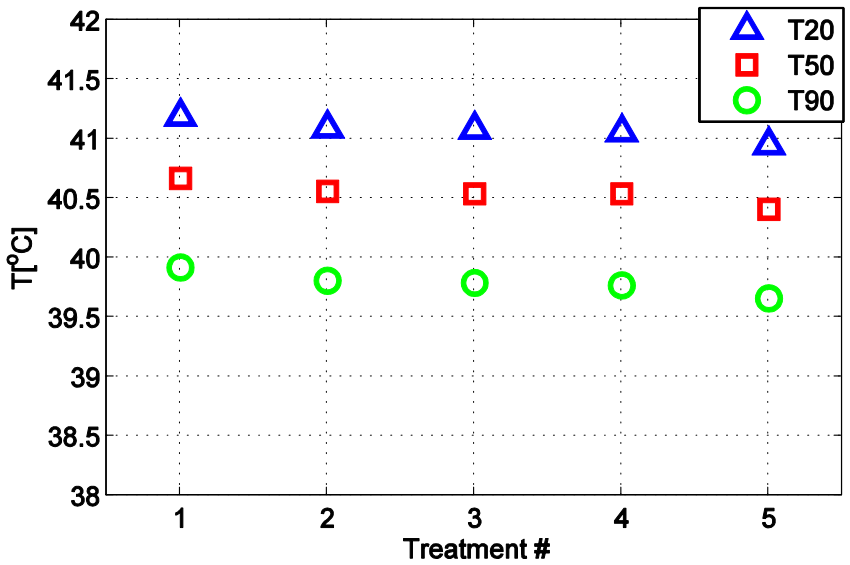

(a)

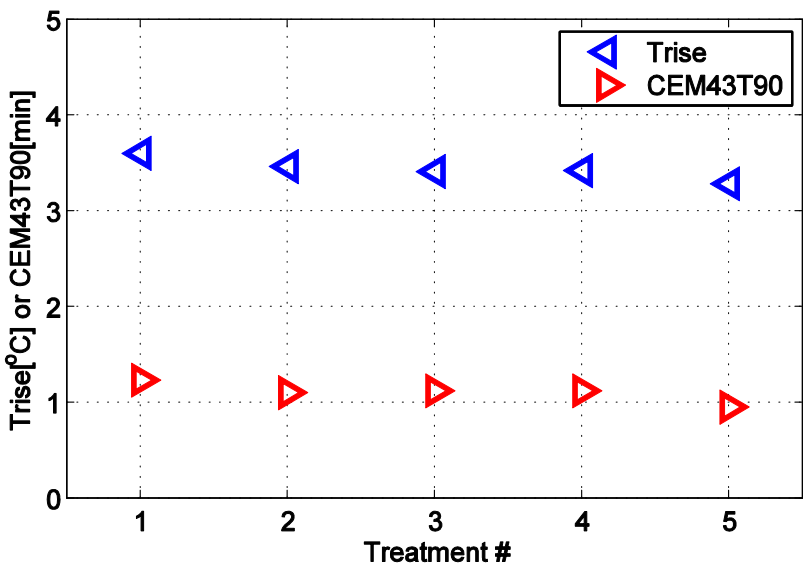

(b)

Figure 6.3: Evolution of temperatures (a) and thermal dose (b) over treatment series based on the data of Franckena et al [33]

Legend:

CEM43T90 = cumulative equivalent minutes of T90 at 43 °C,
TRISE = a local custom-made thermal dose parameter based on T50 and the duration of heating,
T20 = temperature exceeded by 20 % of the monitored sites in bladder, vagina and rectum,
T50 = temperature exceeded by 50 % of the monitored sites in bladder, vagina and rectum,
T90 = temperature exceeded by 90 % of the monitored sites in bladder, vagina and rectum

6.5.1 Lessons learned from the clinical implementation of HTP-guided steering

As to be expected when putting any new technique to clinical use, we encountered a number of challenges. Early on, we noticed that our first optimization routine could insufficiently cope with hotspot-related complaints reported by the patients. This prompted the development of a new optimization routine that did not only maximize power deposition in the tumor, but also minimize power in a specific hotspot-related area.[173]
We also encountered problems in patient positioning, which we were able to overcome with the currently available positioning techniques, although we would like to stress the importance of further improvements needed in this area. Of course, a patient model and optimization routine can be perfect, but when correct patient positioning fails, these are useless.
A much mentioned drawback of hyperthermia treatment planning in general is the time-consuming nature of the process. In this study, one of the rules was that the CT-scan made for hyperthermia treatment planning had to be made at least 3 days before the first study treatment took place. As we gained more experience with the segmentation process, we were able to improve speed. From 8-9 hours per CT-scan in the beginning to 3-4 hours near the end of the study. This may be further improved in the future using atlas-based segmentation. On average, calculation time was 15 hours, a value which may change in time depending on computer speed and segmentation resolution.

6.5.2 Technical limitations

This study was designed to evaluate the efficacy of currently available hyperthermia treatment planning possibilities in the Sigma-60 applicator, with its inherent limitations. From the study by Canters et al. the potential of HGS to optimize the SAR distribution in the Sigma-60 appears to be limited, due to the small amount of degrees of freedom.[112] The potential appearing from this model study could easily be lost due to inaccuracies in the HTP software, the dielectric constants and in the translation from model to clinic. Two important limitations of the system we used in this study are the lack of optimal steering possibilities and the unknown influence of transforming networks. Also, the focus that is created by the BSD-2000 system and the Sigma-60 applicator is quite large and with extreme settings its performance decreases.

6.5.3 Clinical implications

We have no doubt that hyperthermia treatment planning is a necessary and inevitable next step in the development of hyperthermia as an oncological treatment modality. It enables patient-specific optimization of treatment, which should eventually lead to a more standardized application of hyperthermia and better treatment quality. For now, we recommend the use of HGS for clinicians with no or limited experience in the field of hyperthermia as this study shows that with the use of HGS clinical results can be obtained that are approaching our results with 18 years of experience.
Hyperthermia treatment planning can also be a helpful tool in the evaluation of clinical indications; it may help clinicians decide in advance whether a tumor at a specific location can be heated to therapeutic temperatures or not. Further, it can be a great aid in education and training of new hyperthermia staff.
It can also be a helpful tool in the development of new hyperthermia systems. When a hyperthermia treatment planning system is used to develop a new system the technical capabilities can be made better in line with the clinical demands.
Last but not least, hyperthermia treatment planning can be an important tool in more controlled treatment quality.

6.5.4 Future directions

We found that the procedure of online HTP-guided steering is feasible. For maximal exploitation of its possibilities, however, better control and understanding of several patient, tumor and technical parameters is required.
For example, it is mandatory to get more insight into relation between intraluminal temperatures with intratumourally temperature. One could argue that better focusing of energy in the target area could lead to a decline in intraluminal temperatures for some patients, and an increase in others, depending on patient anatomy and tumor vasculature and shrinkage.
Another point that requires further investigation is the relationship between a patient's hotspot-related complaint and a hotspot in the Sigma HyperPlan model, as temperature causes hotspots and not SAR, on which we optimized. This could, in part, explain our difficulties in clearing hotspot-related complaints during the HGS-treatments. In addition, the indication of hotspot-related complaints by a patient is subjective by definition and in our experience there is great variation in how well patients are able to describe sensations in their body during hyperthermia.

6.6 Conclusion

In spite of the problems we encountered during this study and the inherent limitations due the equipment and the current state of hyperthermia treatment planning, HGS performs equally well in treatment two and three when compared to the RESG based on our two decades of clinical experience. This study has been very helpful in identifying some of the challenges and flaws that warrant further investigation in the near future, such as patient positioning and the prevention of hotspot-related complaints. With the progress that has been made during this study, we hope to perfect the principle of hyperthermia treatment planning guided steering in the near future.

7 Optimizing deep hyperthermia treatments: Are locations of patient pain complaints correlated to modeled SAR peak locations?

This chapter was published as:

Canters RAM, Franckena M, Van der Zee J, Van Rhoon GC. Optimizing deep hyperthermia treatments: Are locations of patient pain complaints correlated to modeled SAR peak locations? Phys Med Biol 2011 56(2): 439-451

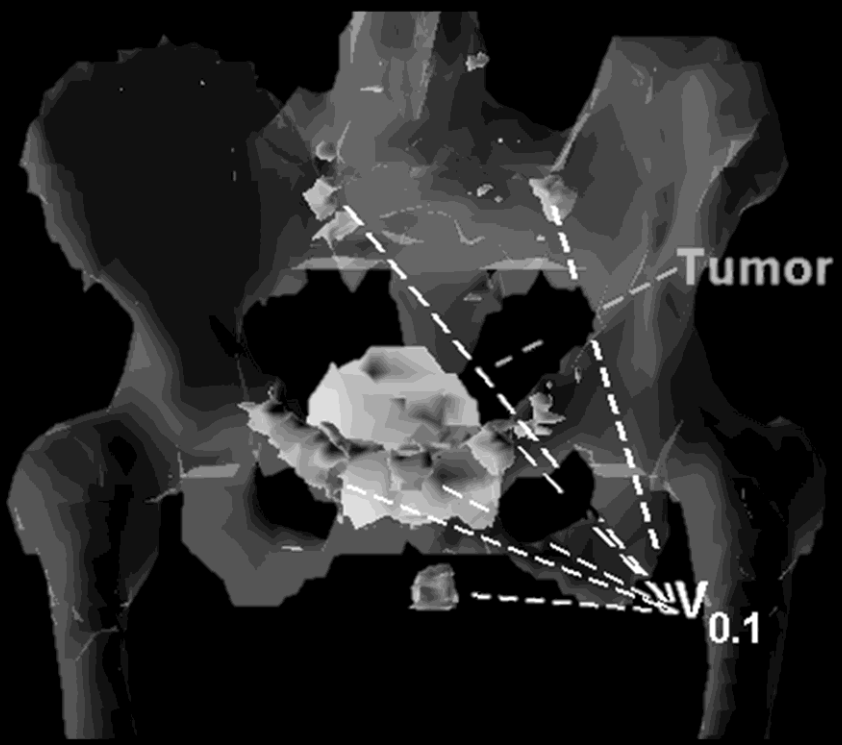

Abstract

Purpose: During deep hyperthermia treatment, patient pain complaints due to heating are common when maximizing power. Hence, there exists a good rational to investigate whether a the location of predicted SAR peaks by hyperthermia treatment planning (HTP) are correlated to the locations of patient pain during treatment.
Methods: A retrospective analysis was performed, using the treatment reports of 35 patients treated with deep hyperthermia controlled by extensive treatment planning. For various SAR indicators, the average distance from a SAR peak to a patient discomfort location was calculated, for each complaint.
Results: Investigated $V_{0.1\ closest}$ (i.e. the part of the 0.1^{th} SAR percentile closest to the patient complaint) performed the best, and leads to an average distance between SAR peak and complaint location of 3.9 cm. Other SAR indicators produced average distances that were all above 10 cm. Further, the predicted SAR peak location with $V_{0.1}$ provides a 77% match with the region of complaint.
Conclusions: The current study demonstrates that HTP is able to provide a global indication of the regions where hotspots during treatment will most likely occur. Further development of this technology is necessary in order to use HTP as a valuable tool for objective and advanced SAR steering. The latter is especially valid for applications that enable 3D SAR steering.

7.1 Introduction

In many hospitals where hyperthermia is added to radiotherapy and/or chemotherapy, electromagnetic fields are used for heating. Loco-regional deep hyperthermia is usually applied by a phased array applicator using constructive interference to deposit sufficient energy at depth, for example for tumours located in the lower pelvis [143] or the head and neck region [74]. Control of the electromagnetic heating of the tumour is realized by changing amplitudes and phases of the signal on pairs of antennas. There exists a broad consensus that the clinical efficacy of a hyperthermia treatment is correlated to the applied thermal dose [26-33]. Hyperthermia treatment planning (HTP) is considered an essential tool to guide SAR steering and to increase the thermal dose [47, 158]. In a recently published patient study on the effectiveness of HTP in deep hyperthermia treatments, Franckena et al. showed that the use of HTP as an objective guide for SAR steering during patient treatments leads to temperature results comparable to the conventional, i.e. subjective, method to control SAR steering during the treatment [108, 135].

Optimization of the SAR distribution in HTP guided steering essentially consists of maximizing SAR in the tumour, and minimizing SAR peaks in the healthy tissue, in the expectation that this leads to maximization of the tumour temperature. Deep hyperthermia treatments are often limited by hotspots[124, 158]. The treatment strategy in Rotterdam is always to heat up to the discomfort limit, and keeping the RF power as high as possible. Therefore, heat induced discomfort in patients (further referred to as complaints) is common. Accurate prediction of SAR peaks that would lead to patient complaints would offer an elegant method to prevent the occurrence of such complaints. This requires however, that a high correlation exists between the predicted SAR peaks and the location of patient complaints. Therefore, this study aims at assessing whether predicted SAR peak locations correlate with the locations of the patient complaints. If so, this enables us to use HTP predicted SAR peak locations as *a-priori* indicators for the occurrence of patient complaints during treatment. This study is a logical follow-up of the previously mentioned study of [108]. Further, the translation from model to clinic is very important when using HTP models. Hence, a sensitivity analysis of the HTP predictions is performed for factors that may determine the quality of this translation: patient positioning, signal of the antennas, dielectric properties, and water bolus shape. Water bolus shape is expected to influence SAR patterns [177], but is not included in this study.

7.2 Materials and methods

7.2.1 Tools

The HTP model Sigma Hyperplan and model generation

Electromagnetic (EM) field calculations for 3D patient models are performed in Sigma Hyperplan using the finite element method (FEM) (Dr. Sennewald Medizintechnik GmbH, München, Germany). The workflow for this modelling has been described extensively before [39]; [100]. On average, the models in this study consisted of 220,000 tetrahedra, with edge lengths between 0.3 and 2.5 cm and with the densest grid near the antennas and in the pelvic area. The Sigma Hyperplan models have demonstrated to be reliable in studies that reported similar numbers of tetrahedral as used in this study [39, 100, 113]. Temperature calculations, based on the Pennes bioheat equation, are calculated with the SAR distribution as input.

The BSD 2000 treatment system

All patients that were analysed in this study were treated for primary cervical cancer in the BSD Sigma 60 applicator [34, 140, 143] (BSD medical corporation, Salt Lake City, USA). The Sigma 60 applicator consists of a ring of 8 dipole antennas that are coupled in 4 channels of paired dipole antennas. Due to the design of the Sigma 60 applicator, i.e. all antennas in one ring in the XY-plane, steering of the electromagnetic field is restricted to the lateral (X) and ventral-dorsal (Y) directions. In addition, physically moving the Sigma 60 applicator in the Z-direction provides a third, limited degree of freedom to control the SAR pattern. Amplitude and phase of the signals that are fed into each antenna can be modified to control the interference pattern of the radiofrequency-field (see figure 7.1).

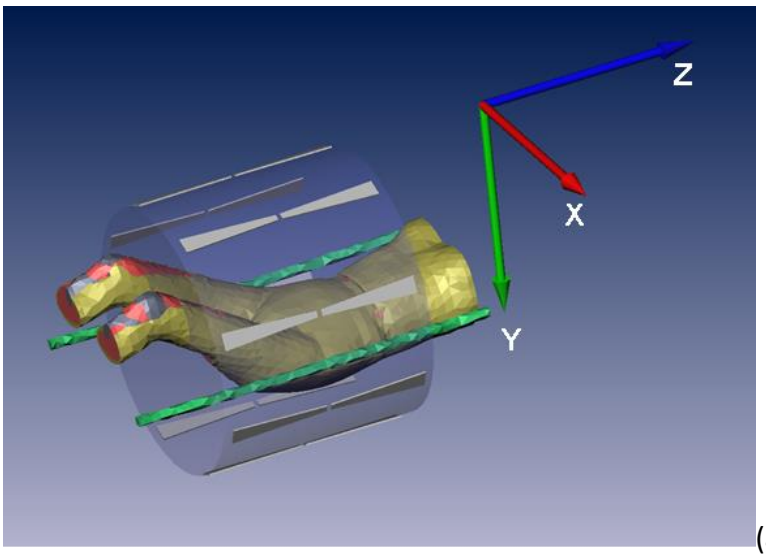

(a)

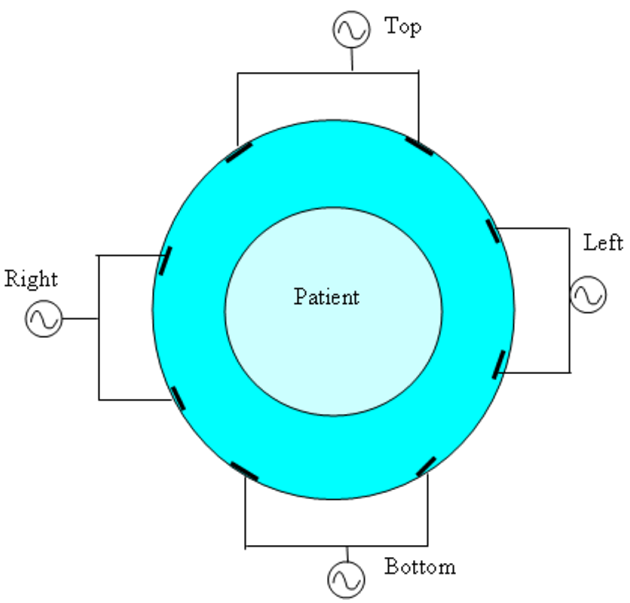

(b)

Figure 7.1. Patient model plus the BSD Sigma 60 applicator with coordinate axes as shown in the graphical user interface of Sigma Hyperplan. The eight dipole antennas are visible. (a) Axial view from the caudal direction of the Sigma 60 applicator, with the four channels, each connected to two antennas (b)

7.2.2 Methods

Prediction of hotspots by HTP models

The anonymized treatment records of 35 patients with locally advanced cervical cancer were analyzed retrospectively in this study. For patient details, see [108]. The considerations regarding our HTP based optimization of the SAR distribution in a patient are extensively described in [47]. For each patient, a HTP model was constructed using a hyperthermia specific CT-scan, i.e. the CT was obtained with the patient positioned in a similar sling as used in the BSD2000 system. During the treatment, each time the heat level exceeded the patient's tolerance, this was registered in a computer database according to figure 7.2, along with the amplitude and phase settings that were in effect. In this retrospective study, HTP is used to reproduce the SAR distribution for the settings that were in effect during each patient complaint. Subsequently, the indicated complaint locations are matched with the location of the nearest SAR peak predicted by the HTP-modeling. Since detailed positioning data and complaint registration are available only for the HTP guided treatments (two of five treatments per patient), only these treatments are analyzed.

Patient complaints

For the registration of patient complaints during treatment, the patient body was subdivided in different regions (see figure 7.2) considering the precision of the patients' ability to locate the pain and to communicate this to the clinical staff. We have chosen a simple approach of a 'top, bottom, left, right' division of the body in the pelvic region, with slightly smaller regions in the genital area, where the patient can localize complaints more accurately.

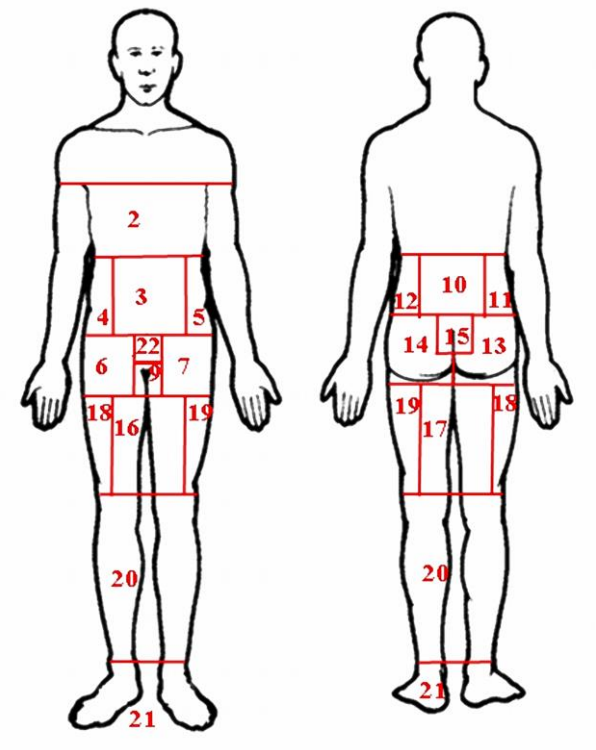

Figure 7.2 Predefined complaint regions

Table 7.1: List of SAR peak indicators .[45]

Indicator	Description
SAR_{max}	Location of maximum SAR
$SAR10g_{max}$	Location of the maximum of the 10g averaged SAR
V_x, with x [0.01, 0.05, 0.1, 0.5, 1, 5]	Location of the largest sub volume of V_x, with V_x the volume where SAR>SARx, i.e. the *x* percent of the patient volume with the highest power absorption.
Average SAR per region	Region with the highest average SAR. The centre of this region is used as hotspot location.
ρ_{HS} V_x, with x [0.01, 0.05, 0.1, 0.5, 1, 5]	Location of the maximum SAR peak density (the largest portion of V_x in a 5cm diameter sphere), with V_x the SAR peak volume
$V_{x\ closest}$ with x [0.01, 0.05, 0.1, 0.5, 1, 5]	Location of the closest SAR peak with regard to the patient complaint
T_{max}	Location of the temperature maximum

Assessment of different SAR peak indicators

Table 7.1 provides a list of all SAR peak indicators.[45] that have been analyzed on their correlation with the location of complaints as identified by the patient. Table 7.1 List of SAR peak indicators .[45]
As an example, figure 7.3 shows the SAR peak indicative$V_{0.1}$. Note that the SAR peak volume is distributed over various sub volumes.
For each SAR peak indicator (table 7.1), the distance is calculated between the complaint location (i.e. the volumetric centre of the complaint region see figure 7.2) and all SAR peak sub volumes,. This is called the 'Distance to complaint' (DTC) and is calculated for all complaints in all 35 treated patients (i.e. a total of 935 complaints).

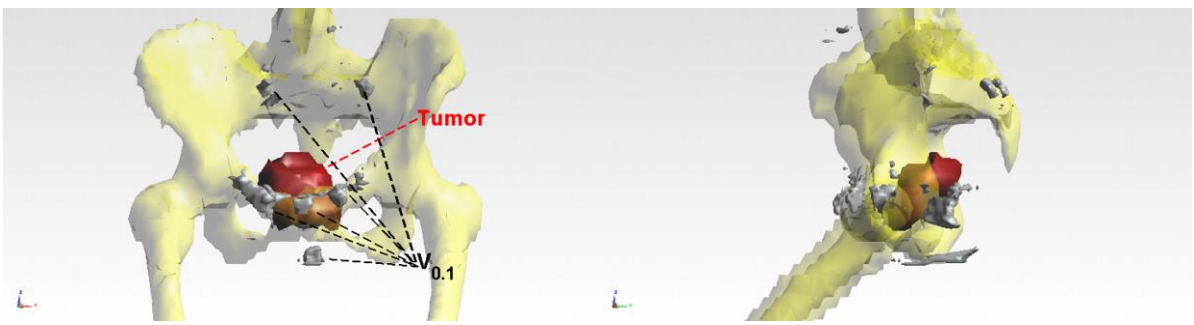

Figure 7.3 Example SAR peak indicative $V_{0.1}$. Note that it consists of various sub volumes. Tumour and bone structure are shown in transparent

7.2.3 Sensitivity analysis

Uncertainties in various input parameters exist as mentioned in the introduction. This can be important for the translation from model to clinic and thus for the spatial accuracy of the prediction of the hotspots. Variations in DTC larger than one centimetre are considered to be relevant [112]. Variations smaller than one centimetre fall within the accuracy of the determination of DTC due to the tetrahedron size in the model. In the sensitivity analysis, the effect of the following 'realistic deviations' on DTC has been evaluated:
Positioning; a realistic uncertainty is 2 cm. For 6 patients, the impact on DTC of position deviations from -2 to 2 cm in steps of 1 cm, along the X-, Y- and Z-axis has been assessed.
Amplitude and phase; deviations of 5%/5^{o} are assumed realistic[178]. This analysis was performed using a Monte Carlo approach, since a maximal deviation in amplitude and

phase does not necessarily result in a maximal variation in DTC. For each amplitude and phase setting, 1000 random amplitudes and phases are calculated. At each complaint that occurred, this bandwidth leads to a spread in DTC per complaint.
Dielectric parameters; Effective conductivity for each tissue is varied between -30% and 30 %. This range is realistic according to Gabriel et al [49] and Van de Kamer et al [96]. Here too, the analyses are performed by varying the effective conductivity (σ) in the various tissues in a Monte Carlo approach, analogous to the amplitude/phase study in previous paragraph.
The average of these deviations over all complaints is used to assess the overall sensitivity.

7.3 Results

In the 70 analyzed treatments, 935 complaints occurred, which means the average number of patient complaints per treatment was 13.3.

7.3.1 Complaint regions distribution

The distribution of complaints over the different complaint regions is displayed in table 7.2. It is clear that by far the most complaints occur in the regions 3 and 10, i.e. the abdomen and the lower back.

Table 7.2. Distribution of occurrence of complaints in all regions, and corresponding DTC values

Region [region nr as in figure 7.2]	Complaint occurrence [%]	Average DTC (±SE)
Abdomen mid [3]	27.6	3.5 ± 0.1
Lower back mid [10]	18.8	3.2 ± 0.1
Tailbone/anus [15]	8.0	2.1 ± 0.2
Buttocks left [14]	7.9	4.9 ± 0.2
Buttocks right [13]	6.4	5.7 ± 0.2
Vagina/perineum [9]	6.3	1.4 ± 0.2
Pubic bone [22]	4.3	1.9 ± 0.2
Groin/Hip right [6]	3.5	7.9 ± 0.3
Bladder [8]	3.2	2.8 ± 0.2
Groin/Hip left [7]	3.1	7.4 ± 0.3
Abdomen left [5]	3.0	5.7 ± 0.7
Abdomen right [4]	1.4	5.5 ± 0.5
Lower back left [12]	1.1	6.9 ± 0.4
Thigh left [19]	0.9	$9.0 \pm 0.1.6$
Legs [20]	0.7	NaN (outside HTP models)
Stomach/upper abdomen [2]	0.7	9.7 ± 1.3
Feet [21]	0.5	NaN (outside HTP models)
Thigh right [18]	0.4	7.7 ± 3.0
Thigh top [16]	0.3	10.8 ± 0.8
Systemic [1]	0.3	NaN (no fixed region)
Lower back right [11]	0.1	7.4 (no SE, single complaint)

Match between patient-indicated complaint regions and location of SAR peak indicators

Table 7.3 shows, the overall match, i.e. the fraction of SAR peak locations and patient complaints in the same region, and the average DTC is shown for each SAR peak indicator (only the indicators with a complaint match larger than 50% are displayed).

Table 7.3. The overall match and distance to complaint, for SAR peak indicators with a complaint match >50%.

Indicator	average complaint match [%]	Average distance to complaint [cm]
$V_{0.01\ closest}$	57	6.2
$V_{0.05\ closest}$	72	4.5
$V_{0.1\ closest}$	77	3.9
$V_{0.5\ closest}$	89	2.8
$V_{1\ closest}$	91	2.4
$V_{5\ closest}$	94	1.6

Evaluation of distance to complaint

As stated in table 7.3, the overall DTC for $V_{0.1\ closest}$ is 3.9 cm, with a standard error of 0.1 cm.

In figure 7.4, the DTC is shown for $V_{0.1closest}$ as SAR peak indicator and as function of time within a treatment.

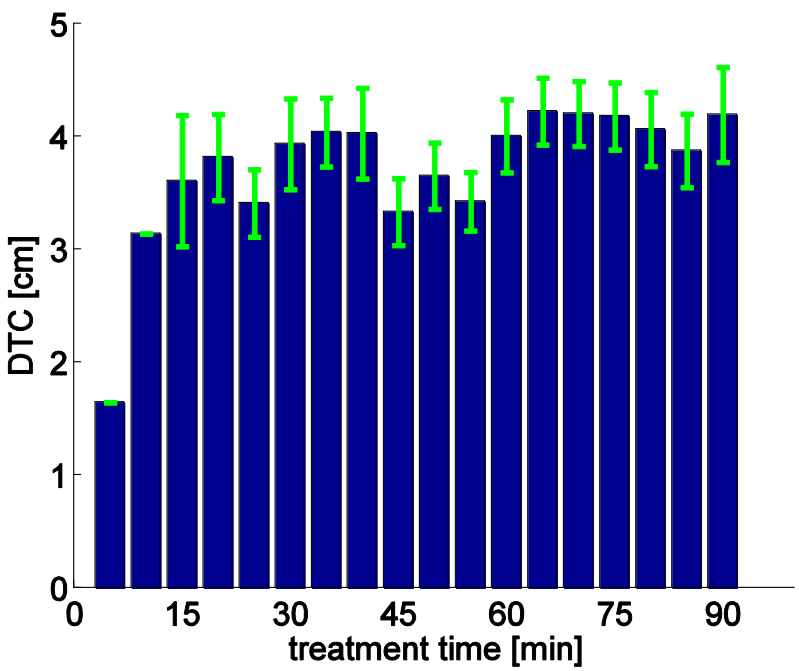

Figure 7.4. Average DTC (distance to complaint) with V0.1 closest as indicator, as a function of the time during a treatment, with the standard error in the error bars.

In general, DTC variations over time are small, as shown in figure 7.4 with $V_{0.1\ closest}$ as an example. over the treatment DTC varies between 3.3 and 4.3 cm. Only in the first 10 treatment minutes, larger differences occur, but these can be attributed to the very low number of complaints that have occurred at the beginning of treatments.

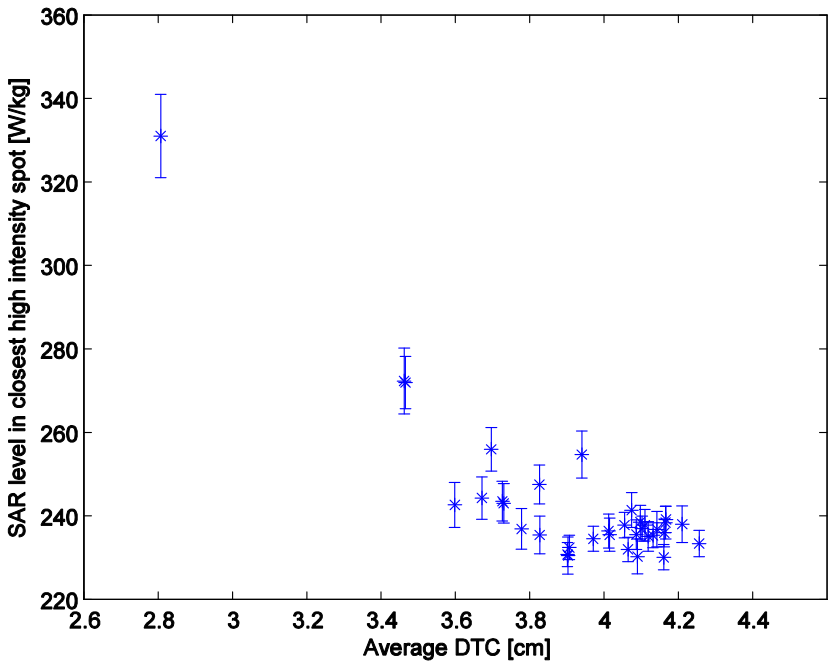

Figure 7.5. SAR level in the SAR peaks versus DTC (distance to complaint). Each point represents a single patient. Treatment specific powers and amplitude/phase settings are taken into account. Errorbars represent the standard error.

In figure 7.5, a closer look is provided on the SAR level of the closest SAR peak against the DTC, where each point represents the average over a single patient. Apart from a few outliers, the average SAR level at complaints appears to be relatively constant at approximately 230 W/kg.

Sensitivity of DTC

As described in section 7.2.3, for each individual complaint, distances to complaint are calculated for a full distribution of amplitudes/phases (range± 5%/5^{o}), for positions (range

± 2cm), and for effective conductivity (range ± 30%). In table 7.4, the results of the sensitivity analysis are presented.

Table 7.4. Sensitivity of DTC for changes in position, amplitude/phase, and effective conductivity

Parameter	Maximum deviation in DTC per complaint, averaged over all complaints [cm]	Overall standard deviation of DTC [cm]
Position	1.15 (31% of average DTC)	0.77 (20% of average DTC)
Amplitude/phase	0.44 (11% of average DTC)	0.15 (4% of average DTC)
Effective conductivity	1.60 (41% of average DTC)	0.55 (14% of average DTC)

7.4 Discussion

In this study we have investigated the correlation between patient experienced discomfort/pain and the location of SAR peaks as predicted by HTP. This correlation is highly important, because pain complaints often limit the hyperthermia treatments. Retrospective data analysis was performed by translating the location of the pain/burning sensation as indicated by the patient to predefined regions. Subsequently, we searched for the SAR peak indicator that predicts these complaints best. This study was retrospective. Therefore, a logical next step is to test the prognostic value of the best SAR peak indicator definitively in a prospective study.

The number of complaints per region

From table 7.2, it is clear that the majority of complaints occur in the abdomen and lower back/tailbone regions. This is most likely caused by the anatomy of the pelvic bones. The general E-field direction in the body is axial. Due to the pelvic bone shape, bone-muscle transitions perpendicular to the E-field occur, especially around the os pubis/lower abdomen and in the lower back. These transitions cause concentrations of energy deposition and hence a high probability of patient complaints.

SAR peak indicators

Table 7.3 shows only those SAR peak indicators with a match between SAR peak location and patient complaint region of at least 50%. In order to select the 'best' SAR peak indicator, it is relevant to consider that a SAR peak indicator containing a large volume at

risk will lead to small DTC values. However, the clinical impact of such an indicator will be low, as it results also in a poor spatial resolution. In addition, we must realize that the V_x indicator is distributed over multiple sub volumes (see figure 7.6), which are spread over multiple regions. Hence, the best SAR peak indicator is a balance between spatial resolution and specificity (high match). On these grounds, we consider $V_{0.1}$ as the golden mean (see figure 7.6). The $V_{0.1}$ volume is around 35 ml for an average patient and still covers the most SAR peak locations in the patient model. Therefore, we decided to use $V_{0.1}$ as SAR peak volume.

In earlier work [45], we already demonstrated a good correlation (approximately R^2=0.75) between modelled temperatures ($T50_{tumour}$) and SAR-peak-SAR-target quotient (i.e. ratio of average SAR in the SAR peak volume and average SAR in the tumor). Since this indicator correlates well with $T50_{tumour}$ (and thus predicts complaint locations well), choosing a similar SAR peak indicator from table 7.3 appears logical.

From the results in table 7.3, it is clear that the closest part of the $V_{0.1}$ volume is close to the complaint location, with an average distance of 3.9 cm, and in 77% of the cases, part of the $V_{0.1}$ volume is in the same region as the complaint. This result shows the actual complaint is in, or close to, the predicted SAR peak volume $V_{0.1}$. This means that $V_{0.1}$ has a predictive value for hotspots, i.e. hotspots occur within or close to a small volume $V_{0.1}$. However, note that this volume is still distributed over a large part of the pelvic area (see figure 7.4), which makes the prediction of the exact complaint location still very hard. Therefore , during HTP guided steering of treatments, patient feedback will still be necessary to reduce hotspots.

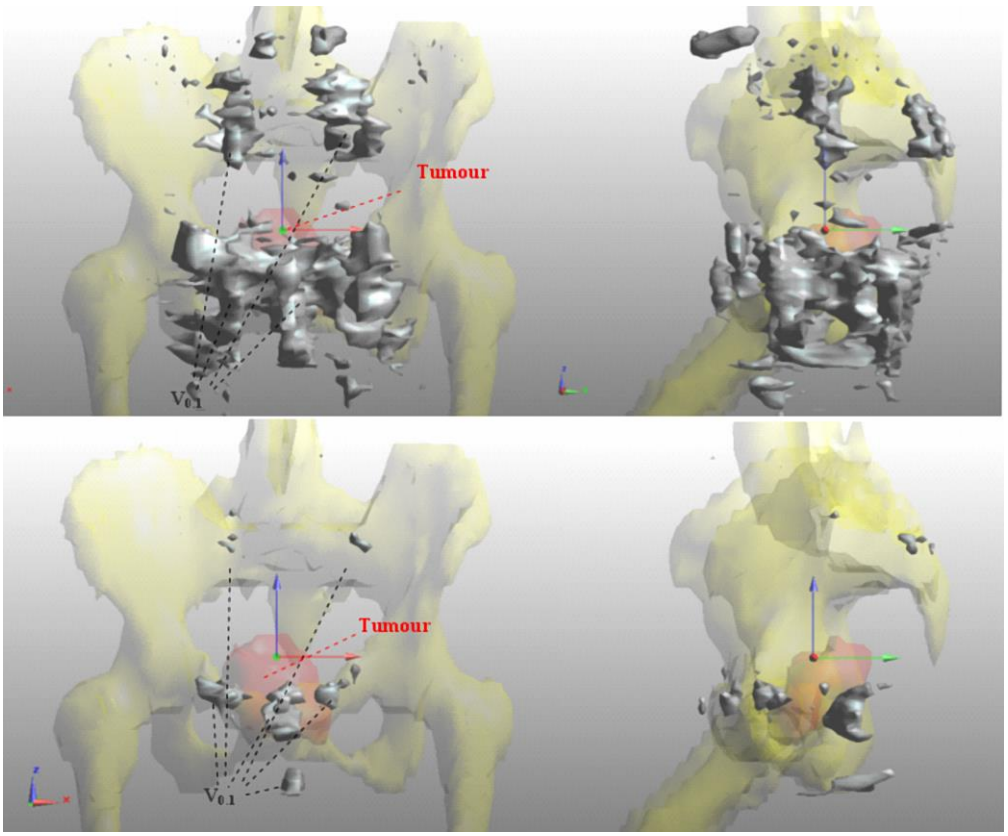

Figure 7.6 Comparison of V1(upper) and V0.1(lower) with in grey the hotspot volumes V0.1 and V1

Other SAR peak indicators that were evaluated, like $V_{0.1,}$ $\rho_{hs\ V0.1}$, and SAR_{max}, appear to have far larger DTC values than $V_{0.1\ closest}$. More than $V_{0.1\ closest}$, these indicators attempt to pinpoint a single SAR peak location in advance. Due to the factors mentioned in the previous paragraph probably, this approach was not successful. The evaluation of the T_{max} indicator showed a large DTC and a low match. Although we would expect a temperature related indicator to predict hotspots better than SAR based indicators, this is clearly not the case in this study. Apparently, other factors besides the SAR-temperature transition play a role.

From figure 7.4, it is clear that the DTC does not significantly change over the course of the treatment. This means that the precision of hotspot prediction does not change during treatment.

Further analysis shows that the DTC is small for commonly occurring complaints, while DTC is generally larger for seldom occurring complaints (see table 7.2). This means that the commonly occurring complaints are on average close to the $V_{0.1}$ volume, while

seldom occurring complaints appear to be harder to predict. It would be interesting to investigate whether this knowledge can be used to provide a risk score (e.g. low-medium-high) to the $V_{0.1}$ indicator that suggests whether a patient complaint will be present. This opens the way to implement *a-priori* measures to prevent patient complaints. When DTC is averaged per patient, a spread is observed between 2.8 and 4.3 cm. Additionally, the absolute SAR value in the high intensity spots appears to be approximately 230 W/kg for most patients (figure 7.5).

Sensitivity in SAR peak-complaint comparison

Although the predicted SAR distribution from the HTP model is considered reliable, the translation to a hotspot location inside the patient can be complicated. Several factors are involved, both patient related or related to the transfer of model predictions to the clinical situation: First, the ability of the patient to localize the complaint plays a role, both in precision and communication. The pain sensation may not be pinpointed to a small spot, but to a region. In addition, referred pain may occur, or nerve damage may cause the patient to indicate a wrong location [179]. Second, the translation from SAR peaks to a temperature causing complaints is dependent on the local blood perfusion, which may vary substantially from day to day and from patient to patient. Third, the accuracy of patient positioning, accuracy of amplitude and phase settings, and uncertainty in dielectric constants influences the outcome of the comparison. Fourth, patient sensitivity differs per patient, and within a patient.
The first factor, localization, is dealt with by defining complaint regions (figure 7.2). From literature, we estimate that the precision with which a patient can locate a hotspot is in the order of the complaint region size, especially when it is located deep and referred pain may occur [179]. Therefore, we estimate that the complaint regions in figure 7.2 are of correct size, since the regions with many nervous receptors are small and vice versa. To asses the second factor, SAR-temperature translation, we evaluated different SAR peak indicators, to find an indicator that covers this translation as much as possible. The third factor, various parameter accuracies, was assessed by the sensitivity analysis, as mentioned in section 7.2.3. Factor four, patient sensitivity, is hard to quantify, and will have to be accepted as source of uncertainties in this study.

Sensitivity analysis

To assess the value of the found ‘distance to complaint’ values, the sensitivity to inaccuracies in amplitude/phase or patient positioning was evaluated. The variation (uniform distribution) of the amplitude and phase with 5%/5^{o} leads to an average

variation in DTC of 0.44 cm Positioning variation from -2 to 2cm leads to an average variation in DTC of 1.15 cm, while variation in effective conductivity leads to an average variation in DTC of 1.60 cm. This suggests that the influence of amplitude and phase inaccuracies is only minimal. Positioning inaccuracies and variation in effective conductivity have a relevant influence, when compared to the average DTC of 3.9 cm. Hence, accurate positioning is very important, as earlier stated [112]. The values for effective conductivity are currently taken from literature [49]. If the inter-patient variation in dielectric parameters is in the order of 30%, the variation in DTC that was found suggests that predicted model high intensity spots can differ by 1-2 cm, dependent on the actual value of sigma. This uncertainty can only be encountered effectively by measuring dielectric properties for each individual patient. The latter is, to our knowledge, an option that not yet can be implemented.
The sensitivity for bolus shape though, was not investigated in this study. From literature, the effects of bolus shape appear to occur close to the bolus edge [177]. However, this is only a relatively basic analysis. A thorough analysis of bolus shape on E-field distribution would require implementation of various bolus shapes, folds, air inclusions etc. Such a study requires an enormous amount of processing and calculation time. Moreover, our current HTP software allows only very little freedom in defining bolus shapes. Therefore, we chose to use a bolus form as standard implemented in Sigma Hyperplan, which is common in literature [100].

7.5 Conclusion

The location of hotspots causing patient complaints and the predicted SAR peak location in a HTP model are highly correlated. The $V_{0.1\ closest}$ indicator was found to produce the best results in terms of 'distance to complaint': 3.9 cm on average. This means that a hotspot will occur in, or close to, the $V_{0.1}$ volume. However, the identification of the 'closest' SAR peak location can only be done in retrospect. Since other high SAR indicators appear to predict hotspots insufficiently, for the time being, patient feedback will still remain necessary to localize the actual hotspots. Yet, the $V_{0,1}$ volume can be used to identify the regions at risk. Further, prospective research is necessary in order to increase the probability of predicting the correct hotspot.

8 The Rotterdam approach of HTP guided treatment in cervical cancer

This chapter is based on:

Canters RAM, Paulides MM, Van der Zee J, Van Rhoon GC. Implementation of treatment planning in the routine clinical procedure of regional hyperthermia treatment of cervical cancer, an overview and the Rotterdam experience, Int J Hyperthermia 2012, 28(6):570-581

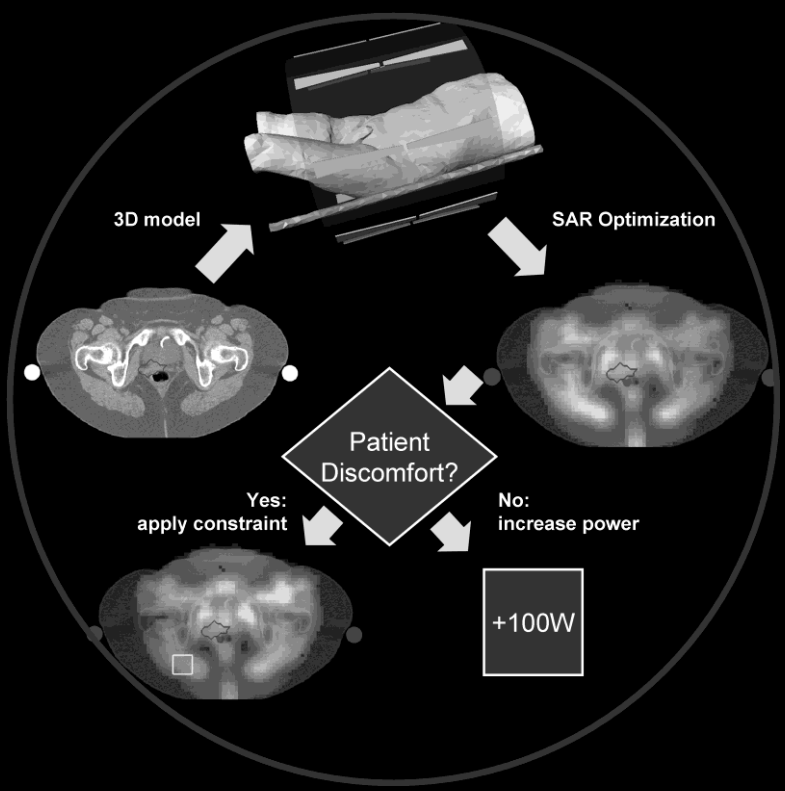

In this chapter, the focus is on the Rotterdam experience of the HTP guided hyperthermia treatments as an illustration of the application of HTP in the clinic. After we successfully demonstrated the potential of HTP guided SAR steering in [108] , on-line HTP guided SAR steering is now applied as standard practice during a deep hyperthermia treatment of cervical cancer. Treatment planning is still SAR based however, as we consider that temperature models still contain too many uncertainties for prospective clinical application. The philosophy behind the use of SAR models is to maximize energy deposition in the tumor and to minimize hotspot SAR. In case hotspots intensity in terms of temperature of patient discomfort is different than predicted by our SAR models, patient feedback gives us the opportunity to re-optimize the SAR distribution with certain constraints.

In figure 8.1, the overall treatment workflow that is currently used in Rotterdam is shown. The preparation of the treatment starts with a CT of the patient in the hammock position. Next, an MD delineates the tumor, in close resemblance to the radiotherapy target volume. After semi-automatic Hounsfield unit segmentation of fat, muscle and bone, the EM calculations are started in Sigma Hyperplan, after which optimization takes place. This results in starting settings for the treatment. During the treatment, SAR levels are monitored using VEDO (Visualization of Electromagnetic fields for Dosimetry and Optimization), a custom tool developed in Rotterdam. In the following sections a number of practical solutions are reported that are used in Rotterdam in order to improve reliability and reproducibility result and still within an acceptable time frame.

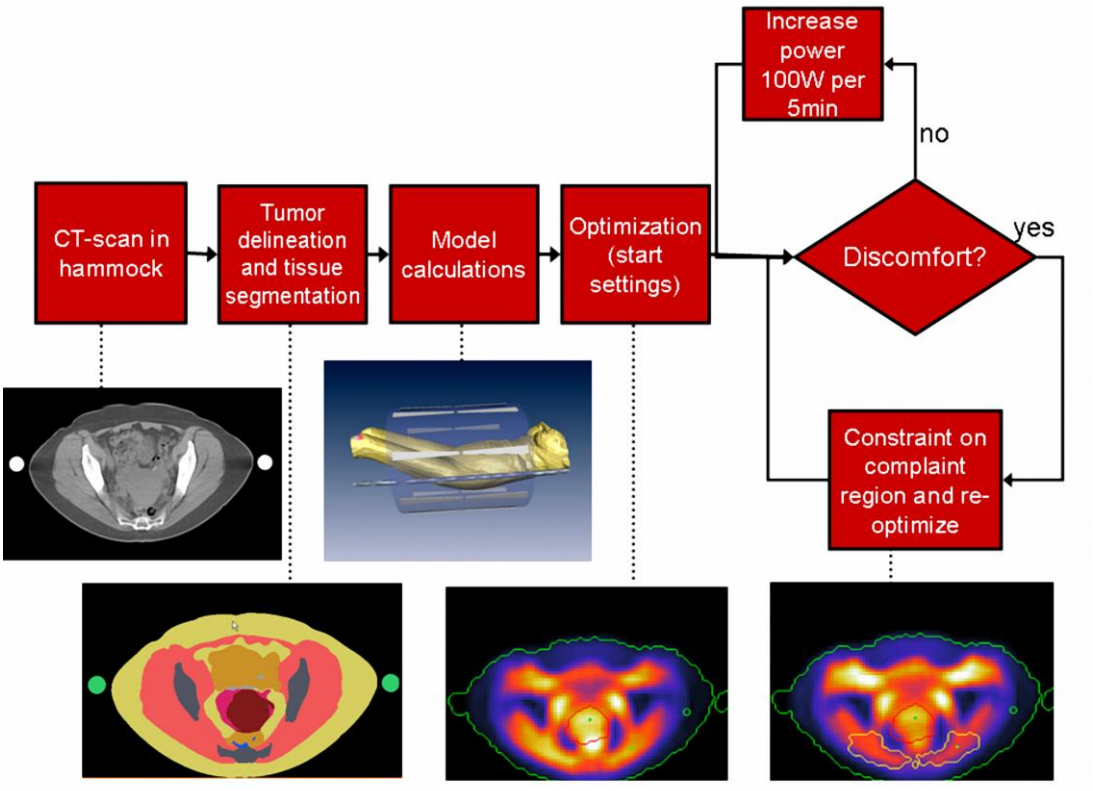

Figure 8.1: Workflow of the HTP guided deep hyperthermia treatments in the Rotterdam clinical practice

CT in treatment position

In figure 8.2, the setup of the hammock CT is illustrated. A BSD hammock, identical to the one used in the clinic, is placed on the CT table on top of two polystyrene blocks. For pelvic tumors, a scan length of 80 cm is used with 0.5 cm slice distance, with the pubic bone in the center of the scan. For an accurate reconstruction of the patient position on the hammock, a marker is placed on a known position on one of the rods. This reconstruction is important to reproduce the patient posture accurately.

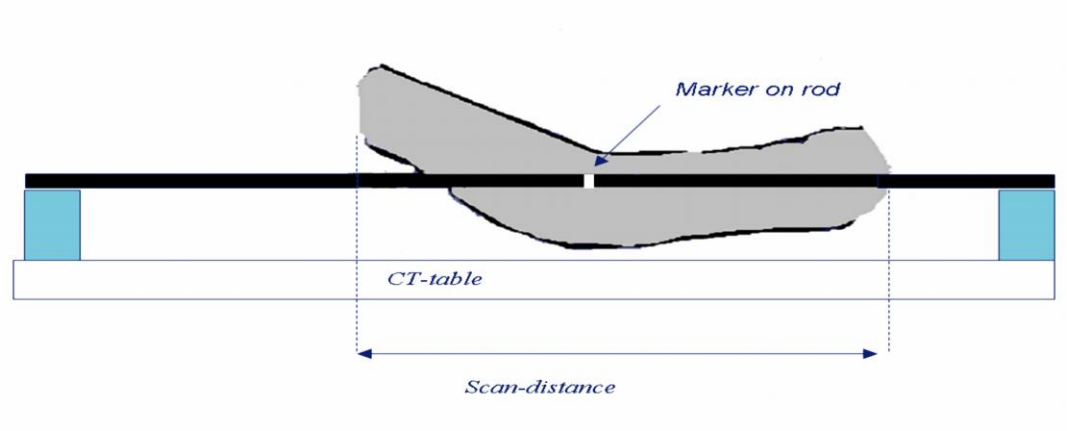

Figure 8.2: Setup of the CT in treatment position

Semi-automatic patient modeling

After the hammock CT is completed, a MD delineates the tumor volume in the segmentation software, equivalently to the radiotherapy volume. Direct import of the radiotherapy delineation is not yet possible due to the different postures in which radiotherapy and hyperthermia CT's are made. Simultaneously to the tumor delineation, an automatic Hounsfield unit (HU) based segmentation takes place. The following tissues are segmented automatically: Exterior/Internal air (HU<-250), fat (-250<HU<-30), muscle (-30<HU<100), Bone (100<HU<1900), and the metal marker on the hammock rod (HU>1900). This automatic segmentation is followed by a number of semi-automatic and manual adaptations: filling holes within the bone, smoothing, island removal, and delineation of the top of the pubic bone (for positioning purposes). Subsequently, the tumor delineation and the semi-automatic segmentation are combined automatically, and a Sigma Hyperplan model is calculated and the results are exported to a Matlab mat file. Patient positioning in the model is as follows: in the lateral and dorsal-ventral directions, the patient is positioned centrally. In the anterior-posterior direction, the tumor is placed centrally in the applicator. After the calculations are finished, a treatment planning report is generated, that includes information for the technicians preparing the treatment. The whole procedure of model preparation takes approximately 1 hour of work and 2 hours of calculations.

Patient positioning

From the treatment planning report, positioning data from the model is available for the actual patient positioning. First, the anterior-posterior position on the hammock can be derived from the locations of the marker and the pubic bone and reproduced in the clinic with a line laser. The lateral position on the hammock is done on sight. We found that due to the fixed rods, a central position is easily achievable. Second the anterior-posterior position of the applicator is derived from the model, using the same line laser. Third, the patient is placed centrally in the dorsal-ventral direction, after which the bolus is filled. After filling, the dorsal-ventral position is fine-tuned using two ultrasound distance measurement probes (see figure 8.3). The correct distances are again derived from the HTP model. We measured that the different positioning steps have an accuracy of about one centimeter. To further improve this accuracy, we are investigating the use 3D US-imaging techniques, or adding more measurement points in the applicator wall.

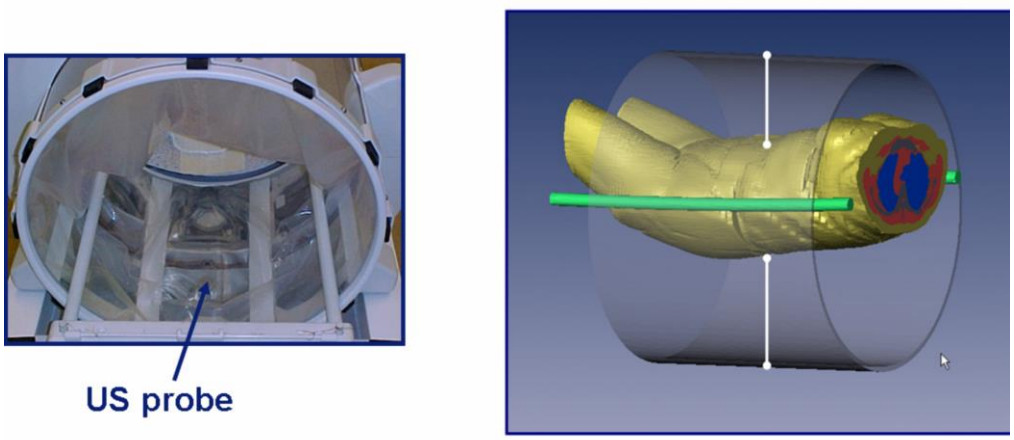

Figure 8.3: Illustration of the used ultrasound positioning probes at the bottom and top of the Sigma-60

Procedure of HTP guided steering

As pointed out before, initial phase and amplitude settings are calculated using a particle swarm algorithm combined with a line search method. The goal function we use for optimization is the aforementioned HTQ, given in section 1.2.5. Optimization is GPU supported, and generally takes less than 30 seconds. Fast enough for use during a clinical treatment. All settings are uploaded to the BSD console via the interface that is present in Sigma Hyperplan. We start in the treatment of cervical tumors with 400W RF-power on the antennas and increase every 5 minutes by 100W until we experience patient

discomfort (see the block diagram in figure 8.1). In case of a complaint power is first switched off until the discomfort has disappeared. We continue the treatment with new phase and amplitude settings obtained from a re-optimization whereby the weight of constraint for the SAR in the complaint region is increased.
Increasing the input power until patient discomfort carries the risk of overheating the patient and thus causing major discomfort and a less effective treatment due to many off-switches. Therefore, we monitor the average power of the last 15 minutes continuously. If this averaged power is >20% below the set input power level, we decrease power by 50 to 100 W, dependent on the power level.

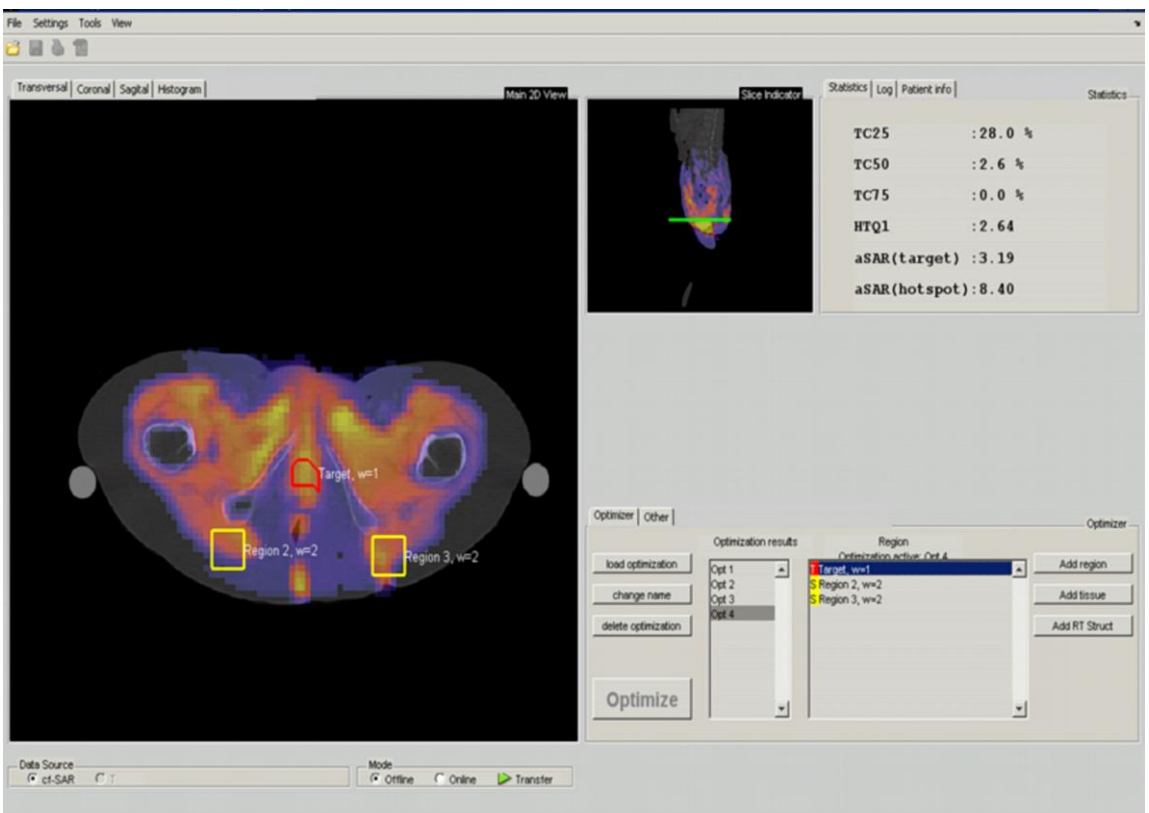

Figure 8.4: Layout of the VEDO software, used for monitoring, optimization and visualization of the treatment. On the left there is an axial slide visible, with the SAR distribution as overlay over the patient CT. Also target (red) and sensitive (yellow) regions are visible. On the right top, several indicators are visible, on the right bottom, the optimizations can be set.

For the online monitoring and control of the treatment using HTP, we created a software package VEDO. In figure 8.4, the layout of this Matlab based software package VEDO is visible. The left half of the screen is reserved for online visualization of the SAR distribution, on basis of measured powers and phases of each antenna. By using a transparent display, the underlying anatomy (CT) is visible. The tumor is displayed with red delineation, while complaint regions can be delineated on any place in the anatomy, and are displayed with yellow delineation. In the top right, various parameters can be monitored, one of which is HTQ. The bottom right part of the screen contains information about optimization settings and current powers and phases. The introduction of this tool enabled the use of HTP in the clinic by MDs and technicians with no or little experience in modeling.

9 General discussion and conclusions

9.1 General discussion

The results presented in this thesis clearly show that applicators with larger number of antennas have the potency for better heating, thus the greatest potential to enhance treatment outcome for pelvic tumors. The larger number of antennas increases complexity to apply to optimal setting and makes the use of hyperthermia treatment planning an absolute necessity. In this thesis it is shown that precise control over the power deposition for optimization purposes considerably improves with the use of HTP. It is also demonstrated that uncertainties in the translation from model to clinic, uncertainties in tissue parameters, and numerical uncertainties will have a considerable influence on the eventual benefit of HTP. Thus far, clinical application of HTP in the Sigma 60 has shown to obtain equally high temperatures as in the years before introduction of HTP. Although the control and uniformity of deep hyperthermia treatments has improved considerably over the last decade, substantial further improvement will still be possible. The current results can serve as a basis to measure the effectiveness of new improvements in the future. In the next sections, the relevance and impact of the various potential improvements is discussed further, and an outlook is given into future research.

9.2 Optimization

An analysis over 420 treated patients of Franckena et al showed that there is a clear dose effect relation in deep hyperthermia treatments [33]. Therefore, to increase overall survival and local control in deep hyperthermia patients, it is highly important to increase the thermal dose. There are two ways of achieving this goal: increasing temperatures in the tumor, or increasing treatment time. Increasing treatment time is not a viable option in our opinion, due to logistics and the burden on a patient of the hyperthermia treatment. Therefore, in this research, we focused on the increase of temperature in the tumor, and the improvement of control of the treatment. The use of HTP offers a great opportunity of optimizing SAR or temperature in the tumor, with amplitude and phase of each antenna as variables, as well as quantification and increased possibilities of control of the hyperthermia treatments. In Rotterdam SAR modeling is still preferred over temperature modeling, because of the large uncertainties in thermal parameters (as shown in chapter 5).

The goal function assessment, described in chapter 2, demonstrates that, for SAR optimization, a goal function taking both hotspot and tumor SAR into account has the best chance of high temperatures. HTQ correlates with tumor T50 with a R^2 value of 0.75

making it the best goal function found in chapter 2. Although the relation of goal functions with temperatures has only been tested in models, it is likely that in clinical practice this correlation will also exist. Limitations of the chosen HTQ parameter are the non linearity, which makes the optimization process less simple, i.e. no analytical solutions can be found. Further, the non-intuitiveness of this parameter makes it difficult to evaluate a SAR distribution by the value of HTQ.
The feasibility of HTP guided steering, as pointed out in chapter 3, has been demonstrated with short calculation times and ability to reduce SAR levels in complaint regions, both in measurements and in model calculations. This paved the way for clinical introduction of HTP guided complaint adaptive steering.

9.3 Uncertainties and their consequences

Chapter 4 showed that accurate positioning has a relevant influence on the HTQ levels in the patient models. Uncertainties in positioning of > 1cm will lead to relevant reductions in tumor SAR and thus temperature. In chapter 5, we compared the Sigma 60 to the Sigma Eye applicator, taking into account uncertainties in thermal and dielectric parameters of tissues via a Monte Carlo analysis. This study showed that the uncertainties, as estimated from literature, have a considerable influence, in SAR distributions, and even more in temperature distributions. The effect of these uncertainties is that a predicted SAR distribution might well be different from the actual distribution in a patient, due to the fact that the actual dielectric and thermal properties of a patient are different from the predicted ones. Therefore, the complaint adaptive steering, i.e. the patient's discomfort indication as a feedback mechanism, remains important in deep hyperthermia treatments. Better thermometry, e.g. noninvasive MR thermometry can potentially replace the patient feedback by direct temperature information.
The positioning study of chapter 4 also showed that the potential for improvement for the 4 antenna Sigma 60 by HTP optimization is relatively small, around 5% HTQ or 0.2^{o}C, due to the limited number of antennas, i.e. degrees of freedom. From the results in chapter 5, we found an interquartile range of ±10% around the median HTQ taking into account realistic uncertainties in dielectric and thermal parameters. This means that the potential benefit of the clinical study of chapter 6 is masked by the uncertainties. This is in agreement with the results found in the clinical study of chapter 6, in which the clinical benefit of the use of HTP guided complaint adaptive steering was tested vs. TCP steering treatments.

As mentioned earlier, apart from the potential direct temperature benefits in an applicator with more antennas, also in the Sigma 60 important benefits exist for increased control, reproducibility, and quantification.
Additionally, chapter 6 shows clearly that, despite uncertainties, it is possible to achieve an improvement in SAR and temperature when switching to applicators with more antennas: the Sigma Eye applicator performs significantly better than the Sigma 60 applicator. This confirms that HTP guided steering is an important tool in the future of hyperthermia treatment, that has the potential to make the potential of more advanced applicators accessible.

9.4 Clinical application of HTP, complaint adaptive steering

Because of the fact that equal temperatures were achieved with HTP guided steering in the clinical study of chapter 6, it was decided to start the clinical implementation of HTP, as described in chapter 8. More importantly, HTP guided steering enables a far more quantitative and standardized approach of deep hyperthermia treatments, which is an absolute prerequisite for the use of more complicated systems, the optimization of the SAR distribution, and a quantitative and uniform response on complaints. Furthermore, HTP guided steering enables the quantitative evaluation of treatments, which facilitates the more widespread use of hyperthermia and the comparison of hyperthermia treatment results between different institutes.
Implementation of this steering technique in the Sigma 60, which is a relatively easy step, enables optimization of the treatment approach in clinical practice, and preparation for the next step towards HTP guided treatments with more advanced applicators.

9.5 Conclusions

From the research in this thesis, it is clear that the clinical use of hyperthermia treatment planning enables the controlled and optimized administration of power and/or heat to the patient. The complaint adaptive approach that was taken has been proven to be effective in reducing the SAR levels in complaint regions, especially when they are located away from the tumor. This strategy can be an effective method to further optimize the treatment via patient specific feedback. Tumor powers however have to be monitored when using this strategy, to make sure that no over-constraining takes place.
The influence of uncertainties on the correct prediction of the SAR distribution inside a

patient appears to be considerable. This makes exact prediction of hotspot locations still difficult and causes temperatures and SAR levels in the tumor to be sub-optimal. Nevertheless, despite the uncertainties, significant improvements were found when switching from the 4 antenna Sigma 60 to the 12 antenna Sigma Eye. This provides a solid basis for development of applicators with more antennas. The uncertainty make temperature based simulations on average not advantageous over SAR based simulations and therefore, with the current level of uncertainties, SAR simulations are sufficient for clinical use of HTP. Future research however, first has to focus on reduction of uncertainties by measuring the various parameters. Second, image guided hyperthermia can act as a feedback mechanism for online optimization during treatment. Both these lines of research will enable the use of more complicated applicators that can generate custom heating patterns. Overall, unlike the intuitive TCP steering, HTP guided steering still has a considerable potential for further improvement of the hyperthermia treatments, and should be part of all current deep hyperthermia systems.

9.6 Outlook and future research directions

Hyperthermia treatment planning is without doubt a very useful tool to optimize deep hyperthermia treatment, and to increase thermal dose inside the tumor. Furthermore, it is absolutely necessary for the use of more complicated applicators with more antennas. In this way, HTP enables the advancement towards more complicated applicator designs. The main foci for future research should be reduction of uncertainties and development of treatment routines that make use of non-invasive thermometry. When uncertainties are reduced, this paves the way for development of new advanced applicators with arrays of antennas far larger than the current applicators, and thus more focused heating of the tumor. In order to achieve this challenging objective future research should aim at:

Reduction of the influence of uncertainties

The benefit of using treatment planning is partly hampered by the amount and size of the various uncertainty factors, of which the dielectric parameters and the perfusion probably make up the largest part. Figure 5.3 showed that these uncertainties cause a drop of temperatures of more than 0.5^{o}C. Despite the fact that there still is an improvement when switching to the Sigma Eye, this unused potential is fairly large. To use this potential, the various uncertainty factors have to be reduced by controlling them using measurements. Currently we are already in the process of reducing uncertainties in

antenna behaviour, by measuring the EM field inside the applicator. Further, patient positioning errors are being reduced by placing ultrasound distance measurement sensors in the applicator. The main uncertainties, i.e. dielectric parameters and perfusion, still need to be addressed. A possibility to do this would be to perform perfusion measurements with MR techniques, e.g. dynamic contrast enhanced imaging. Also, the uncertainty of the dielectric parameters might be reduced by patient measurements using MR imaging and B1+ field extraction.
When uncertainties are reduced, HTP will become more reliable and precise. This enables improved HTP guided treatments with more complex applicators that lead to higher temperatures.

Image guided hyperthermia.
Considerable improvement of the quality of a hyperthermia treatment is also expected from visualizing the actual temperature distribution in 3D by non-invasive thermometry (NIT) using an MR scanner. An almost real-time temperature overview would enable correction of the effects of uncertainties and re-optimization as described in the work of the group of Duke university [66, 72]. With a NIT-HTP feedback loop, the effect of uncertainties on HTP results can be corrected . Before the NIT measurements can be used for actual steering of the treatment, the impact of several artifacts has to be reduced. Although the fat referenced PRFS method corrects for the drift occurring during the treatment, motion of blood and other body fluids can potentially disrupt the thermometry images. Therefore, correction methods for these artifacts need to be investigated.

Towards improved applicators

HTP models are also suitable for parameterized applicator development. Several studies in the past have already shown this [61, 80, 180]. On one side, the HTP models enable the development of optimized applicator design, as is currently done in a Dutch Cancer Society project EMCR2009-4448. On the other side, as mentioned, HTP guided steering enables the clinical use of these applicators with optimized settings.

10 Summary

Deep hyperthermia is a treatment used in concurrence with radiation therapy or chemotherapy in the treatment of deep seated tumors. In hyperthermia, tumor temperatures are elevated 3 to 7^{o}C above normal body temperature, up to a temperature of 44^{o}C. In a randomized trial, the 3 year overall survival of cervical cancer patients was almost doubled by adding hyperthermia to radiotherapy. There is a clear dose-effect relation in hyperthermia, and therefore increasing the temperature in the tumor is an important factor to further increase survival rates in cervical cancer.
Until recently, hyperthermia treatments in Rotterdam were performed by aiming a focus point that was calculated using a cylindrical representation of the patient. Because of the inhomogeneous nature of a patient, this representation is far from accurate. For the 4 antenna Sigma 60, the calculated focus point may still be close to the optimum, but for applicators with more antennas, and a high number of degrees of freedom, this approach will certainly be inadequate.
Originating in the 1970's, electromagnetic numerical and thermal modeling of 3D structures is currently possible with a precision and speed that is sufficient for routine use. When the electromagnetic and thermal properties of a patient are known, the energy and thermal distributions can be calculated for each antenna of the applicator. With this information, the interference pattern can be determined, dependent on phase and amplitude of the emitted signals by the antennas, and thus can be optimized. When performing these patient specific calculations, i.e. treatment planning, and optimizations, the resulting settings can be applied on-line in the clinic.
This thesis covers the clinical introduction of hyperthermia treatment planning, the assessment of the various uncertainties that should be taken into account, and the results of clinical implementation.

Optimization

The successful application of hyperthermia treatment planning requires optimization routines that optimize the SAR distribution in such manner that the eventual dose in the tumor is maximized. In chapter 2, various SAR based goal functions were assessed. This assessment showed that a goal function taking into account hotspot minimization as well as maximization of the SAR in the tumor has the highest probability to lead to high tumor temperatures. Eventually, two goal functions were chosen for clinical assessment: average tumor SAR normalized on whole body average SAR (Opt1), and hotspot tumor quotient (HTQ), the ratio between SAR in the 0.1th percentile and the tumor SAR (Opt2).

Further, the concept of complaint adaptive steering is tested, i.e. local reduction of SAR in case of patient discomfort by adapting the goal function.
The phantom test and a sensitivity study in 10 patient models, show that complaint adaptive steering is most effective in peripheral complaint regions. Clinical evaluation in two groups of five patients shows that time between complaints is longer using Opt2 ($p=0.007$), i.e. a higher comfort of the patient during treatment. It does, however, not yet lead to significantly different temperatures [T50's of 40.3(Opt1) vs. 40.1^{o}C (Opt2) ($p=0.898$)]. From this study we concluded that complaint adaptive steering is feasible in terms of SAR-reduction in complaint regions and in time consumption. Moreover, complaint adaptive HTP guided steering has the potential for further improvement and thus higher temperatures, when the degrees of freedom are increased, i.e. in more advanced applicators. Opt2 (i.e. HTQ) is used in further clinical application, because of better complaint reduction and control.

Uncertainties

The clinical use of hypethermia treatment planning can be influenced considerably by various uncertainties. These uncertainties are either related to the reproduction of the model setup in the clinic (e.g. positioning, water bolus shape, antenna signals), or deviations of patient tissue properties from literature values, and cause differences in heating between model predictions and the actual patient. In chapter 4, we investigated the influence of positioning uncertainties on power deposition in the Sigma 60 applicator. Position inaccuracies of less than 1 cm appear not to affect SAR patterns relevantly. Current positioning precision is sufficient in the X (right-left)-direction but precision measurements are needed to reach the desired accuracy in the Y (anterior posterior)-direction.
In chapter 5, a closer look was taken at the influence of tissue parameter uncertainties on the tumor SAR and temperature levels for 20 patient models. A Monte Carlo analysis, simulating many uncertainty scenarios, shows a variation of HTQ of approximately 25% (interquartile range) and a variation of 0.7 to 1^{o}C (interquartile range) for temperatures, due to the uncertainties in tissue parameters. Difference between the Sigma 60 and Sigma Eye applicators however, still remain significant ($p<0.001$ for SAR and temperature distributions). The additional benefit that could be expected from temperature modeling is canceled out by the uncertainties. This means that SAR modeling is sufficient, as long as uncertainties persist. Moreover, these results show that with uncertainty reduction, the potential of HTP guided steering can be increased considerably.

Clinical implementation of HTP guided steering

HTP guided steering was tested for clinical use in a randomized trial, comparing TCP steering with HTP guided steering in the Sigma 60 applicator (see chapter 6). Results of 36 patients showed equal temperatures in these two steering modes. This means that, despite the fact that the potential gain in the Sigma 60 was only small, HTP guided steering has matched the 20 year experience in TCP steering. After the conclusion of this study, we decided to implement HTP guided steering in the clinic. Besides the expected advantages in applicators with more degrees of freedom, it offers improved control and quantification of the treatment. The VEDO tool, that controls the visualization and optimization of the HTP guided steering, was developed to assist a uniform and optimized application of deep hyperthermia treatments.

Future research

Three main directions of future research are:
Uncertainty reduction. By measurements the various parameters could be assessed patient specific, to create more accurate HTP models.
Image guided hyperthermia. Non invasive thermometry offers great possibilities to visualize actual temperatures in 3D. Combined with HTP, efficient optimization is possible.
Development of advanced applicators. When reduced uncertainties are in effect, advanced applicators can be developed, which can focus the heat anywhere in the pelvic area, without causing hotspots outside the target volume.

11 Samenvatting

Diepe hyperthermie is een behandeling die samen met radiotherapie of chemotherapie wordt gebruikt in de behandeling van diepliggende tumoren. Tijdens de hyperthermie worden temperaturen van 3 tot 7 ^{o}C boven de normale lichaamstemperatuur gebruikt, oplopend tot 44^{o}C. In een gerandomiseerde studie werd gevonden dat de overlevingskans voor patiënten met baarmoederhalskanker bijna verdubbelde als hyperthermie werd toegevoegd aan de radiotherapie. Er is een duidelijke dosis-effect relatie in hyperthermie, en daarom is het verhogen van de behaalde temperaturen in de tumor een belangrijke factor in het verhogen van de overlevingskansen in baarmoederhalskanker.
Tot onlangs werden hyperthermie behandelingen in Rotterdam gedaan door een focuspunt te definiëren voor de verhitting, waarbij de daaruit volgende instellingen berekend werden met behulp van een simpel cilindrisch model van de patiënt. Vanwege de inhomogene samenstelling van een patiënt, is deze manier van focusseren verre van accuraat. Voor de Sigma 60 applicator, die 4 antennes heeft, leidt deze manier van focusseren wellicht nog resultaten die dicht bij het optimum uitkomen. Echter voor applicators met meer antennes, en dus een hoger aantal vrijheidsgraden, zal deze benadering zeker inadequaat zijn.
Numeriek modelleren van elektromagnetische en thermische problemen gaat terug tot de 70-er jaren. Met de huidige stand van zaken in de computertechniek is het op dit moment mogelijk om 3D structuren door te rekenen met voldoende precisie en snelheid voor routinegebruik. Als de elektromagnetische en thermische eigenschappen van een patiënt bekend zijn, kunnen energie- en temperatuurverdelingen berekend worden voor iedere antenne afzonderlijk. Met deze informatie kan het interferentiepatroon bepaald worden voor willekeurige amplitudes en fases van het signaal op iedere antenne. Hiermee kan vervolgens een optimalisatie plaatsvinden. Als deze patiëntspecifieke berekeningen gedaan zijn (berekeningen en optimalisatie), kunnen de resulterende instellingen meteen in de kliniek worden toegepast.
Dit proefschrift gaat over de klinische introductie van ‘hyperthermia treatment planning’ (HTP), de analyse van de verschillende onzekerheden, en de resultaten van de klinische implementatie.

Optimalisatie

Het succesvol toepassen van HTP vereist optimalisatieroutines die de SAR verdeling zodanig optimaliseren dat de uiteindelijke dosis in de tumor gemaximaliseerd wordt. In hoofdstuk 2 worden verschillende SAR-gebaseerde doelfuncties geanalyseerd. Deze analyse liet zien dat een doelfunctie die naast tumor maximalisatie ook hotspot

minimalisatie meeneemt, de grootste kans heeft om tot hoge tumortemperaturen te leiden. Uiteindelijk werden twee doelfuncties gekozen voor een klinische test: 1) de gemiddelde SAR in de tumor, genormaliseerd op de totale SAR in het lichaam (Opt1), 2) het quotiënt van tumor SAR en de SAR in het 0.1^{de} percentiel (Opt2). Verder werd het concept van klachtgebaseerd sturen getest: lokale reductie van SAR bij klachten door de doelfunctie aan te passen.
Een fantoomtest en een gevoeligheidsanalyse in 10 patiënten liet zien dat klachtgebaseerd sturen het meest effectief is in perifere regio's, ver van de tumor verwijderd. Klinische evaluatie in twee groepen van 5 patiënten liet zien dat de tijd tussen klachten groter is in Opt2 ($p=0.007$), wat een groter comfort voor de patiënt betekent. Er was echter geen verschil in temperaturen [T50's van 40.3 ^{o}C (Opt1) vs. 40.1^{o}C (Opt2), $p=0.898$]. Hieruit is de conclusie getrokken dat klachtgebaseerd sturen mogelijk is wat betreft SAR-reductie in klachtregio's en wat betreft tijdsconsumptie. Bovendien heeft klachtgebaseerd sturen m.b.v. HTP het potentieel om tot verdere verbetering te leiden als het aantal antennes (dus vrijheidsgraden) verhoogd wordt in geavanceerdere applicators. Opt2 wordt verder gebruikt in klinische toepassing, vanwege betere klachtreductie en controle.

<u>Onzekerheden</u>

Het klinische gebruik van HTP kan behoorlijk beïnvloed worden door verschillende onzekerheden. Deze onzekerheden zijn of gerelateerd aan reproduceerbaarheid van het model in de kliniek (bijv. positionering, waterbolus vorm, antenne signalen), of aan afwijkingen in weefseleigenschappen van de patiënt ten opzichte van literatuurwaarden. Dit zorgt voor verschillen in verwarming tussen model en de eigenlijke patiënt. In hoofdstuk 4 is de invloed onderzocht van positieonzekerheden in de Sigma 60 op de vermogensdistributie in de patiënt. Onzekerheden in positionering van minder dan 1 cm blijken de SAR verdeling niet relevant te beïnvloeden. De huidige positioneringmethode is voldoende in de X-richting (links-rechts), maar meer precieze metingen zijn nodig in de Y-richting (anterior-posterior).
In hoofdstuk 5 is voor 20 patiëntmodellen verder ingegaan op onzekerheden in weefselparameters en hun invloed op de tumor-SAR en –temperaturen. Een Monte Carlo analyse, waarbij vele onzekerheidsscenario's werden gesimuleerd, liet een variatie in HTQ van ongeveer 25% zien (interquartiel afstand) en een variatie van 0.7 tot 1^{o}C (interquartiel afstand) wat betreft temperatuur. Er bleef echter nog steeds een significant verschil bestaan tussen de Sigma 60 en de Sigma Eye ($p<0.001$ voor zowel SAR- als temperatuurverdelingen). Het extra voordeel dat verwacht werd met

temperatuuroptimalisatie werd teniet gedaan door de onzekerheden. Dit betekent dat SAR-modellering voldoet, zolang als de onzekerheden blijven. Verder laten deze resultaten zien dat met onzekerheidreductie het potentieel voor HTP geleid sturen aanzienlijk kan worden vergroot.

Klinische implementatie van HTP geleid sturen

HTP geleid sturen is in een gerandomiseerde studie getest voor klinisch gebruik, waarin TCP sturen vergeleken werd met HTP geleid sturen in de Sigma 60 applicator (zie hoofdstuk 6). De resultaten van 36 patiënt lieten gelijke temperaturen zien in deze twee stuurmodaliteiten. Dit betekent dat, ondanks het feit dat de potentiële winst in de Sigma 60 maar zeer klein was, HTP geleid sturen de 20 jaar ervaring met TCP sturen geëvenaard heeft. Op basis van deze studie is besloten om HTP geleid sturen klinisch te implementeren. Naast de verwachte voordelen in applicators met meer vrijheidsgraden, leidt HTP geleid sturen ook tot verbeterde controle en quantificatie van de behandeling. De VEDO tool, die de visualisatie en optimalisatie controleert in HTP geleid sturen, is ontwikkeld om een uniforme en geoptimaliseerde toepassing in diepe hyperthermie behandelingen te ondersteunen.

Toekomstig onderzoek

Drie hoofdrichtingen voor toekomstig onderzoek zijn:
Onzekerheidsreductie. Door metingen kunnen de verschillende parameters patiëntspecifiek gemaakt worden, om zo meer accurate HTP modellen te kunnen berekenen.
Beeldgeleide hyperthermie. Niet invasieve thermometrie biedt veel mogelijkheden om temperaturen in 3D zichtbaar te maken. Gecombineerd met HTP is efficiënte optimalisatie mogelijk.
Ontwikkeling van geavanceerdere applicators. Als onzekerheden gereduceerd zijn, kunnen geavanceerde applicators ontwikkeld worden. Deze zullen de warmte beter en overal in het lichaam kunnen focusseren, zonder hotspot buiten het doelgebied.

12 PhD portfolio

Courses

2006	Advanced use of Hyperplan for hyperthermia treatment planning
2007	Classical methods for data analysis (NIHES)
2008	Biomedical English writing
2011	Research management for postdocs

Teaching activities

- Workshop on Hyperthermia treatment planning, Educational day, ESHO 2010, Rotterdam
- Guest lecture on Hyperthermia treatment of cancer, The Hague University, 2010
- Lecture on Physical effects in Hyperthermia for the resident radiation oncologist, Erasmus MC, 2012
- Supervision of several graduation projects of Applied Physics students, mainly from The Hague University
- Supervision of bachelor graduation projects from Eindhoven University of Technology

Organization

Organization of meetings of the Working group Clinical Hyperthermia of the Dutch cancer society.

Review

Reviewing of several papers for the International Journal of Hyperthermia

Honors

ESHO Rosner travel award for the 11th ICHO, Kyoto, Japan

Peer-reviewed journal publications 1st author

- Complaint-adaptive power density optimization as a tool for HTP-guided steering in deep hyperthermia treatment of pelvic tumors. Canters RA, Franckena M, van der Zee J, Van Rhoon GC. *Phys Med Biol.* 2008; 53(23):6799-820
- Patient positioning in deep hyperthermia: influences of inaccuracies, signal correction possibilities, and optimization potential. Canters RA, Franckena M, Paulides MM ,Van Rhoon GC. *Phys Med Biol. 2009; 54(12):3923-36*

- A literature survey on indicators for characterisation and optimisation of SAR distributions in deep hyperthermia, a plea for standardisation. Canters RA, Wust P, Bakker J ,Van Rhoon GC. *Int J Hyperthermia. 2009; 25(7):593-608*
- Optimizing deep hyperthermia treatments: are locations of patient pain complaints correlated with modelled SAR peak locations? Canters RA, Franckena M, van der Zee J, van Rhoon GC. *Phys Med Biol*. 2011; 21;56(2):439-51.
- Implementation of treatment planning in the routine clinical procedure of regional hyperthermia treatment of cervical cancer. An overview and the Rotterdam experience. Canters RA, Paulides MM, Franckena M,Van der Zee J, Van Rhoon GC. *Int J hyperthermia*. 2012; 28(6):570-581
- Benefit of replacing the Sigma-60 by the Sigma-Eye applicator: a Monte Carlo based uncertainty analysis. Canters RAM, Paulides MM, Franckena M, Mens JW, Van Rhoon GC. *Strahlenther Onkol*. 2013; 189(1):74-80

Conference oral presentations

- Hyperthermia treatment planning: Real-time clinical use of model guided steering. Canters RAM, Franckena M, Van der Zee J. Van Rhoon GC. ESHO 2007, Prague, Czech Republic
- Prediction of hot spots by calculation models, a patient study. Canters RAM, Franckena M, Van der Zee J, Van Rhoon GC. ESHO 2009, Verona, Italy
- Improvement treatment planning in deep hyperthermia, a new study and preliminary results. Canters RAM, Franckena M, Van der Zee J, Van Rhoon GC. ESHO 2010, Rotterdam, The Netherlands
- Towards controlled dose delivery in deep hyperthermia. First results and overview. Canters RAM, Franckena M, Van der Zee J, Van Rhoon GC. BME 2011, Egmond aan Zee, The Netherlands
- Assessment of optimization results as a tool for applicator selection and development in deep hyperthermia. Canters RAM, Paulides MM, Van Rhoon GC. ESHO 2011, Aarhus, Denmark
- EMF dose in patients and medical staff during hyperthermia treatment of cancer. Bakker JF, Canters RAM, Paulides MM, Van Rhoon GC. EMC Europe 2012, Rome, Italy

Conference posters

- Putting the patient in the center: a model study to find an optimum in patient position. Canters RAM, Franckena M, Van der Zee J, Van Rhoon GC. ICHO 2008, Munich, Germany
- Clinical benefit of replacing the Sigma 60 by the Sigma Eye applicator. A Monte Carlo based uncertainty analysis. Canters RAM, Paulides MM, Van Rhoon GC. ICHO 2012, Kyoto, Japan

13 Curriculum vitae

Richard Adrianus Maria Canters, born August 29th, 1978 in Venlo, The Netherlands

1990-1996	Secondary school (Gymnasium), Collegium Marianum, Venlo
1996-2002	Masters degree in Applied Physics, Eindhoven University of Technology, The Netherlands
2003-2006	Research scientist at Wageningen UR, The Netherlands
2006-2013	Research scientist at the Unit Hyperthermia, Erasmus MC - Daniel den Hoed Cancer Center, Rotterdam, The Netherlands
2013-present	Medical physicist in training, UMC St Radboud, Nijmegen, The Netherlands

14 Dankwoord

Zo, het is af. Na een heel aantal jaren van onderzoek en werk in de unit hyperthermie, is tenslotte dit boekje geschreven. Hoewel ik het natuurlijk zelf geschreven heb, zijn er een hele hoop mensen die in meer of mindere mate hebben meegeholpen aan dit onderzoek. Hoewel ik niet iemand ben van heel uitgebreide dankwoorden, zijn er stiekem toch wel veel mensen die ik hier even wil noemen.

Allereerst wil ik mijn promotor bedanken. Gerard, Prof. Van Rhoon, je altijd enthousiaste benadering van de hyperthermie en je vele originele ideeën zijn een grote stimulans voor me geweest tijdens mijn onderzoek. Je weet mensen te inspireren, en een groep te creëren met een prettige en collegiale sfeer.

Verder natuurlijk Cobi, mijn co-promotor. Samen met Gerard ben je altijd de drijvende kracht achter de hyperthermie afdeling geweest. Het was altijd fijn dat je mijn vrij technische onderzoek zo wist te verbinden aan de klinische praktijk.

Maarten, in het begin van mijn tijd op de hyperthermie ben je zelf gepromoveerd. In de afgelopen jaren ben je uitgegroeid tot iemand die de lijnen uitstippelt en de onderzoekers stuurt en begeleidt. Bedankt voor alle constructieve commentaar op mijn onderzoek en papers, voor de discussies en feedback.

Tomas, I liked to get to know you better in the last couple of years. It was good to drive together and I liked our dicussions and the regular drinks with you and the other guys.

Martine, in de eerste jaren van mijn promotie hebben we samen op een KWF project gewerkt. Bedankt voor de fijne samenwerking! Het was altijd erg fijn om zaken ook regelmatig vanuit een ander perspectief van jou te horen en gewoon leuk om samen de treatment planning in de hyperthermie op te zetten.

Daniel, we hebben de afgelopen jaren nauw samengewerkt in het KWF project. Bedankt voor al je support en de goede samenwerking. Je bent iemand die praktisch erg goed is en ook het inzicht in de materie heeft.
Verder wil ik alle andere onderzoekers bedanken voor de goede tijd op de hyperthermie, voor alle samenwerking, en de gezelligheid. Jurriaan, Paolo, Zef, René, Tom, Wouter, Maarten B, Marianne, Fatemeh, Citlalli, Roel, bedankt!

Wat zou de hyperthermie behandeling zijn zonder de artsen, nurse practitioners en laboranten? Heleen, Eva, Dennis,Lia, Laurens, Pia, Greta, Aleida, Audrey en Deborah, bedankt voor alle samenwerking en voor alle geduld en flexibiliteit met het invoeren van door mij bedachte nieuwigheden.

Verder wil ik de afdelingen waarmee we samenwerken bedanken: het AMC, Instituut Verbeeten, de verschillende Duitse hyperthermiecentra, de afdeling electromagnetics van de TU Eindhoven.

Ook de support vanuit Dr. Sennewald Medizintechnik en BSD was altijd goed en is door mij zeer gewaardeerd.

Dan wil ik hier tegen het eind van mijn dankwoord ook niet in het minst mijn ouders, familie en vrienden noemen. Bedankt voor alle vriendschap, liefde en alle steun!

En natuurlijk wil ik mijn lieve vrouw Wendy en Kristine, Simon en Louise bedanken. Jullie zijn de zon in mijn leven!

Tenslotte wil ik de Heer God bedanken. Uw zegeningen zijn ontelbaar.

References

1. Robinson, J.E., M.J. Wizenberg, and W.A. McCready, *Combined hyperthermia and radiation suggest and alternative to heavy particle therapy for reduced oxygen enhancement ratios.* Nature, 1974. **251**(5475): 521-2.
2. Dewey, W.C., *Arrhenius relationships from the molecule and cell to the clinic.* Int J Hyperthermia, 1994. **10**(4): 457-83.
3. Overgaard, J., D. Gonzalez Gonzalez, M.C. Hulshof, G. Arcangeli, O. Dahl, O. Mella*, et al.*, *Randomised trial of hyperthermia as adjuvant to radiotherapy for recurrent or metastatic malignant melanoma. European Society for Hyperthermic Oncology.* Lancet, 1995. **345**(8949): 540-3.
4. van der Zee, J., D. Gonzalez Gonzalez, G.C. van Rhoon, J.D. van Dijk, W.L. van Putten, and A.A. Hart, *Comparison of radiotherapy alone with radiotherapy plus hyperthermia in locally advanced pelvic tumours: a prospective, randomised, multicentre trial. Dutch Deep Hyperthermia Group.* Lancet, 2000. **355**(9210): 1119-25.
5. Datta, N.R., A.K. Bose, H.K. Kapoor, and S. Gupta, *Head and neck cancers: results of thermoradiotherapy versus radiotherapy.* Int J Hyperthermia, 1990. **6**(3): 479-86.
6. Perez, C.A., T. Pajak, B. Emami, N.B. Hornback, L. Tupchong, and P. Rubin, *Randomized phase III study comparing irradiation and hyperthermia with irradiation alone in superficial measurable tumors. Final report by the Radiation Therapy Oncology Group.* Am J Clin Oncol, 1991. **14**(2): 133-41.
7. Valdagni, R. and M. Amichetti, *Report of long-term follow-up in a randomized trial comparing radiation therapy and radiation therapy plus hyperthermia to metastatic lymph nodes in stage IV head and neck patients.* Int J Radiat Oncol Biol Phys, 1994. **28**(1): 163-9.
8. Berdov, B.A. and G.Z. Menteshashvili, *Thermoradiotherapy of patients with locally advanced carcinoma of the rectum.* Int J Hyperthermia, 1990. **6**(5): 881-90.
9. Harima, Y., K. Nagata, K. Harima, V.V. Ostapenko, Y. Tanaka, and S. Sawada, *A randomized clinical trial of radiation therapy versus thermoradiotherapy in stage IIIB cervical carcinoma.* Int J Hyperthermia, 2001. **17**(2): 97-105.
10. Emami, B., C. Scott, C.A. Perez, S. Asbell, P. Swift, P. Grigsby*, et al.*, *Phase III study of interstitial thermoradiotherapy compared with interstitial radiotherapy alone in the treatment of recurrent or persistent human tumors. A prospectively controlled randomized study by the Radiation Therapy Group.* Int J Radiat Oncol Biol Phys, 1996. **34**(5): 1097-104.
11. Sneed, P.K., P.R. Stauffer, M.W. McDermott, C.J. Diederich, K.R. Lamborn, M.D. Prados*, et al.*, *Survival benefit of hyperthermia in a prospective randomized trial of brachytherapy boost +/- hyperthermia for glioblastoma multiforme.* Int J Radiat Oncol Biol Phys, 1998. **40**(2): 287-95.
12. Kitamura, K., H. Kuwano, M. Watanabe, T. Nozoe, M. Yasuda, K. Sumiyoshi*, et al.*, *Prospective randomized study of hyperthermia combined with chemoradiotherapy for esophageal carcinoma.* J Surg Oncol, 1995. **60**(1): 55-8.
13. Sugimachi, K., H. Kuwano, H. Ide, T. Toge, M. Saku, and Y. Oshiumi, *Chemotherapy combined with or without hyperthermia for patients with oesophageal carcinoma: a prospective randomized trial.* Int J Hyperthermia, 1994. **10**(4): 485-93.
14. Hamazoe, R., M. Maeta, and N. Kaibara, *Intraperitoneal thermochemotherapy for prevention of peritoneal recurrence of gastric cancer. Final results of a randomized controlled study.* Cancer, 1994. **73**(8): 2048-52.

15. Ghussen, F., K. Nagel, W. Groth, J.M. Muller, and H. Stutzer, *A prospective randomized study of regional extremity perfusion in patients with malignant melanoma.* Ann Surg, 1984. **200**(6): 764-8.
16. Hafstrom, L., C.M. Rudenstam, E. Blomquist, C. Ingvar, P.E. Jonsson, B. Lagerlof*, et al.*, *Regional hyperthermic perfusion with melphalan after surgery for recurrent malignant melanoma of the extremities. Swedish Melanoma Study Group.* J Clin Oncol, 1991. **9**(12): 2091-4.
17. Koops, H.S., M. Vaglini, S. Suciu, B.B. Kroon, J.F. Thompson, J. Gohl*, et al.*, *Prophylactic isolated limb perfusion for localized, high-risk limb melanoma: results of a multicenter randomized phase III trial. European Organization for Research and Treatment of Cancer Malignant Melanoma Cooperative Group Protocol 18832, the World Health Organization Melanoma Program Trial 15, and the North American Perfusion Group Southwest Oncology Group-8593.* J Clin Oncol, 1998. **16**(9): 2906-12.
18. Engin, K., D.B. Leeper, L. Tupchong, and F.M. Waterman, *Thermoradiotherapy in the management of superficial malignant tumors.* Clin Cancer Res, 1995. **1**(2): 139-45.
19. Kapp, D.S., I.A. Petersen, R.S. Cox, G.M. Hahn, P. Fessenden, S.D. Prionas*, et al.*, *Two or six hyperthermia treatments as an adjunct to radiation therapy yield similar tumor responses: results of a randomized trial.* Int J Radiat Oncol Biol Phys, 1990. **19**(6): 1481-95.
20. Verwaal, V.J., S. van Ruth, E. de Bree, G.W. van Sloothen, H. van Tinteren, H. Boot*, et al.*, *Randomized trial of cytoreduction and hyperthermic intraperitoneal chemotherapy versus systemic chemotherapy and palliative surgery in patients with peritoneal carcinomatosis of colorectal cancer.* J Clin Oncol, 2003. **21**(20): 3737-43.
21. Colombo, R., L.F. Da Pozzo, A. Salonia, P. Rigatti, Z. Leib, J. Baniel*, et al.*, *Multicentric study comparing intravesical chemotherapy alone and with local microwave hyperthermia for prophylaxis of recurrence of superficial transitional cell carcinoma.* J Clin Oncol, 2003. **21**(23): 4270-6.
22. Jones, E.L., J.R. Oleson, L.R. Prosnitz, T.V. Samulski, Z. Vujaskovic, D. Yu*, et al.*, *Randomized trial of hyperthermia and radiation for superficial tumors.* J Clin Oncol, 2005. **23**(13): 3079-85.
23. Issels, R.D., L.H. Lindner, J. Verweij, P. Wust, P. Reichardt, B.C. Schem*, et al.*, *Neo-adjuvant chemotherapy alone or with regional hyperthermia for localised high-risk soft-tissue sarcoma: a randomised phase 3 multicentre study.* Lancet Oncol, 2010. **11**(6): 561-70.
24. Hua, Y., S. Ma, Z. Fu, Q. Hu, L. Wang, and Y. Piao, *Intracavity hyperthermia in nasopharyngeal cancer: a phase III clinical study.* Int J Hyperthermia, 2011. **27**(2): 180-6.
25. Huilgol, N.G., S. Gupta, and C.R. Sridhar, *Hyperthermia with radiation in the treatment of locally advanced head and neck cancer: a report of randomized trial.* J Cancer Res Ther, 2010. **6**(4): 492-6.
26. van der Zee, J., G.C. van Rhoon, J.L. Wike-Hooley, and H.S. Reinhold, *Clinically derived dose effect relationship for hyperthermia given in combination with low dose radiotherapy.* Br J Radiol, 1985. **58**(687): 243-50.
27. Cox, R.S. and D.S. Kapp, *Correlation of thermal parameters with outcome in combined radiation therapy-hyperthermia trials.* Int J Hyperthermia, 1992. **8**(6): 719-32.

28. Wust, P., H. Stahl, K. Dieckmann, S. Scheller, J. Loffel, H. Riess*, et al.*, *Local hyperthermia of N2/N3 cervical lymph node metastases: correlationof technical/thermal parameters and response.* Int J Radiat Oncol Biol Phys, 1996. **34**(3): 635-46.
29. Sherar, M., F.F. Liu, M. Pintilie, W. Levin, J. Hunt, R. Hill*, et al.*, *Relationship between thermal dose and outcome in thermoradiotherapy treatments for superficial recurrences of breast cancer: data from a phase III trial.* Int J Radiat Oncol Biol Phys, 1997. **39**(2): 371-80.
30. Maguire, P.D., T.V. Samulski, L.R. Prosnitz, E.L. Jones, G.L. Rosner, B. Powers*, et al.*, *A phase II trial testing the thermal dose parameter CEM43 degrees T90 as a predictor of response in soft tissue sarcomas treated with pre-operative thermoradiotherapy.* Int J Hyperthermia, 2001. **17**(4): 283-90.
31. Thrall, D.E., S.M. LaRue, D. Yu, T. Samulski, L. Sanders, B. Case*, et al.*, *Thermal dose is related to duration of local control in canine sarcomas treated with thermoradiotherapy.* Clin Cancer Res, 2005. **11**(14): 5206-14.
32. Gellermann, J., B. Hildebrandt, R. Issels, H. Ganter, W. Wlodarczyk, V. Budach*, et al.*, *Noninvasive magnetic resonance thermography of soft tissue sarcomas during regional hyperthermia: correlation with response and direct thermometry.* Cancer, 2006. **107**(6): 1373-82.
33. Franckena, M., D. Fatehi, M. de Bruijne, R.A. Canters, Y. van Norden, J.W. Mens*, et al.*, *Hyperthermia dose-effect relationship in 420 patients with cervical cancer treated with combined radiotherapy and hyperthermia.* Eur J Cancer, 2009. **45**(11): 1969-78.
34. Wust, P., B. Hildebrandt, G. Sreenivasa, B. Rau, J. Gellermann, H. Riess*, et al.*, *Hyperthermia in combined treatment of cancer.* Lancet Oncol, 2002. **3**(8): 487-97.
35. van der Zee, J. and G.C. van Rhoon, *Cervical cancer: radiotherapy and hyperthermia.* Int J Hyperthermia, 2006. **22**(3): 229-34.
36. Lagendijk, J.J., *Hyperthermia treatment planning.* Phys Med Biol, 2000. **45**(5): R61-76.
37. Paulsen, K.D., P.M. Meaney, M.J. Moskowitz, and J.R. Sullivan, *A dual mesh scheme for finite element based reconstruction algorithms.* IEEE Trans Med Imaging, 1995. **14**(3): 504-14.
38. Yee, K.S., *Numerical solutions of initial boundary value problems involving Maxwell's equations in isotropic media.* IEEE Trans Antennas Propag, 1966(14): 302-307.
39. Sreenivasa, G., J. Gellermann, B. Rau, J. Nadobny, P. Schlag, P. Deuflhard*, et al.*, *Clinical use of the hyperthermia treatment planning system HyperPlan to predict effectiveness and toxicity.* Int J Radiat Oncol Biol Phys, 2003. **55**(2): 407-19.
40. Pennes, H.H., *Analysis of tissue and arterial blood temperatures in the resting human forearm.* J Appl Physiol, 1948. **1**(2): 93-122.
41. Raaymakers, B.W., J. Crezee, and J.J. Lagendijk, *Modelling individual temperature profiles from an isolated perfused bovine tongue.* Phys Med Biol, 2000. **45**(3): 765-80.
42. Raaymakers, B.W., A.N. Kotte, and J.J. Lagendijk, *How to apply a discrete vessel model in thermal simulations when only incomplete vessel data are available.* Phys Med Biol, 2000. **45**(11): 3385-401.
43. Kotte, A.N., G.M. van Leeuwen, and J.J. Lagendijk, *Modelling the thermal impact of a discrete vessel tree.* Phys Med Biol, 1999. **44**(1): 57-74.
44. Van den Berg, C.A., J.B. Van de Kamer, A.A. De Leeuw, C.R. Jeukens, B.W. Raaymakers, M. van Vulpen*, et al.*, *Towards patient specific thermal modelling of the prostate.* Phys Med Biol, 2006. **51**(4): 809-25.

45. Canters, R.A., P. Wust, J.F. Bakker, and G.C. Van Rhoon, *A literature survey on indicators for characterisation and optimisation of SAR distributions in deep hyperthermia, a plea for standardisation.* Int J Hyperthermia, 2009. **25**(7): 593-608.
46. Stalling, D., M. Seebass, H. Hege, P. Wust, P. Deuflhard, and R. Felix, *Hyperplan -An integrated system for treatment plannign in regianal hyperthermia*. 1996, Konrad Zuse Zentrum für Informationstechnik Berlin.
47. Canters, R.A., M. Franckena, J. van der Zee, and G.C. Van Rhoon, *Complaint-adaptive power density optimization as a tool for HTP-guided steering in deep hyperthermia treatment of pelvic tumors.* Phys Med Biol, 2008. **53**(23): 6799-820.
48. Gabriel, S., R.W. Lau, and C. Gabriel, *The dielectric properties of biological tissues: III. Parametric models for the dielectric spectrum of tissues.* Phys Med Biol, 1996. **41**(11): 2271-93.
49. Gabriel, S., R.W. Lau, and C. Gabriel, *The dielectric properties of biological tissues: II. Measurements in the frequency range 10 Hz to 20 GHz.* Phys Med Biol, 1996. **41**(11): 2251-69.
50. Gabriel, C., S. Gabriel, and E. Corthout, *The dielectric properties of biological tissues: I. Literature survey.* Phys Med Biol, 1996. **41**(11): 2231-49.
51. Hasgall, P.A., E. Neufeld, G.M. C., A. Klingenböck, and N. Kuster, *IT'IS Database for thermal and electromagnetic parameters of biological tissues*. 2011.
52. McIntosh, R.L. and V. Anderson, *Comprehensive Tissue Properties Database Provided for the Thermal Assessment of a Human at Rest.* Biophysical Reviews and Letters, 2010. **5**(3): 129-151.
53. Song, C.W., A. Lokshina, J.G. Rhee, M. Patten, and S.H. Levitt, *Implication of blood flow in hyperthermic treatment of tumors.* IEEE Trans Biomed Eng, 1984. **31**(1): 9-16.
54. Tompkins, D.T., R. Vanderby, S.A. Klein, W.A. Beckman, R.A. Steeves, D.M. Frye*, et al.*, *Temperature-dependent versus constant-rate blood perfusion modelling in ferromagnetic thermoseed hyperthermia: results with a model of the human prostate.* Int J Hyperthermia, 1994. **10**(4): 517-36.
55. Lang, J., B. Erdmann, and M. Seebass, *Impact of nonlinear heat transfer on temperature control in regional hyperthermia.* IEEE Trans Biomed Eng, 1999. **46**(9): 1129-38.
56. Cheng, K.S. and R.B. Roemer, *Blood perfusion and thermal conduction effects in Gaussian beam, minimum time single-pulse thermal therapies.* Med Phys, 2005. **32**(2): 311-7.
57. Sekins, K.M., J.F. Lehmann, P. Esselman, D. Dundore, A.F. Emery, B.J. deLateur*, et al.*, *Local muscle blood flow and temperature responses to 915MHz diathermy as simultaneously measured and numerically predicted.* Arch Phys Med Rehabil, 1984. **65**(1): 1-7.
58. Roemer, R.B., A.M. Fletcher, and T.C. Cetas, *Obtaining local SAR and blood perfusion data from temperature measurements: steady state and transient techniques compared.* Int J Radiat Oncol Biol Phys, 1985. **11**(8): 1539-50.
59. Akyurekli, D., L.H. Gerig, and G.P. Raaphorst, *Changes in muscle blood flow distribution during hyperthermia.* Int J Hyperthermia, 1997. **13**(5): 481-96.
60. de Greef, M., H.P. Kok, D. Correia, A. Bel, and J. Crezee, *Optimization in hyperthermia treatment planning: the impact of tissue perfusion uncertainty.* Med Phys, 2010. **37**(9): 4540-50.

61. de Greef, M., H.P. Kok, D. Correia, P.P. Borsboom, A. Bel, and J. Crezee, *Uncertainty in hyperthermia treatment planning: the need for robust system design.* Phys Med Biol, 2011. **56**(11): 3233-50.
62. Wust, P., R. Beck, J. Berger, H. Fahling, M. Seebass, W. Wlodarczyk*, et al.*, *Electric field distributions in a phased-array applicator with 12 channels: measurements and numerical simulations.* Med Phys, 2000. **27**(11): 2565-79.
63. Neufeld, E., *High resolution hyperthermia treatment planning*, in *ETH Zürich*. 2008, ETH Zürich: Zürich.
64. Wust, P., J. Berger, H. Fahling, J. Nadobny, J. Gellermann, W. Tilly*, et al.*, *Scanning E-field sensor device for online measurements in annular phased-array systems.* Int J Radiat Oncol Biol Phys, 1999. **43**(4): 927-37.
65. Wust, P., T. Meier, M. Seebass, H. Fahling, K. Petermann, and R. Felix, *Noninvasive prediction of SAR distributions with an electro-optical E field sensor.* Int J Hyperthermia, 1995. **11**(2): 295-310.
66. Cheng, K.S., M.W. Dewhirst, P.F. Stauffer, and S. Das, *Mathematical formulation and analysis of the nonlinear system reconstruction of the online image-guided adaptive control of hyperthermia.* Med Phys, 2010. **37**(3): 980-94.
67. Cheng, K.S., Y. Yuan, Z. Li, P.R. Stauffer, P. Maccarini, W.T. Joines*, et al.*, *The performance of a reduced-order adaptive controller when used in multi-antenna hyperthermia treatments with nonlinear temperature-dependent perfusion.* Phys Med Biol, 2009. **54**(7): 1979-95.
68. Stakhursky, V.L., O. Arabe, K.S. Cheng, J. Macfall, P. Maccarini, O. Craciunescu*, et al.*, *Real-time MRI-guided hyperthermia treatment using a fast adaptive algorithm.* Phys Med Biol, 2009. **54**(7): 2131-45.
69. Ranneberg, M., M. Weiser, M. Weihrauch, V. Budach, J. Gellermann, and P. Wust, *Regularized antenna profile adaptation in online hyperthermia treatment.* Med Phys, 2010. **37**(10): 5382-94.
70. Weihrauch, M., P. Wust, M. Weiser, J. Nadobny, S. Eisenhardt, V. Budach*, et al.*, *Adaptation of antenna profiles for control of MR guided hyperthermia (HT) in a hybrid MR-HT system.* Med Phys, 2007. **34**(12): 4717-25.
71. Cheng, K.S., V. Stakhursky, P. Stauffer, M. Dewhirst, and S.K. Das, *Online feedback focusing algorithm for hyperthermia cancer treatment.* Int J Hyperthermia, 2007. **23**(7): 539-54.
72. Cheng, K.S., M.W. Dewhirst, P.R. Stauffer, and S. Das, *Effective learning strategies for real-time image-guided adaptive control of multiple-source hyperthermia applicators.* Med Phys, 2010. **37**(3): 1285-97.
73. Kowalski, M.E. and J.M. Jin, *A temperature-based feedback control system for electromagnetic phased-array hyperthermia: theory and simulation.* Phys Med Biol, 2003. **48**(5): 633-51.
74. Paulides, M.M., J.F. Bakker, E. Neufeld, J. van der Zee, P.P. Jansen, P.C. Levendag*, et al.*, *Winner of the "New Investigator Award" at the European Society of Hyperthermia Oncology Meeting 2007. The HYPERcollar: a novel applicator for hyperthermia in the head and neck.* Int J Hyperthermia, 2007. **23**(7): 567-76.
75. Paulides, M.M., J.F. Bakker, A.P. Zwamborn, and G.C. Van Rhoon, *A head and neck hyperthermia applicator: theoretical antenna array design.* Int J Hyperthermia, 2007. **23**(1): 59-67.

76. Nadobny, J., W. Wlodarczyk, L. Westhoff, J. Gellermann, R. Felix, and P. Wust, *A clinical water-coated antenna applicator for MR-controlled deep-body hyperthermia: a comparison of calculated and measured 3-D temperature data sets.* IEEE Trans Biomed Eng, 2005. **52**(3): 505-19.
77. Kennedy, J. and R. Eberhart, *Particle swarm optimization.* 1995 Ieee International Conference on Neural Networks Proceedings, Vols 1-6, 1995: 1942-1948.
78. Bardati, F., A. Borrani, A. Gerardino, and G.A. Lovisolo, *SAR optimization in a phased array radiofrequency hyperthermia system. Specific absorption rate.* IEEE Trans Biomed Eng, 1995. **42**(12): 1201-7.
79. Das, S.K., S.T. Clegg, and T.V. Samulski, *Electromagnetic thermal therapy power optimization for multiple source applicators.* Int J Hyperthermia, 1999. **15**(4): 291-308.
80. Seebass, M., R. Beck, J. Gellermann, J. Nadobny, and P. Wust, *Electromagnetic phased arrays for regional hyperthermia: optimal frequency and antenna arrangement.* Int J Hyperthermia, 2001. **17**(4): 321-36.
81. Wust, P., M. Seebass, J. Nadobny, P. Deuflhard, G. Monich, and R. Felix, *Simulation studies promote technological development of radiofrequency phased array hyperthermia.* Int J Hyperthermia, 1996. **12**(4): 477-94.
82. Paulsen, K.D., S. Geimer, J. Tang, and W.E. Boyse, *Optimization of pelvic heating rate distributions with electromagnetic phased arrays.* Int J Hyperthermia, 1999. **15**(3): 157-86.
83. Sandrini, L., A. Vaccari, C. Malacarne, L. Cristoforetti, and R. Pontalti, *RF dosimetry: a comparison between power absorption of female and male numerical models from 0.1 to 4 ghz.* Phys Med Biol, 2004. **49**(22): 5185-201.
84. Wiersma, J., *Hyperthermia treatment planning*. 2000, UMC Utrecht
85. Wiersma, J., R.A. van Maarseveen, and J.D. van Dijk, *A flexible optimization tool for hyperthermia treatments with RF phased array systems.* Int J Hyperthermia, 2002. **18**(2): 73-85.
86. Kroeze, H., J.B. Van de Kamer, A.A. De Leeuw, and J.J. Lagendijk, *Regional hyperthermia applicator design using FDTD modelling.* Phys Med Biol, 2001. **46**(7): 1919-35.
87. Kuster, N., V.B. Torres, N. Nikoloski, M. Frauscher, and W. Kainz, *Methodology of detailed dosimetry and treatment of uncertainty and variations for in vivo studies.* Bioelectromagnetics, 2006. **27**(5): 378-91.
88. IEEE-1529, *Recommended Practice for Determining the Peak Spatial-Average Specific Absorption Rate (SAR) associated with the use of wireless handsets—computational techniques*.
89. Keshvari, J. and S. Lang, *Comparison of radio frequency energy absorption in ear and eye region of children and adults at 900, 1800 and 2450 MHz.* Phys Med Biol, 2005. **50**(18): 4355-69.
90. Bahr, A., H. Dorn, and T. Bolz, *Dosimetric assessment of an exposure system for simulating GSM and WCDMA mobile phone usage.* Bioelectromagnetics, 2006. **27**(4): 320-7.
91. Bernardi, P., M. Cavagnaro, S. Pisa, and E. Piuzzi, *Specific absorption rate and temperature elevation in a subject exposed in the far-field of radio-frequency sources operating in the 10-900-MHz range.* IEEE Trans Biomed Eng, 2003. **50**(3): 295-304.
92. ICNIRP, *Guidelines for limiting exposure to time-varying electric, magnetic, and electromagnetic fields (up to 300 GHz). International Commission on Non-Ionizing Radiation Protection.* Health Phys, 1998. **74**(4): 494-522.

93. Myerson, R.J., C.A. Perez, B. Emami, W. Straube, R.R. Kuske, L. Leybovich*, et al.*, *Tumor control in long-term survivors following superficial hyperthermia.* Int J Radiat Oncol Biol Phys, 1990. **18**(5): 1123-9.
94. Lee, H.K., A.G. Antell, C.A. Perez, W.L. Straube, G. Ramachandran, R.J. Myerson*, et al.*, *Superficial hyperthermia and irradiation for recurrent breast carcinoma of the chest wall: prognostic factors in 196 tumors.* Int J Radiat Oncol Biol Phys, 1998. **40**(2): 365-75.
95. Gelvich, E.A., V.N. Mazokhin, and Troshin, II, *An attempt at quantitative specification of SAR distribution homogeneity.* Int J Hyperthermia, 1996. **12**(3): 431-6.
96. Van de Kamer, J.B., N. Van Wieringen, A.A. De Leeuw, and J.J. Lagendijk, *The significance of accurate dielectric tissue data for hyperthermia treatment planning.* Int J Hyperthermia, 2001. **17**(2): 123-42.
97. De Greef, M., H.P. Kok, A. Bel, and J. Crezee, *3D versus 2D steering in patient anatomies: a comparison using hyperthermia treatment planning.* Int J Hyperthermia, 2011. **27**(1): 74-85.
98. Kok, H.P., M. de Greef, P.P. Borsboom, A. Bel, and J. Crezee, *Improved power steering with double and triple ring waveguide systems: the impact of the operating frequency.* Int J Hyperthermia, 2011. **27**(3): 224-39.
99. Das, S.K., S.T. Clegg, and T.V. Samulski, *Computational techniques for fast hyperthermia temperature optimization.* Med Phys, 1999. **26**(2): 319-28.
100. Gellermann, J., P. Wust, D. Stalling, M. Seebass, J. Nadobny, R. Beck*, et al.*, *Clinical evaluation and verification of the hyperthermia treatment planning system hyperplan.* Int J Radiat Oncol Biol Phys, 2000. **47**(4): 1145-56.
101. Erdmann, B., J. Lang, and M. Seebass, *Optimization of temperature distributions for regional hyperthermia based on a nonlinear heat transfer model.* Ann N Y Acad Sci, 1998. **858**: 36-46.
102. Cheng, K.S., V. Stakhursky, O.I. Craciunescu, P. Stauffer, M. Dewhirst, and S.K. Das, *Fast temperature optimization of multi-source hyperthermia applicators with reduced-order modeling of 'virtual sources'.* Phys Med Biol, 2008. **53**(6): 1619-35.
103. Jia, X., K.D. Paulsen, D.N. Buechler, F.A. Gibbs, Jr., and P.M. Meaney, *Finite element simulation of Sigma 60 heating in the Utah phantom: computed and measured data compared.* Int J Hyperthermia, 1994. **10**(6): 755-74.
104. Craciunescu, O.I., S.K. Das, R.L. McCauley, J.R. MacFall, and T.V. Samulski, *3D numerical reconstruction of the hyperthermia induced temperature distribution in human sarcomas using DE-MRI measured tissue perfusion: validation against non-invasive MR temperature measurements.* Int J Hyperthermia, 2001. **17**(3): 221-39.
105. Wiersma, J. and J.D. Van Dijk, *RF hyperthermia array modelling; validation by means of measured EM-field distributions.* Int J Hyperthermia, 2001. **17**(1): 63-81.
106. Gellermann, J., W. Wlodarczyk, H. Ganter, J. Nadobny, H. Fahling, M. Seebass*, et al.*, *A practical approach to thermography in a hyperthermia/magnetic resonance hybrid system: validation in a heterogeneous phantom.* Int J Radiat Oncol Biol Phys, 2005. **61**(1): 267-77.
107. de Bruijne, M., T. Samaras, N. Chavannes, and G.C. van Rhoon, *Quantitative validation of the 3D SAR profile of hyperthermia applicators using the gamma method.* Phys Med Biol, 2007. **52**(11): 3075-88.
108. Franckena, M., R. Canters, F. Termorshuizen, J. Van Der Zee, and G. Van Rhoon, *Clinical implementation of hyperthermia treatment planning guided steering: A cross over trial to*

assess its current contribution to treatment quality. Int J Hyperthermia, 2010. **26**(2): 145-57.

109. Li, Z., M. Vogel, P.F. Maccarini, V. Stakhursky, B.J. Soher, O.I. Craciunescu*, et al.*, *Improved hyperthermia treatment control using SAR/temperature simulation and PRFS magnetic resonance thermal imaging.* Int J Hyperthermia, 2011. **27**(1): 86-99.
110. Voet, P.W., M.L. Dirkx, D.N. Teguh, M.S. Hoogeman, P.C. Levendag, and B.J. Heijmen, *Does atlas-based autosegmentation of neck levels require subsequent manual contour editing to avoid risk of severe target underdosage? A dosimetric analysis.* Radiother Oncol, 2011. **98**(3): 373-7.
111. Teguh, D.N., P.C. Levendag, P.W. Voet, A. Al-Mamgani, X. Han, T.K. Wolf*, et al.*, *Clinical validation of atlas-based auto-segmentation of multiple target volumes and normal tissue (swallowing/mastication) structures in the head and neck.* Int J Radiat Oncol Biol Phys, 2011. **81**(4): 950-7.
112. Canters, R.A., M. Franckena, M.M. Paulides, and G.C. Van Rhoon, *Patient positioning in deep hyperthermia: influences of inaccuracies, signal correction possibilities and optimization potential.* Phys Med Biol, 2009. **54**(12): 3923-36.
113. Gellermann, J., J. Goke, R. Figiel, M. Weihrauch, C.H. Cho, V. Budach*, et al.*, *Simulation of different applicator positions for treatment of a presacral tumour.* Int J Hyperthermia, 2007. **23**(1): 37-47.
114. Bruggmoser, G., S. Bauchowitz, R. Canters, H. Crezee, M. Ehmann, J. Gellermann*, et al.*, *Quality assurance for clinical studies in regional deep hyperthermia.* Strahlenther Onkol, 2011. **187**(10): 605-10.
115. Berger, J., K. Petermann, H. Fahling, and P. Wust, *Calibrated electro-optic E-field sensors for hyperthermia applications.* Phys Med Biol, 2001. **46**(2): 399-411.
116. Thrall, D.E., G.L. Rosner, C. Azuma, S.M. Larue, B.C. Case, T. Samulski*, et al.*, *Using units of CEM 43 degrees C T90, local hyperthermia thermal dose can be delivered as prescribed.* Int J Hyperthermia, 2000. **16**(5): 415-28.
117. Fatehi, D., J. van der Zee, M. de Bruijne, M. Franckena, and G.C. van Rhoon, *RF-power and temperature data analysis of 444 patients with primary cervical cancer: deep hyperthermia using the Sigma-60 applicator is reproducible.* Int J Hyperthermia, 2007. **23**(8): 623-43.
118. Sugahara, T., J. van der Zee, H.H. Kampinga, Z. Vujaskovic, M. Kondo, T. Ohnishi*, et al.*, *Kadota Fund International Forum 2004. Application of thermal stress for the improvement of health, 15-18 June 2004, Awaji Yumebutai International Conference Center, Awaji Island, Hyogo, Japan. Final report.* Int J Hyperthermia, 2008. **24**(2): 123-40.
119. van der Zee, J., Z. Vujaskovic, M. Kondo, and T. Sugahara, *The Kadota Fund International Forum 2004--clinical group consensus.* Int J Hyperthermia, 2008. **24**(2): 111-22.
120. van Rhoon, G.C. and P. Wust, *Introduction: non-invasive thermometry for thermotherapy.* Int J Hyperthermia, 2005. **21**(6): 489-95.
121. Dewhirst, M.W., Z. Vujaskovic, E. Jones, and D. Thrall, *Re-setting the biologic rationale for thermal therapy.* Int J Hyperthermia, 2005. **21**(8): 779-90.
122. Nadobny, J., M. Szimtenings, D. Diehl, E. Stetter, G. Brinker, and P. Wust, *Evaluation of MR-induced hot spots for different temporal SAR modes using a time-dependent finite difference method with explicit temperature gradient treatment.* IEEE Trans Biomed Eng, 2007. **54**(10): 1837-50.

123. de Bruijne, M., D.H. Wielheesen, J. van der Zee, N. Chavannes, and G.C. van Rhoon, *Benefits of superficial hyperthermia treatment planning: five case studies.* Int J Hyperthermia, 2007. **23**(5): 417-29.
124. Kok, H.P., P.M. van Haaren, J.B. van de Kamer, P.J. Zum Vorde Sive Vording, J. Wiersma, M.C. Hulshof*, et al.*, *Prospective treatment planning to improve locoregional hyperthermia for oesophageal cancer.* Int J Hyperthermia, 2006. **22**(5): 375-89.
125. Rossetto, F., P.R. Stauffer, V. Manfrini, C.J. Diederich, and G. Biffi Gentili, *Effect of practical layered dielectric loads on SAR patterns from dual concentric conductor microstrip antennas.* Int J Hyperthermia, 1998. **14**(6): 553-71.
126. Rossetto, F. and P.R. Stauffer, *Effect of complex bolus-tissue load configurations on SAR distributions from dual concentric conductor applicators. Specific absorption rate.* IEEE Trans Biomed Eng, 1999. **46**(11): 1310-9.
127. Samaras, T., P.J.M. Rietveld, and G.C. van Rhoon, *Effectiveness of FDTD in predicting SAR distributions from the lucite cone applicator.* Ieee Transactions on Microwave Theory and Techniques, 2000. **48**(11): 2059-2063.
128. Rossetto, F. and P.R. Stauffer, *Theoretical characterization of dual concentric conductor microwave applicators for hyperthermia at 433 MHz.* Int J Hyperthermia, 2001. **17**(3): 258-70.
129. Paulides, M.M., S.H. Vossen, A.P. Zwamborn, and G.C. van Rhoon, *Theoretical investigation into the feasibility to deposit RF energy centrally in the head-and-neck region.* Int J Radiat Oncol Biol Phys, 2005. **63**(2): 634-42.
130. Paulides, M.M., D.H. Wielheesen, J. Van der Zee, and G.C. Van Rhoon, *Assessment of the local SAR distortion by major anatomical structures in a cylindrical neck phantom.* Int J Hyperthermia, 2005. **21**(2): 125-40.
131. Van der Gaag, M.L., M. De Bruijne, T. Samaras, J. Van der Zee, and G.C. Van Rhoon, *Development of a guideline for the water bolus temperature in superficial hyperthermia.* Int J Hyperthermia, 2006. **22**(8): 637-56.
132. de Bruijne, M., T. Samaras, J.F. Bakker, and G.C. van Rhoon, *Effects of waterbolus size, shape and configuration on the SAR distribution pattern of the Lucite cone applicator.* Int J Hyperthermia, 2006. **22**(1): 15-28.
133. Paulides, M.M., J.F. Bakker, N. Chavannes, and G.C. Van Rhoon, *A patch antenna design for application in a phased-array head and neck hyperthermia applicator.* IEEE Trans Biomed Eng, 2007. **54**(11): 2057-63.
134. Kok, H.P., P.M. Van Haaren, J.B. Van de Kamer, J. Wiersma, J.D. Van Dijk, and J. Crezee, *High-resolution temperature-based optimization for hyperthermia treatment planning.* Phys Med Biol, 2005. **50**(13): 3127-41.
135. van der Wal, E., M. Franckena, D.H. Wielheesen, J. van der Zee, and G.C. van Rhoon, *Steering in locoregional deep hyperthermia: evaluation of common practice with 3D-planning.* Int J Hyperthermia, 2008. **24**(8): 682-93.
136. Van de Kamer, J.B., A.A. De Leeuw, S.N. Hornsleth, H. Kroeze, A.N. Kotte, and J.J. Lagendijk, *Development of a regional hyperthermia treatment planning system.* Int J Hyperthermia, 2001. **17**(3): 207-20.
137. Paulides, M.M., J.F. Bakker, and G.C. van Rhoon, *Electromagnetic head-and-neck hyperthermia applicator: experimental phantom verification and FDTD model.* Int J Radiat Oncol Biol Phys, 2007. **68**(2): 612-20.

138. Raaymakers, B.W., M. Van Vulpen, J.J. Lagendijk, A.A. De Leeuw, J. Crezee, and J.J. Battermann, *Determination and validation of the actual 3D temperature distribution during interstitial hyperthermia of prostate carcinoma.* Phys Med Biol, 2001. **46**(12): 3115-31.
139. Turner, P.F. and T. Schaefermeyer, *BSD-2000 approach for deep local and regional hyperthermia: clinical utility.* Strahlenther Onkol, 1989. **165**(10): 700-4.
140. Van Rhoon, G.C., D.J. Van Der Heuvel, A. Ameziane, P.J. Rietveld, K. Volenec, and J. Van Der Zee, *Characterization of the SAR-distribution of the Sigma-60 applicator for regional hyperthermia using a Schottky diode sheet.* Int J Hyperthermia, 2003. **19**(6): 642-54.
141. Neuman, D.G., P.R. Stauffer, S. Jacobsen, and F. Rossetto, *SAR pattern perturbations from resonance effects in water bolus layers used with superficial microwave hyperthermia applicators.* Int J Hyperthermia, 2002. **18**(3): 180-93.
142. Johnson, J.E., D.G. Neuman, P.F. Maccarini, T. Juang, P.R. Stauffer, and P. Turner, *Evaluation of a dual-arm Archimedean spiral array for microwave hyperthermia.* Int J Hyperthermia, 2006. **22**(6): 475-90.
143. Turner, P.F., A. Tumeh, and T. Schaefermeyer, *BSD-2000 approach for deep local and regional hyperthermia: physics and technology.* Strahlenther Onkol, 1989. **165**(10): 738-41.
144. Vaupel, P., F. Kallinowski, and P. Okunieff, *Blood flow, oxygen and nutrient supply, and metabolic microenvironment of human tumors: a review.* Cancer Res, 1989. **49**(23): 6449-65.
145. Kotte, A., G. van Leeuwen, J. de Bree, J. van der Koijk, H. Crezee, and J. Lagendijk, *A description of discrete vessel segments in thermal modelling of tissues.* Phys Med Biol, 1996. **41**(5): 865-84.
146. Gellermann, J., M. Weihrauch, C.H. Cho, W. Wlodarczyk, H. Fahling, R. Felix*, et al.*, *Comparison of MR-thermography and planning calculations in phantoms.* Med Phys, 2006. **33**(10): 3912-20.
147. Kok, H.P., *Treatment planning for locoregional and intraluminal hyperthermia*. 2007: Amsterdam.
148. Wust, P., H. Fahling, T. Helzel, M. Kniephoff, W. Wlodarczyk, G. Monich*, et al.*, *Design and test of a new multi-amplifier system with phase and amplitude control.* Int J Hyperthermia, 1998. **14**(5): 459-77.
149. Kongsli, J., B.T. Hjertaker, and T. Froystein, *Evaluation of power and phase accuracy of the BSD Dodek amplifier for regional hyperthermia using an external vector voltmeter measurement system.* Int J Hyperthermia, 2006. **22**(8): 657-71.
150. van Rhoon, G.C., A. Ameziane, W.M. Lee, D.J. van der Heuvel, H.J. Klinkhamer, C. Barendrecht*, et al.*, *Accuracy of electrical field measurement using the flexible Schottky diode sheet at 433 MHz.* Int J Hyperthermia, 2003. **19**(2): 134-44.
151. Lee, W.M., A. Ameziane, A.M. van den Biggelaar, P.J. Rietveld, and G.C. van Rhoon, *Stability and accuracy of power and phase measurements of a VVM system designed for online quality control of the BSD-2000 (-3D) DHT system.* Int J Hyperthermia, 2003. **19**(1): 74-88.
152. Siauve, N., L. Nicolas, C. Vollaire, and C. Marchal, *Optimization of the sources in local hyperthermia using a combined finite element-genetic algorithm method.* Int J Hyperthermia, 2004. **20**(8): 815-33.
153. Kohler, T., P. Maass, P. Wust, and M. Seebass, *A fast algorithm to find optimal controls of multiantenna applicators in regional hyperthermia.* Phys Med Biol, 2001. **46**(9): 2503-14.

154. Schittkowski, K., *NLQPL: A FORTRAN-Subroutine Solving Constrained Nonlinear Programming Problems.* Ann of Oper Res, 1985. **5**: 485-500.
155. Franckena, M., L.J. Stalpers, P.C. Koper, R.G. Wiggenraad, W.J. Hoogenraad, J.D. van Dijk*, et al.*, *Long-term improvement in treatment outcome after radiotherapy and hyperthermia in locoregionally advanced cervix cancer: an update of the Dutch Deep Hyperthermia Trial.* Int J Radiat Oncol Biol Phys, 2008. **70**(4): 1176-82.
156. Fatehi, D., J. van der Zee, E. van der Wal, W.N. Van Wieringen, and G.C. Van Rhoon, *Temperature data analysis for 22 patients with advanced cervical carcinoma treated in Rotterdam using radiotherapy, hyperthermia and chemotherapy: a reference point is needed.* Int J Hyperthermia, 2006. **22**(4): 353-63.
157. Paulsen, K.D., *Principles of power deposition models*, in *Principles and practice of thermoradiotherapy and thermochemotherapy*, M.H. Seegenschmiedt, Editor. 1995, Springer Verlag: Berlin. p. 399-423.
158. Wiersma, J., N. van Wieringen, H. Crezee, and J.D. van Dijk, *Delineation of potential hot spots for hyperthermia treatment planning optimisation.* Int J Hyperthermia, 2007. **23**(3): 287-301.
159. Wust, P., J. Nadobny, M. Seebass, D. Stalling, J. Gellermann, H.C. Hege*, et al.*, *Influence of patient models and numerical methods on predicted power deposition patterns.* Int J Hyperthermia, 1999. **15**(6): 519-40.
160. Gibbs, F.A., Jr., *personal communication*. 2008.
161. de Bruijne, M., B. van der Holt, G.C. van Rhoon, and J. van der Zee, *Evaluation of CEM43 degrees CT90 thermal dose in superficial hyperthermia: a retrospective analysis.* Strahlenther Onkol, 2010. **186**(8): 436-43.
162. Sauer, R., H. Creeze, M. Hulshof, R. Issels, O. Ott, S. Interdisciplinary Working Group for Clinical Hyperthermia of the German Cancer*, et al.*, *Concerning the final report "Hyperthermia: a systematic review" of the Ludwig Boltzmann Institute for Health Technology Assessment, Vienna, March 2010.* Strahlenther Onkol, 2012. **188**(3): 209-13.
163. Trefna, H.D., P. Togni, R. Shiee, J. Vrba, and M. Persson, *Design of a wideband multi-channel system for time reversal hyperthermia.* Int J Hyperthermia, 2012. **28**(2): 175-83.
164. Paulides, M.M., J.F. Bakker, M. Linthorst, J. van der Zee, Z. Rijnen, E. Neufeld*, et al.*, *The clinical feasibility of deep hyperthermia treatment in the head and neck: new challenges for positioning and temperature measurement.* Phys Med Biol, 2010. **55**(9): 2465-80.
165. Linthorst, M., T. Drizdal, H. Joosten, G.C. van Rhoon, and J. van der Zee, *Procedure for creating a three-dimensional (3D) model for superficial hyperthermia treatment planning.* Strahlenther Onkol, 2011. **187**(12): 835-41.
166. Canters, R.A., M. Franckena, J. van der Zee, and G.C. van Rhoon, *Optimizing deep hyperthermia treatments: are locations of patient pain complaints correlated with modelled SAR peak locations?* Phys Med Biol, 2011. **56**(2): 439-51.
167. Bakker, J.F., M.M. Paulides, E. Neufeld, A. Christ, N. Kuster, and G.C. van Rhoon, *Children and adults exposed to electromagnetic fields at the ICNIRP reference levels: theoretical assessment of the induced peak temperature increase.* Phys Med Biol, 2011. **56**(15): 4967-89.
168. Datta, N.R., A.K. Bose, and H.K. Kapoor, *Thermoradiotherapy in the management of carcinoma cervix (stage IIIB): A controlled clinical study.* Indian Med Gaz, 1987. **121**: 68-71.

169. Sharma, S., F.D. Patel, A.P. Sandhu, B.D. Gupta, and N.S. Yadav, *A prospective randomized study of local hyperthermia as a supplement and radiosensitizer in the treatment of carcinoma of the cervix with radiotherapy. .* Endocuriether/Hyperthermia Oncol, 1989. **5**: 151-159.
170. van der Zee, J. and G.D. Gonzalez, *The Dutch Deep Hyperthermia Trial: results in cervical cancer.* Int J Hyperthermia, 2002. **18**(1): 1-12.
171. Chen, H., F. Jun-Lie, and L. Wei, *A randomized trial of hyperthermo-radiochemotherapy for uterine cervix cancer. .* Chin J Clin Oncol, 1997. **24**: 249-251.
172. Franckena, M., L.C. Lutgens, P.C. Koper, C.E. Kleynen, E.M. van der Steen-Banasik, J.J. Jobsen*, et al.*, *Radiotherapy and hyperthermia for treatment of primary locally advanced cervix cancer: results in 378 patients.* Int J Radiat Oncol Biol Phys, 2009. **73**(1): 242-50.
173. van Haaren, P.M., H.P. Kok, C.A. van den Berg, P.J. Zum Vorde Sive Vording, S. Oldenborg, L.J. Stalpers*, et al.*, *On verification of hyperthermia treatment planning for cervical carcinoma patients.* Int J Hyperthermia, 2007. **23**(3): 303-14.
174. Fatehi, D., J. van der Zee, A. Notenboom, and G.C. van Rhoon, *Comparison of intratumor and intraluminal temperatures during locoregional deep hyperthermia of pelvic tumors.* Strahlenther Onkol, 2007. **183**(9): 479-86.
175. Fatehi, D., M. de Bruijne, J. van der Zee, and G.C. van Rhoon, *RHyThM, a tool for analysis of PDOS formatted hyperthermia treatment data generated by the BSD2000/3D system.* Int J Hyperthermia, 2006. **22**(2): 173-84.
176. Rabe-Hesketh, S. and A. Skrondal, *Multilevel and longitudinal modeling using stata*. 2nd ed. 2008, College Station, Tex.: Stata Press Publication. xxxiii, 562 p.
177. Hornsleth, S.N., *Radiofrequency regional hyperthermia*. 1996.
178. Hornsleth, S.N., L. Frydendal, O. Mella, O. Dahl, and P. Raskmark, *Quality assurance for radiofrequency regional hyperthermia.* Int J Hyperthermia, 1997. **13**(2): 169-85.
179. Victor, M. and A.H. Ropper, *Pain*, in *Adams and Victor's Principles of Neurology*. 2002, McGraw-Hill: New York. p. 135-156.
180. Arcangeli, G., P.P. Lombardini, G.A. Lovisolo, G. Marsiglia, and M. Piattelli, *Focusing of 915 MHz electromagnetic power on deep human tissues: a mathematical model study.* IEEE Trans Biomed Eng, 1984. **31**(1): 47-52.